DIPPED ADCLUSTER MODEL FOR CHEMISORPTION AND CATALYTIC REACTIONS

HIROSHI NAKATSUJI

Department of Synthetic Chemistry and Biological Chemistry,
Graduate School of Engineering, Kyoto University,
Sakyo-ku, Kyoto 606-01, Japan,

Department of Applied Chemistry, Graduate School of Engineering,
The University of Tokyo, Tokyo 113, Japan
and
Institute for Fundamental Chemistry, 34-4 Takano-Nishihiraki-cho,
Sakyo-ku, Kyoto 606, Japan

Abstract

Dipped adcluster model (DAM) is a model for surface reactions involving electron transfer between surface and adsorbates. *Adcluster* is a combined system of the adsorbate and cluster directly interacting, and it is *dipped* onto the *electron bath* of the solid metal. Spin and electron exchange occur between the adcluster and the bulk metal, and the equilibrium is established when the chemical potential of the adcluster, which is $-\partial E(n)/\partial n$ with $E(n)$ being the energy of the adcluster as a function of the number n of electrons transferred into the adcluster, becomes equal with the chemical potential μ of the metal surface. Here, n can be non-integer because we are dealing with a partial system. The shape of the $E(n)$ curve as a function of n, in particular, the upper or lower convex nature, determines whether integral or non-integral number of electrons, respectively, is transferred from the bulk metal. This shape is closely related with the spin-coupling of the transferred electrons in the active orbital and therefore with the surface magnetism. A molecular orbital model of the dipped adcluster was summarized and the shape was related with the electron-electron repulsions within the active molecular orbitals. *Image force*, which is an electrostatic interaction between admolecule and surface, is an important long-range force and is included in the DAM. Using the DAM, the size of the adcluster can be much reduced. Otherwise, in the cluster model, a very large cluster must be used for correctly describing chemisorption and catalytic reactions in which electron transfer is important.

For surface reactions, electron correlations are often very important and further the catalytically active states are not necessarily the ground state of the adcluster. Sometimes, we have to describe several different electronic states along the reaction dynamics. The SAC (symmetry-adapted-cluster)/SAC-CI (configuration-interaction) method is a method for calculating effectively the correlated wave functions for ground, excited, ionized, and electron attached states and offers a convenient method for studying surface reactions.

The DAM has been applied to palladium-O_2 system and halogen chemisorptions on alkali metal surfaces. In the latter subject, interesting electron transfer processes such as harpooning, surface chemiluminescence and surface electron emission were successfully described by the DAM combined with the SAC/SAC-CI method. The same method was also applied to the O_2 chemisorption, molecular and dissociative, on a silver surface. Using the DAM, we could describe, for the first time, the chemisorption and the molecular and dissociative adsorptions of O_2 on a silver surface. The reaction of O_2 on a silver surface which is important in both science and industry is the partial oxidation of ethylene and propylene. Silver is a good catalyst for the epoxidation of ethylene but a very poor catalyst for the same reaction of propylene. We have clarified the active oxygen species of the reaction and the mechanism of the partial oxidation of ethylene. We have further clarified the reason why the same silver catalyst is poor for the epoxidation of propylene and leads to a complete oxidation. Concluding remarks are given in the final section.

Contents

Acronyms

AO	Atomic orbital	RHF	Restricted Hartree-Fock
CM	Cluster model	SAC	Symmetry adapted cluster
DAM	Dipped adcluster model	SAC-CI	Symmetry adapted cluster-configuratioin interaction
ECM	Embedded cluster model		
HF	Hartree-Fock	STM	Scanning tunneling microscope
MO	Molecular orbital	TS	Transition state
MP2	Second-order Møller-Plesset-perturbation theory	UHF	Unrestricted Hartree-Fock

1. Introduction

Chemistry and physics of surface-molecule interaction and reaction systems are of much interest from both purely scientific and industrial points of view. Since these interactions involve finite and infinite systems, modeling is necessary for theoretical studies of these systems. Further, since the result of the study is largely dependent upon the nature and the quality of the model adopted, we have to carefully examine the model for the surface-molecule interaction and reactions.

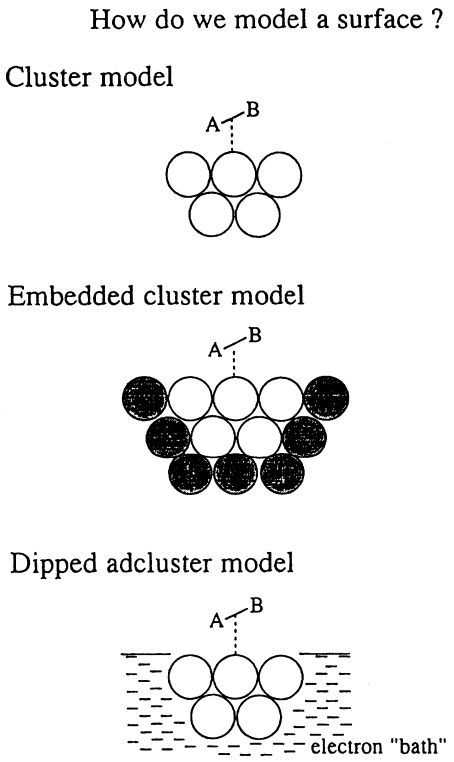

Fig. 1. Conceptual sketch of the cluster model (CM), embedded cluster model (ECM), and dipped adcluster model (DAM).

Figure 1 shows some existing models of the surface-molecule interacting system. *Cluster model* (CM) has been most frequently used by quantum chemists for investigating chemisorption and catalytic reactions on metal and metal-oxide surfaces. The reaction of a molecule with a model cluster is approximated as the reaction on a surface. The effects of the bulk solid are completely neglected in the CM. To include such an effect, Grimley, Pisani, and others developed the *embedded cluster model* (ECM) [1-4]. The cluster was embedded into a larger cluster illustrated by the filled-in atoms in Figure 1, and through the interaction with it, the effect of the bulk solid was incorporated. There are other embedding methods which were reviewed recently by Whitten and Yang [5].

Dipped adcluster model (DAM) has been proposed as a theoretical model for studying chemisorption and surface reactions involving electron transfer between an admolecule and a surface [6]. It was proposed since the conventional CM neglects the effect of a bulk metal. Figure 2 shows a conceptual sketch of the DAM. An *adcluster*, a combined system of an admolecule and a cluster, is

dipped into the electron *bath* of a solid metal and an equilibrium is established for electron and/or spin transfer between them. In the CM, all the electrons transferred into the admolecule must be supplied from the cluster, sometimes by sacrificing the chemical bonds within the cluster leading to an unphysical destabilization of the cluster, while in the DAM, some of the electrons are supplied from the electron bath of the bulk metal. Since the adcluster itself is a partial system of the surface-molecule interacting system, the number of electrons, n, transferred from (or to) the bulk metal can be a non-integer.

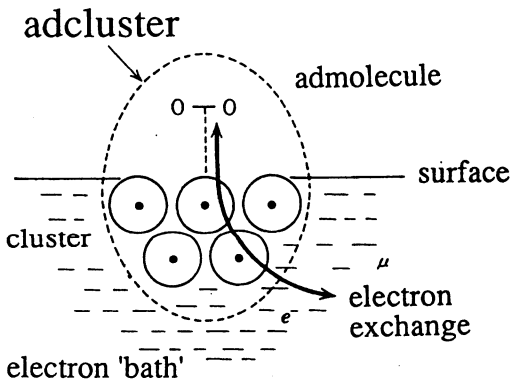

Fig. 2. Concept of the dipped adcluster model (DAM).

Chemisorption and surface catalytic reaction involve the formation and breaking of the chemical bond between admolecule and surface atoms. Since chemical force is a short-range force, mostly decaying exponentially as a function of a distance, the number of the metal atoms *directly* interacting with the admolecule is small. This is the *locality of the interaction* between admolecule and surface and this is why the most important chemical interaction involved in the surface-molecule interaction can be represented by a small number of surface atoms, justifying the CM and the DAM.

In the system the DAM is applied, the admolecule is usually charged and therefore, the electrostatic interaction between admolecule and surface should be important. On a metal surface, this force is approximated as *image* force, though it may overestimate the real such interaction. In the CM, this image force is neglected, but in the DAM, such force is taken into account as *image force correction* [7].

Now, having a rough image of the DAM, let us consider what aspects should be taken into account for studying surface reactions. We may summarize some important aspects as follows.

1. Locality of surface-molecule interaction.
2. Effect of bulk solid.
3. Electron and spin transfer between adsorbate and surface.
4. Surface magnetism.
5. Surface-adsorbate electrostatic interaction.
6. Role of surface dangling orbitals.
7. Two-dimensional coagulating field (two-dimensional liquid).

8. Importance of electron correlation.
9. Importance of several lower surface states (ground, excited, ionized, and electron-transferred states).
10. Roles of photons.
11. Effect of external electric and magnetic fields.
12. Surface geometrical structures and reconstructions.
13. Interaction between adsorbates (direct and indirect).
14. Effect of promoters.

First, what makes the surface chemically active seems to be the existence of the dangling bonds or orbitals on the surface. When a bulk metal is forced to be separated into two parts, a surface is generated, so that surface is essentially chemically active. There are a lot of broken bonds (dangling bonds) on the surface which promote chemisorption and catalytic reaction on the surface. They also cause a reorganization of the surface structure into a stable form. Bulk metal works like a storage of electrons and spins, and they are transferred from or to the admolecule through the dangling bond in the course of the surface reaction, thereby regulating the reaction barrier and realizing the catalytic cycle of reactions.

Surface provides a two-dimensional coagulating field by exerting two kinds of forces to the admolecules. One is the chemical force which is a short-range force and the other is the electrostatic force which is a long-range force. When a molecule approaches on a surface, the long-range force is first important, and then the short-range force. These forces work to coagulate molecules on a surface, increasing a chance of collisions like in a liquid phase. Generally speaking, the barriers for migrations of admolecules from site to site are smaller on metal surface than on metal oxide surface.

Interesting surface reactions very often take place on transition metal surfaces and on transition metal oxide surfaces. It is generally known that electron correlations are very important for describing the formation and breaking of the chemical bond involving metal atoms, especially, transition metal atoms. In particular, for studying the course and the mechanism of the catalytic reaction on a surface, we have to be able to calculate the energy of the system in a chemical accuracy, i.e., in kcal/mol. This is certainly a severe requirement very often conflicting with a hope to make our model cluster and adcluster as large as possible.

When we actually study surface reactions, the most interesting reaction is not necessarily the reaction of the ground state, but it is often the reaction of the lower excited state of the system. For example, oxygen exists on a metal surface in a variety of states, e.g., superoxide, peroxide, atomic, etc., and one may be a ground state at some situation and then the others are excited states. For studying the chemistry of oxygens adsorbed on a surface, we need a method which can describe both ground and excited states in the same chemical accuracy.

Surface photochemistry is a very interesting field of surface chemistry being developed quite rapidly in recent years. It deals with the dynamics of the electronic excited states of the surface-molecule interacting system, and there are many possibilities about where the initial excitation takes place. We have studied recently the photo-stimulated desorption of CO from the Pt surface [8]: we

have calculated the potential curves of many excited states of the surface-molecule interacting system and clarifed the mechanism of the photo-stimulated desorption. Further, in such a system, electron emission and photo-emission often take place. We, therefore, have to prepare a useful and reliable method which is able to describe both ground and excited states of the surface-adsorbate system.

External fields are often applied to the surface-molecule interacting system. When we study *scanning tunneling microscope* (STM) and surface manipulations, we actually deal with the tip-sample interaction in an external electric field [9-11]. Electrochemical reactions on an electrode may also be studied by a similar methodology. External magnetic field may also be important for studying spin alignment property on a surface.

Surface geometrical dependence of chemisorption and catalytic reaction is very well known. For example, oxygen chemisorption on a Ag surface differs between Ag(110) and Ag(111) surfaces [12]. Though only silver is effective for the partial oxidation of ethylene to ethylene oxide, the selectivity and activity differs between these surfaces. The activity for ethylene conversion to both partial and complete oxidation is higher on Ag(110) than on Ag(111), while the selectivity for ethylene oxide is lower on Ag(110) than on Ag(111) [12]. We think that this geometrical dependence is related with the stability of the superoxide species on a different surface. For studying such geometrical factors of the surface, we have to use relatively large clusters which can simulate the difference in the surface geometry.

This review is an exposition of the DAM concept and our studies on the surface reactions in which electron transfer between admolecule and surface is important. The DAM has been proven to be useful to study such surface reactions. When the amount of such electron transfer is small, the conventional CM is useful. For example, we have successfully studied hydrogen chemisorption on palladium [13] and platinum [14] and the hydrogenation reaction of acetylene on palladium surface [15]. The mechanism of the photo-stimulated desorption of CO on platinum was studied using the CM [8]. The CM was also useful to study the reactions on the metal oxide surfaces such as ZnO [16,17], ZrO_2 [18], and MgO [19], and to study the mechanism of GaAs epitaxial crystal growth [20]. We have also examined the ECM applying it to hydrogen chemisorption on lithium surface [4]. We refer to the review articles summarizing the studies on surface reactions performed in our laboratory [21-25].

2. Dipped Adcluster Model

We define *adcluster* as a combined system of a metal cluster and admolecule [6]. Figure 2 shows an illustration of this system. When this adcluster is dipped onto the electron *bath* of the solid metal, electron transfer would occur between them until the chemical potential of the adcluster becomes equal to the chemical potential of the solid surface, i.e., when

$$\frac{\partial E(n)}{\partial n} = -\mu \ , \tag{2.1}$$

where $E(n)$ is the energy of the adcluster with n being the number of electrons transferred from the solid into the adcluster and μ the chemical potential of the electrons of the metal surface. This electron flow is not between separated systems but between partial systems artificially divided, so that n is not necessarily an integer, but can be a non-integer. Since $E(n)$ is not necessarily a monotomic function of n, as shown in some examples, the equilibrium holds more generally

$$at\ the\ min[E(n)]\ in\ the\ range\ of\ \frac{\partial E(n)}{\partial n} \leq -\mu\ . \tag{2.2}$$

When a reverse flow of electrons is considered, n in the above equations should be replaced by $-n$.

For metals, Fermi levels and work functions are used for μ, and for semiconductors and insulators, the ionization potential Ip (or Ev), electron affinity Ea (or Ec), or the Mulliken's electronegativity $(1/2)(Ip + Ea)$ is used for μ, depending on the nature of the electron transfer under consideration. For some metals, the chemical potential corresponding to the density of active state may be used. The effects of promoters, cocatalysts, and supports are taken into account through the variations in the chemical potential μ, as well as the effects of the external electric field [9] which may be important in the study of STM [10,11].

In the dipped adcluster model, the cluster atoms need not supply all the electrons transferred into the admolecule: some are supplied from the electron bath of the solid metal. The metal atoms of the adcluster play not only as an interaction counterpart of the admolecule, which is chemically very specific, but also as a passage of electrons and spins. The charge polarization locally produced in this way is very important, since it is an origin of the image force.

A. Behavior of $E(n)$ curve and implications

Let us consider the general behaviors of the energy $E(n)$ of the dipped adcluster as a function of the number of electrons transferred into the adcluster, n, and the implications of the equilibrium conditions given by (2.1) and (2.2). Generally speaking, $E(n)$ is a continuous function of n, but its derivative is not necessarily continuous at n being an integer. Figure 3 shows several different behaviors of the $E(n)$ curve. The *lhs* figures show lower convex, and the *rhs* ones upper convex. In case A, the condition given by (1) is realized at $n = n_0$, but in cases B and C, it is not realized.

We discuss first the $E(n)$ curves given by case A, since they show two very important patterns of electron transfer. When the $E(n)$ curve is a lower convex (case A-1), the system initially at $n = 0$ and $E = E(0)$ carries out electron flow and the equilibrium is established at $n = n_0$ and $E = E(n_0)$. Namely, n_0 electrons flow into the adcluster and it is stabilized to $E(n_0)$. Note that n_0 is usually a non-integer and that $E(n_0)$ is higher than the minimum of the $E(n)$ curve, since the condition given by (2.1) is not a variational-type condition.

On the other hand, when the $E(n)$ curve is an upper convex (case A-2), there is a barrier, initially, for the electron flow from n=0 to n=n_0: electron flow would not occur until n_0 electrons *sink* into the adcluster through, say, tunneling or activation, and at n=n_0 it looks down a deep valley, so that afterwards, electrons flow into the adcluster up to n=i, as (2.2) indicates, with i being an integer. At n=i, the system is most stable, and when n exceeds i, the gradient suddenly becomes very high (even positive), so that the electron flow ceases at n=i. The energy of the system is $E(i)$. It is interesting to note that in this case, a transfer of an *integral* number of electrons naturally results from the shape of the potential curve, so that case A-2 is in some sense *quantum*. We further note that the *tunneling* in this case is not the tunneling in the coordinate space, but in the space of n. We will actually see the occurrence of such a tunneling in the harpooning of electron in the halogen chemisorption on an alkali metal surface [26] as explained in § 5.

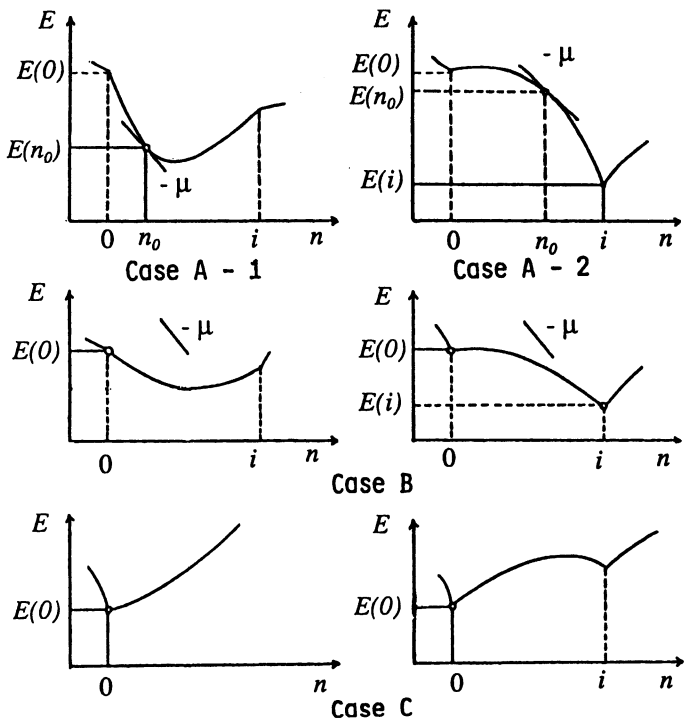

Fig. 3. Some typical behaviours of the $E(n)$ curve as a function of n, the number of electrons transferred into the adcluster. On the horizontal axis, i denotes an integer number of electrons. The gradient μ is the chemical potential of the metal surface.

It is now clear that whether the number of electrons transferred from the bulk metal to the adcluster is integer or non-integer depends on the upper or lower convex natures, respectively, of the $E(n)$ curve. We will see in the next section from the molecular orbital model of the dipped adcluster that this upper and lower natures are reflected from the spin properties of the chemisorptions.

Let us return back again to Figure 3. In case B, there is a region of n where $E(n)$ is lower than $E(0)$, but the gradient is always smaller than μ. Referring to (2.1) and (2.2), we see that the electron

flow does not occur in this case, since the potential of the metal is always lower than that of the adcluster. However, when the chemical potential of the metal is modified by an addition of promoters, raising temperature, applying electric field, exposing it to light, etc., the electron flow may be able to be realized. Such a device is important for catalyst design.

In case C, *E(0)* is most stable in some wide region of *n*. In this case, electron transfer can not be expected, and the isolated adcluster model, which is the conventional cluster model, would be appropriate, as far as the image force correction is small.

We note that the above pattern of the *E(n)* curve is not an intrinsic property of the admolecule-solid pair, but a property depending on the distance, geometry, etc., and other external conditions as described above. In particular, when an electric potential is applied between an admolecule and a solid [9], as in STM [10,11], the electron flow would be facilitated and regulated. In the above considerations, an electron flow from the bulk metal to the adcluster was implicitly assumed. The reverse flow is realized simply by changing *n* to *-n*.

B. Molecular orbital model of dipped adcluster

We here explain a molecular orbital (MO) model of the dipped adcluster for calculating the energy *E(n)* and the electronic structure of the adcluster. We assume that the adcluster exchanges electrons and spins with the solid through its HOMO (highest occupied MO), LUMO (lowest unoccupied MO), SOMO (singly occupied MO), or some other active MO, with the other MOs being doubly occupied or completely unoccupied. Such active MO is denoted by *m*. Two different extreme ways of occupations of electron spins in the active MO are assumed. One is called *highest-spin coupling*, in which the active MO is first occupied by α spin electron and after its occupation becomes equal to unity, it is then occupied by β spin electron. In this case, the adcluster is paramagnetic and the surface is ferromagnetic or antiferromagnetic. The other is *paired-spin coupling* in which the same amounts of α and β spin electrons occupy the active MO. Here, the adcluster is always diamagnetic.

We calculate the energy of the adcluster in which *x* electrons occupy the active MO denoted by *m*. This *x* is proportional to the number of the transferred electron, *n*, in the preceding section. First we assume that this active MO is nondegenerate. Then, the electronic energy of the adcluster is written as

$$E^{(0)} = 2\sum_{k} H_k + \sum_{k,l}(2J_{kl} - K_{kl}) + x\sum_{k}(2J_{km} - K_{km}) + xH_m + Q, \qquad (2.3)$$

where *k*, *l* run over the doubly occupied MO's. H_k, J_{kl}, and K_{kl} denote core-Hamiltonian integral, Coulomb repulsion integral, and exchange repulsion integral, respectively. The superscript (0) on the energy *E* means that this energy is due to the interactions only within the adcluster. The quantity *Q* represents the electron repulsion within the active orbital *m* and depends on the way of the spin and electron accommodation in the active orbital *m*. It is given by

$$Q = (x/2)^2 J_{mm} \tag{2.4}$$

for the paired-spin coupling and by

$$Q = \|x\text{-}1\| J_{mm} \tag{2.5}$$

for the highest-spin coupling. Here, $\|a\| = 0$ if $a < 0$, $\|a\| = a$ if $0 < a < 1$, and $\|a\| = 1$ if $a > 1$. It is easy to prove that Q is minimum for the highest-spin coupling and maximum for the paired-spin coupling. Therefore, the energy of the adcluster is lower in the highest-spin coupling than in the paired-spin coupling. The actual preference of the spin coupling would also depend on the nature of the solid and the nature of the interaction between the adcluster and the solid. Further, an intermediate spin coupling is also possible, because these two spin couplings are just two-extreme cases. For example, when some amount of α spin is transferred from the solid metal to the adcluster (highest-spin coupling), the adcluster is spin polarized and locally paramagnetic.

Let us now calculate the chemical potential of the adcluster by differentiating $E(x)$ with x. Neglecting the change of the MOs due to the change in x, we get

$$\frac{\partial E^{(0)}}{\partial x} = \varepsilon_m + \frac{\partial Q}{\partial x}, \tag{2.6}$$

where ε_m is the orbital energy of the active orbital m,

$$\varepsilon_m = H_m + \sum_k (2J_{km} - K_{km}), \tag{2.7}$$

and the last term of (2.6) is calculated in the highest-spin coupling case as

$$\begin{aligned} \frac{\partial Q}{\partial x} &= x, & x \le 1, \\ &= J_{mm}, & 1 < x \le 2, \end{aligned} \tag{2.8}$$

and in the paired-spin coupling case as

$$\frac{\partial Q}{\partial x} = \frac{1}{2} x J_{mm} \tag{2.9}$$

for all the range of x. At x=0 and x=2, both spin-couplings give

$$\left(\frac{\partial E^{(0)}}{\partial x} \right)_{x=0} = \varepsilon_m , \tag{2.10}$$

$$\left(\frac{\partial E^{(0)}}{\partial x} \right)_{x=2} = \varepsilon_m + J_{mm} . \tag{2.11}$$

Figure 4 shows the $E(x)$ curve roughly estimated from the above results, (2.6)-(2.11). The real lines correspond to the case when the relaxation of the orbitals with the change of x is neglected, while

the broken line shows when such effect is included. An important deduction from this figure is that the upper convex $E(x)$ curve is associated with the highest-spin coupling and the lower convex curve with the paired-spin coupling. Reminding that the integer and non-integer number of electrons are transferred in the upper-convex and lower-convex cases, respectively, we can predict that an integer electron transfer tends to occur in the highest-spin coupling case, while non-integer electron transfer in the paired-spin coupling case. It is interesting that the *surface magnetism* is thus connected with the manner of the spin-coupling in the active orbital of the adcluster.

In the above formulation, the effect of the electrostatic force, like image force, due to the bulk solid is neglected. This effect will be discussed in detail in § 2C. When the surface-molecule interacting system is neutral in a separated limit, the energy tends to be stabilized as x increase, since the electrostatic interaction between the admolecule and surface would increase as the admolecule is more and more changed as x increase. This effect increases the upper convex component of the curve.

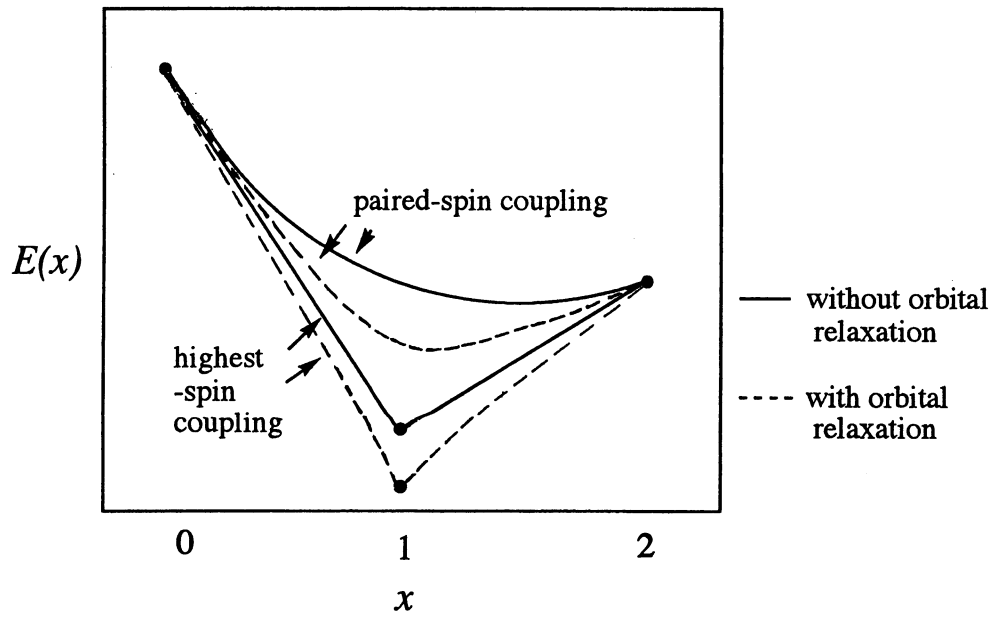

Fig. 4. $E(n)$ curves for the non-degenerate active orbital

When the active orbital is twofold degenerate, m and n, the energy of the dipped adcluster is calculated as

$$E^{(0)} = 2\sum_{k} H_k + \sum_{k,l}(2J_{kl} - K_{kl}) + \frac{x}{2}\sum_{k}\sum_{m}(2J_{km} - K_{km}) + \frac{x}{2}(H_m + H_n) + Q, \tag{2.12}$$

where $Q$is written as

$$Q = \left(\frac{x}{4}\right)^2 \sum_{m,n}(2J_{mn} - K_{mn}), \tag{2.13}$$

for the paired-spin coupling.

In the highest-spin coupling case, two different ways of accommodation may be considered. Figure 5 gives an illustrative explanation of the two different accommodations. In type I case, α-spin electron is first accommodated in one of the degenerate orbital, and after its occupation becomes unity, next α-spin electron is accommodated in the other degenerate MO until its occupation becomes unity. In this process, the roles of the MOs m and n are always symmetrized to keep the degeneracy. Then, β-spin electron is added to one of the degenerate MOs until its occupation becomes two and then another β-spin electron is added to the other MO until its occupation becomes two: then the two degenerated orbitals are fully occupied. In this type I case, the repulsion term Q is given as

$$Q_I = \|x - 1\|(J_{mn} - K_{mn}) + \|x - 2\|J_{mn} + \|x - 3\|(2J_{mn} - K_{mn}) + \|\frac{1}{2}(x-2)\|(J_{mm} + J_{nn}) . \quad (2.14)$$

In type II case, two degenerate MOs accommodate equal number of electrons in the same way, so that the repulsion term Q is written as

$$Q_{II} = \|\frac{x}{2}\|^2(J_{mn} - K_{mn}) + \|\frac{1}{2}(x-2)\|^2(J_{mn} - K_{mn}) + \|x - 2\|(J_{mn} + \frac{1}{2}J_{mm} + \frac{1}{2}J_{nn}) . \quad (2.15)$$

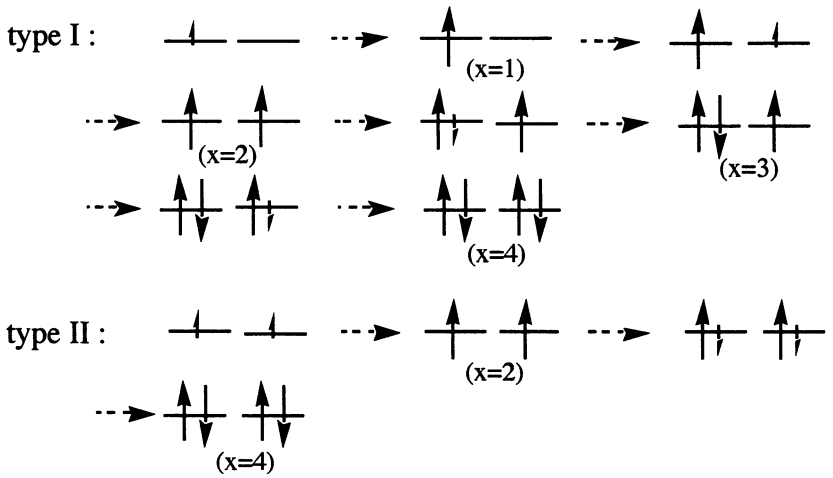

Fig. 5. Two different accomodation schemes in the two-fold degenerate active orbitals in the highest-spin coupling case.

The eigenvalue of the S_z operator is the same between type I and type II: they are equally paramagnetic. Note that the repulsion energy Q is largest in the paired-spin coupling, then type II of the highest spin coupling, and then type I of the highest-spin coupling. The stability of the adcluster is in the reverse order. We further note that types I and II have the same energy at x=0, 2, and 4. In ref.6, we gave only type I case of the highest-spin coupling.

The chemical potential of the adcluster in the case of the two-fold degenerate active orbitals is calculated as

$$\frac{\partial E^{(0)}}{\partial x} = \frac{1}{2}(H_m + H_n) + \frac{1}{2}\sum_k \sum_m (2J_{km} - K_{km}) + \frac{\partial Q}{\partial x}\ , \tag{2.16}$$

where we again neglected the orbital reorganization effect due to the change in x, since the purpose here is not a quantitative calculation but to get a rough idea. The last term of (2.16) is given in the paired-spin coupling case as

$$\frac{\partial Q}{\partial x} = \frac{1}{8}x(2J_{mn} - K_{mn})\ . \tag{2.17}$$

while in type I of the highest-spin coupling case, it is given by

$$\begin{aligned} \frac{\partial Q_I}{\partial x} &= 0, && 0 \le x \le 1, \\ &= J_{mn} - K_{mn}, && 1 < x \le 2, \\ &= J_{mn} + \frac{1}{2}(J_{mm} + J_{nn}), && 2 < x \le 3, \\ &= (2J_{mn} - K_{mn}) + \frac{1}{2}(J_{mm} + J_{nn}), && 3 < x \le 4, \end{aligned} \tag{2.18}$$

and in type II case, it is given by

$$\begin{aligned} \frac{\partial Q_{II}}{\partial x} &= \frac{1}{2}x(J_{mn} - K_{mn}), && 0 \le x \le 2, \\ &= \frac{1}{2}x(J_{mn} - K_{mn}) + K_{mn} + \frac{1}{2}(J_{mm} + J_{nn}), && 2 \le x \le 4, \end{aligned} \tag{2.19}$$

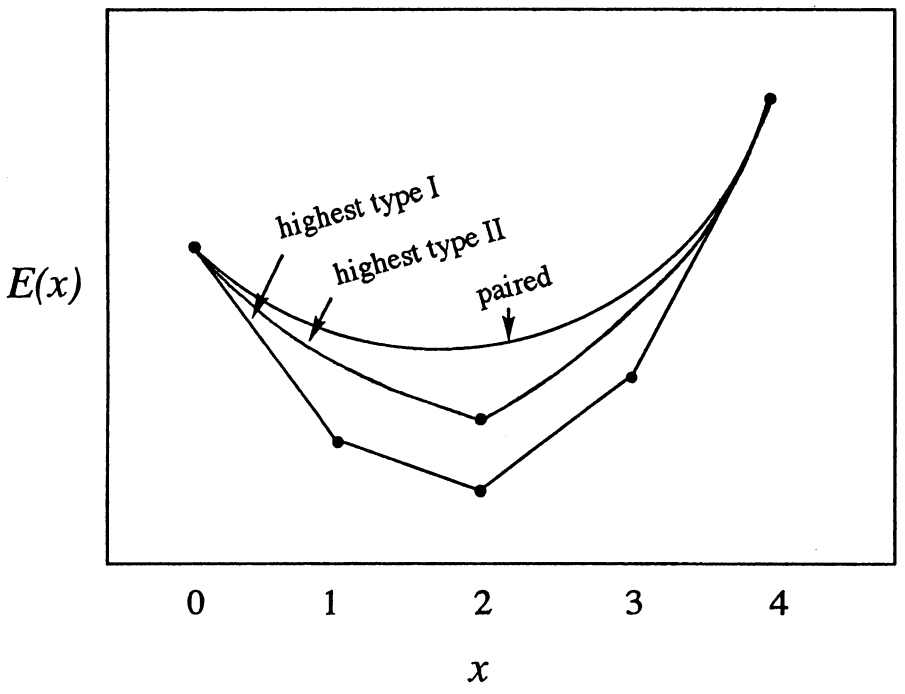

Fig. 6. $E(x)$ curves for the two-fold degenerate active orbitals.

Figure 6 shows a schematic picture of the $E(n)$ curve drawn based on the information given by (2.16)-(2.19). The curves are drawn neglecting the relaxation of the orbitals. We expect from this figure that the non-integer electron transfer is possible in the paried-spin coupling case and in type II of the highest-spin coupling case, while the integer electron transfer would occur in type I of the highest-spin coupling case. When the orbital relaxation effect is taken into account, an upper convex nature increases in all cases. Further, when the system is neutral in a separated limit, the electrostatic effect due to the bulk solid would also work to increase the upper convex nature.

When n electrons flow from the solid into the adcluster, positive n holes would be created in the solid near the adcluster. On the surface of insulators, these holes would be localized near the adcluster, and since the electrostatic interaction between the electrons on the admolecule and the holes in the solid stabilizes the system, the holes in the solid would not be easily neutralized. When the solid is a good conductor like a metal, this electrostatic interaction would be represented by the image force. Denoting such electrostatic term as $E^{(1)}$, the energy of the adcluster is written as

$$E = E^{(0)} + E^{(1)} . \tag{2.20}$$

The detailed forms of the electrostatic term $E^{(1)}$ would be discussed in the next section.

We note that the geometry of the solid surface, such as (111) and (100) planes and a step, kink, terrace, etc., is described by the structure of the cluster part of the adcluster and by the functional form of $E^{(1)}$. $E^{(0)}$ includes both of the short-range and long-range forces, but $E^{(1)}$ is a long-range force. Because of the long-range nature of the Coulombic interaction, the electrostatic energy $E^{(1)}$ is insensitive to the detailed chemical structure of the adcluster.

The energy and the orbitals of the dipped adcluster are calculated using the conventional open-shell *restricted Hartree-Fock* (RHF) program. The energy of the open-shell RHF method is written as [27]

$$E = \sum_k \lambda_k H_k + \frac{1}{2}\sum_k \sum_l \lambda_k \lambda_l (\alpha_{kl} J_{kl} - \beta_{kl} K_{kl}) . \tag{2.21}$$

By a comparison betwee (2.21) and (2.3) or (2.12), the occupation parameters λ and the spin coupling parameters α and β in (2.21) are fixed. So, performing the RHF MO SCF calculations involving nonintegral occupation number x for the active orbitals, we obtain the molecular orbitals and the energy $E(x)$ of the adcluster.

The molecular orbital model of the dipped adcluster given above may be viewed in a different way, as described in the Appendix of ref. 6. Namely, the molecular orbitals of the dipped adcluster under the electrostatic influence of the surrounding solid atoms are obtained from the MO formalism for the total (adcluster plus solid) system with the zero-differential overlap and zero bond order approximations between the AO's belonging to the adcluster and the surrounding solid. In this approximation, the Fock matrix of the total system is written in a block-diagonal form of the Fock matrices of the adcluster and the solid. The same is true for the overlap matrix. Therefore, the adcluster

and the solid system are separately solved, mutually giving electrostatic influences. The number of the electrons of each system need not be an integer, though the sum of them should be an integer, which is possible when a number of degenerate orbitals exist between the adcluster and the solid system. This is possible since our total system is an infinite system.

C. Electrostatic interaction between adcluster and solid

The electrostatic term $E^{(1)}$ is different depending on whether the solid is metal (conductor) or insulator. Semiconductor has a nature median of these two.

When we deal with a metal surface, the so-called *image force* would represent well the electrostatic term $E^{(1)}$. When an adatom A at the position $\boldsymbol{a}$ has a charge q, it induces an opposite charge on a metal surface. At point $\boldsymbol{x}$ (x, y, 0) of the surface, the induced charge density is given by [28]

$$\sigma(\boldsymbol{x}) = -\frac{q|\boldsymbol{a}-\boldsymbol{a}'|}{4\pi|\boldsymbol{a}-\boldsymbol{x}|^3}, \tag{2.22}$$

where $\boldsymbol{a}'$ is the positional vector of the mirror image of the adatom A. The electrostatic interaction between the charge q and the hole $\sigma(\boldsymbol{x})$ sums up to the well-known image force given by

$$\mathbf{F}_{if} = \int\int_{xy}^{surface} \frac{\sigma(\boldsymbol{x})q}{|\boldsymbol{a}-\boldsymbol{x}|^3}(\boldsymbol{a}-\boldsymbol{x})dxdy = \frac{q^2(\boldsymbol{a}'-\boldsymbol{a})}{|\boldsymbol{a}-\boldsymbol{a}'|^3}, \tag{2.23}$$

and the stabilization energy is given by

$$E_{if} = \int\int_{xy}^{surface} \frac{\sigma(\boldsymbol{x})q}{2|\boldsymbol{a}-\boldsymbol{x}|}dxdy = -\frac{q^2}{2|\boldsymbol{a}'-\boldsymbol{a}|}, \tag{2.24}$$

where the factor 2 in the denominator is due to the integration over the half space.

When the energy $E^{(0)}$ of the adcluster is calculated by an *ab initio* MO method, the electrostatic interaction within the adcluster is already included. Therefore, the electrostatic term $E^{(1)}$ is estimated, as illustrated in Figure 7, by integrating the electrostatic interaction between the charge q and the hole $\sigma(\boldsymbol{x})$ at the point $\boldsymbol{x}$ outside the cluster region of the surface. In practice, the energy $E^{(1)}$ is calculated by subtracting from E_{if} the electrostatic energy (E_{in}) for $\sigma(\boldsymbol{x})$ inside the cluster region, that is,

$$E^{(1)} = E_{if} - E_{in}. \tag{2.25}$$

As sketched in Figure 7, the cluster region of the surface is estimated by the Van der Waals radius of the metal atom, and the Mulliken's atomic charge is used for q.

When we have to consider several charges q_i on the atoms A_i of an admolecule, the charge density $\sigma(\boldsymbol{x})$ induced on the surface is given by

$$\sigma(x) = \sum_i \sigma_i(x) = -\sum_i \frac{q_i |a_i - a_i'|}{4\pi |a_i - x|^3}, \tag{2.26}$$

where a_i is the positional vector of the atom A_i and a_i' that of the mirror image. The image force acting on the atom A_i is given by

$$\mathbf{F}_{if,i} = \sum_j \frac{q_i q_j (a_j' - a_i)}{|a_i - a_j'|^3}, \tag{2.27}$$

and the total image force energy by

$$E_{if} = -\sum_i \sum_j \frac{q_i q_j}{2|a_i - a_j'|}, \tag{2.28}$$

The electrostatic term $E^{(1)}$ is calculated similarly by (2.25).

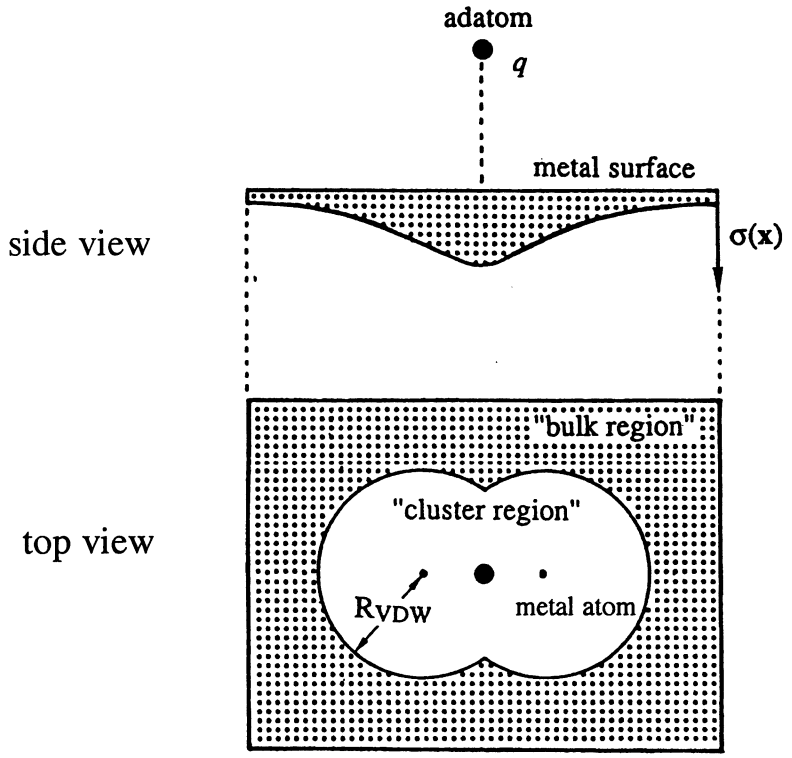

Fig. 7. Schematic representation of the adatom and the induced charge density on the surface. Cluster region is estimated using the van der Waals radius of the metal atom.

The estimation of the electrostatic energy may be done before or after MO calculations. In principle, the effect should be included before MO calculation because then, we can include the relaxation of the electron cloud of the adcluster in the electrostatic field of the surface. Since q_i and $\sigma(x)$ depends on each other, the calculations should be done iteratively. We have shown in ref. [6] that these two methods give similar results, though the iterative method usually overestimates the $E^{(1)}$ term.

When we deal with a semi-conductor surface for which more localized electrostatic term is

desirable, we may use the expression

$$E^{(1)} = \sum_A \sum_R g_A g_R / R_{AR} + \sum_{R>S} g_R g_S / R_{RS} \quad , \tag{2.29}$$

where A runs over the atoms of the adcluster, R, S over the solid atoms. g_A is the gross charge of atom A of the adcluster. g_R is the gross charge of atom R and may be calculated as n/M where n is the number of the transferred electrons and M the number of the solid atoms over which n holes are distributed.

We note that the image force correction can be used even for n=0, but the correction based on (2.29) vanishes when n=0.

D. Brief remark

Here, we have explained the dipped adcluster model (DAM) for the study of chemisorption and catalytic reactions on a metal surface which involve a large electron transfer between admolecule and surface. The size of the cluster necessary for investigating such electronic processes would be reduced if the dipped adcluster model is adopted instead of the conventional cluster model. This merit is practically very important since electron correlations are often very important, and further since sometimes the catalytically active state is not necessarily the ground state but an excited state of the surface cluster. Therefore, sometimes we have to use an advanced electronic theory for the calculations, so that we have to make the size of the cluster as small as possible. Although we have restricted the present formulation only within the molecular orbital model, the inclusion of electron correlation is necessary. Further, it is interesting to investigate the effect of the cluster size on the dipped adcluster model. If the size is large enough to be able to describe the real surface, the dipped adcluster model would, in principle, become unnecessary. But, how large is such size is an interesting question which must be investigated in future.

3. SAC/SAC-CI Method

Electron correlations are sometimes very important for the surface phenomena. In particular, when the surface is a transition metal, the Hartree-Fock model is insufficient for describing the bonding between an admolecule and the surface. Furthermore, the catalytically active states are sometimes the excited states of the adcluster [14]. Therefore, we need a theory which can describe both ground and excited states in a same accuracy. The SAC (symmetry-adapted-cluster) / SAC-CI (configuration interaction) theory is such a theory.

The SAC theory [29] provides a method for calculating the ground state and the SAC-CI method [30-32] is the method for calculating correlated wave functions for excited, ionized, and electron attached states. The SAC/SAC-CI wave functions satisfy the correct relations among these states and are based on the approximate transferability of electron correlations among these states. It is more rapidly convergent than ordinary CI expansion and furthermore it gives directly comparable results for

the energies and the wave functions of many different states, different in energy and in the number of electrons. The theoretical simplicity, reliability, and usefulness have been shown in many publications in molecular spectroscopy [33] and excited state chemistry [8,34]. We believe that the method is simple and accurate enough to be useful. Since I have recently written review articles of the SAC/SAC-CI method [35,36], the details are not given here. The SAC/SAC-CI code [37] is available from the author on request.

4. Palladium-O_2 System

The first subject the DAM was applied was the chemisorption of O_2 on a palladium surface [6,7]. We approximated the surface by a single Pd atom and O_2 was approached vertically on top of the atom. A linear Pd-O-O system was taken as an adcluster and the Pd atom was dipped onto the electron bath of the palladium. Both of the highest-spin coupling and the paired-spin coupling were applied. The electrostatic interaction was calculated by the image force correction.

A. Highest-spin coupling

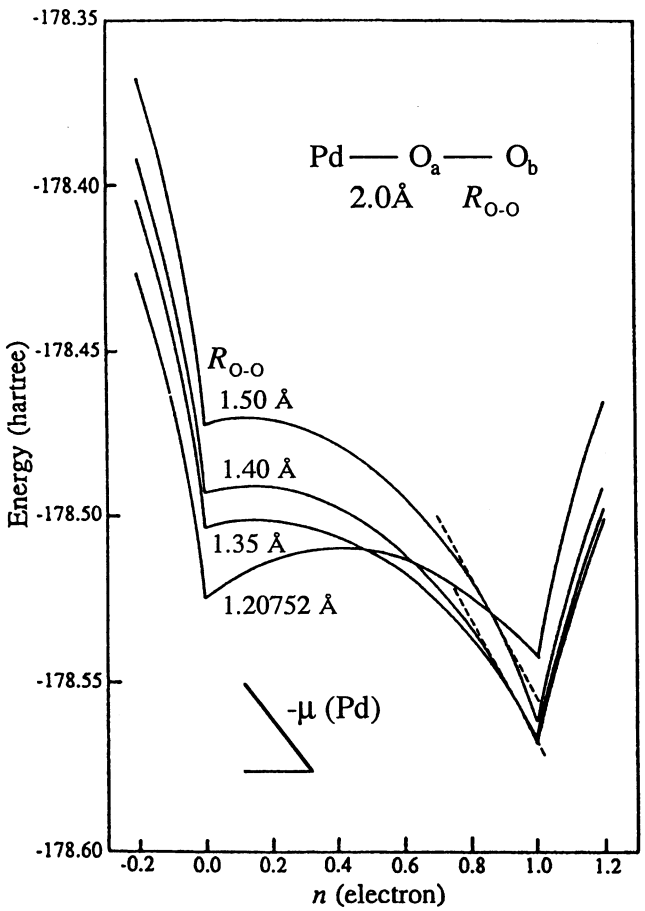

Fig. 8. *E(n)* curves of the Pd-O_a-O_b system in the highest-spin coupling model for the O-O distances of 1.20752, 1.35, 1.40, and 1.50Å and the Pd-O_a distance fixed at 2.00Å .

The $E(n)$ curves of the system calculated by the highest-spin coupling model for different O-O distances(R_{OO}) are shown in Figure 8. The curves are upper convex and the curvature is discontinuous at n=0.0 and 1.0. At n=0.0, R_{OO} =R_{eq} (equilibrium distance 1.20752 Å) [38] is most stable, but at n=1.0, R_{OO}=1.4 Å is most stable. When R_{OO} is fixed to R_{eq}, the tangent of the $E(n)$ curve is too small to become equal with -μ, where μ is the chemical potential of the palladium surface, 5.12 eV [39]. However, when R_{OO} is relaxed, the $E(n)$ curve is stabilized at large n and longer R_{OO} region, so that the tangent can exceed the chemical potential μ. Therefore, as discussed in Figure 3, case A-2, one electron flows from the metal into the adcluster, after some barrier.

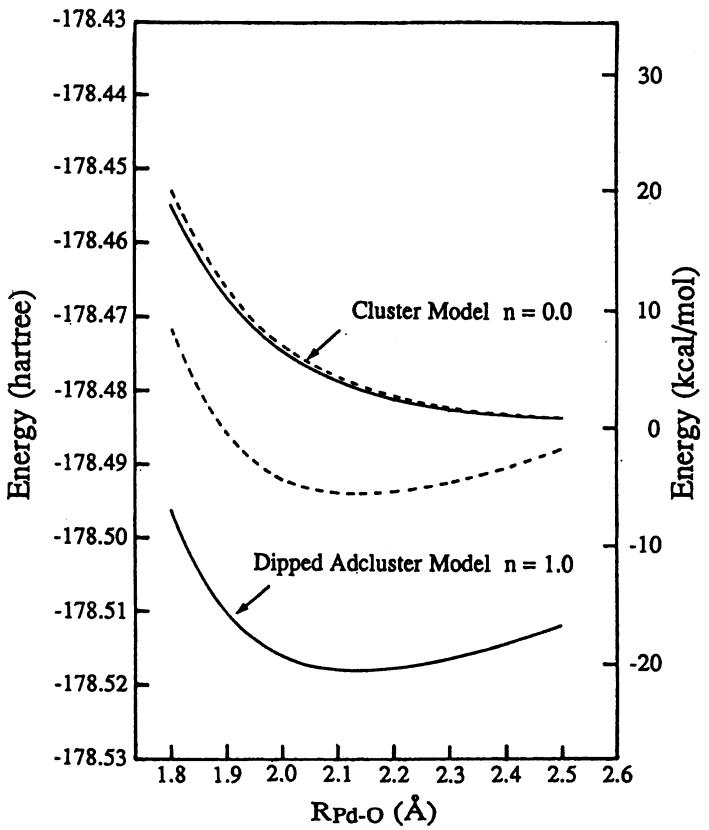

Fig. 9. Potential energy curves for the end-on approach of the O_2 molecule onto palladium calculated by the highest-spin coupling. The O-O length was fixed at 1.20752Å (equilibrium length of the free O_2) for the upper one and at 1.35 Å for the lower one. Broken and solid lines are calculated, respectively, without and with the image force correction $E^{(1)}$. The upper broken line with n=0.0 corresponds to the cluster model. The energy scale on the right-hand side is in kcal/mol relative to the free Pd plus O_2 system.

Figure 9 shows the potential energy curve for the end-on approach of the O_2 molecule to the palladium surface. The broken lines are for $E^{(0)}$ alone and the solid lines for $E^{(0)}$+$E^{(1)}$. The broken and solid curves for n=0.0 nearly overlap each other, since the electrostatic term is very small. The broken curve for n=0.0 corresponds to the cluster model. The potential curve of the cluster model is repulsive at any distance, so that the cluster model indicates that the O_2 molecule is not adsorbed on the Pd surface in contrary to the experiment. On the other hand, when the electron transfer from the bulk metal

to the adcluster is admitted, the system becomes stable as O_2 approaches Pd, and the chemisorption occurs in agreement with the experiment. Furthermore, the image force is important for stabilizing the system, though it is overstimated because the adcluster size is too small in this example.

The equilibrium Pd-O length and the Pd-O stretching frequency of the adsorbed state are calculated to be 2.15 and 338 cm^{-1}, respectively. The experimental frequency is 485 cm^{-1} for the O_2 molecule on a Pt(111) surface [40]. The equilibrium O-O length is calculated to be 1.22 and 1.40 Å for the free and adsorbed states, respectively. The experimental value for the former is 1.20752 Å [38]. The NEXAFS measurement for the superoxide on the Pt(111) surface has given the O-O bond length of 1.32±0.05 Å [41], which is shorter than our highest spin coupling result. The O-O vibrational frequencies are calculated to be 1707 and 1272 cm^{-1} for the free and adsorbed states, respectively, in comparison with the experimental values of 1580 [38] and 1035 [42] cm^{-1}, respectively. As is well known, the Hartree-Fock model overestimates the vibrational frequency. The adsorption energy is calculated to be 21.9 and 6.4 kcal/mol, respectively, with and without including the image force correction. The molecular adsorption energy observed by the *temperature programmed desorption* (TPD) experiment [43-46] is 7.5~12.3 kcal/mol.

It is noted that the cluster model using one Pd atom fails to describe the end-on adsorption of an O_2 molecule. This failure is mainly due to the limitation of the cluster model. Namely, all the electrons transferred to O_2 must be supplied from the cluster. A larger-size cluster must be used for describing within the cluster model. Then, how large should the size of the cluster be? For example, Upton *et al.* used Ag_{24} cluster for studying O_2 chemisorption on an Ag surface by the GVB and GVB-CI methods [47]. Geometric and spectroscopic parameters were calculated in good agreement with the available experimental data. However, the adsorption energy relative to the ground state of the cluster and O_2 was calculated to be *negative*, -14.8 kcal/mol. On the other hand, the DAM has been able to give reasonable positive adsorption energies for the O_2 adsorptions on an Ag surface with the use of the Ag-O_2, Ag_2-O_2 and Ag_4-O_2 adclusters [48-50]. The geometric and spectroscopic properties calculated by the DAM have also excellently reproduced the observed values.

TABLE 1. Energy (a.u.) and atimic charge of the Pd-O_a-O_b system[a]

R_{OO}	n=0.0						n=1.0					
(Å)	$E^{(0)}$	$E^{(1)}$	Pd	O_a	O_b	O_a+O_b	$E^{(0)}$	$E^{(1)}$	Pd	O_a	O_b	O_a+O_b
1.20752	-178.47428	-0.00037	+0.093	-0.120	+0.027	-0.093	-178.46929	-0.02278	-0.218	-0.479	-0.303	-0.782
1.35	-178.45172	-0.00112	+0.169	-0.140	-0.029	-0.169	-178.49180	-0.02440	-0.193	-0.555	-0.252	-0.807
1.50	-178.41973	-0.00226	+0.262	-0.064	-0.198	-0.262	-178.48611	-0.02540	-0.172	-0.563	-0.265	-0.828

[a] Pd-O_a length is 2.0 Å.

When one electron is transferred to the adcluster, it is mostly distributed into the O_2 molecule. Table 1 shows the atomic charge of the PdO_2 system. When n=1.0, about 0.56 electron lies on O_a, 0.25 electron on O_b, and 0.19 electron on the Pd atom: the inside oxygen O_a is more negatively charged

than the outside one O_b. Such polarization of O_2 on an Ag surface was also reported by Broomfield *et al.* [51], and Nakatsuji *et al.* [48-50]. When n is fixed to zero, the negative charge of the O_2 molecule is donated only by th Pd atom, so that the amount of the electron transfer is limited and the Pd atom becomes very positively charged. In the DAM, such electrons are supplied by the electron bath of the solid metal.

It is interesting to note that on palladium, the O_2 molecule is as if it breathes the electron gas; viz., when the O-O distance is elongated, the electron enters into the O_2 region and vice versa. This implies that the intensity of the IR vibrational peaks of O_2 should be larger on a metal surface than in a gas phase. There is an experimental observation supporting this result as surface enhanced IR spectroscopy [52].

Figure 10 illustrates the frontier orbital map, which is related to the reactivity of the adsorbed oxygen species. It consists mainly of the π^* orbital of O_2 and partly the $4d_{xz}$ (or $4d_{yz}$) orbital of Pd. In contrast to the charge distribution, the frontier orbital is larger at O_b than at O_a, which indicates that the former is more reactive than the latter.

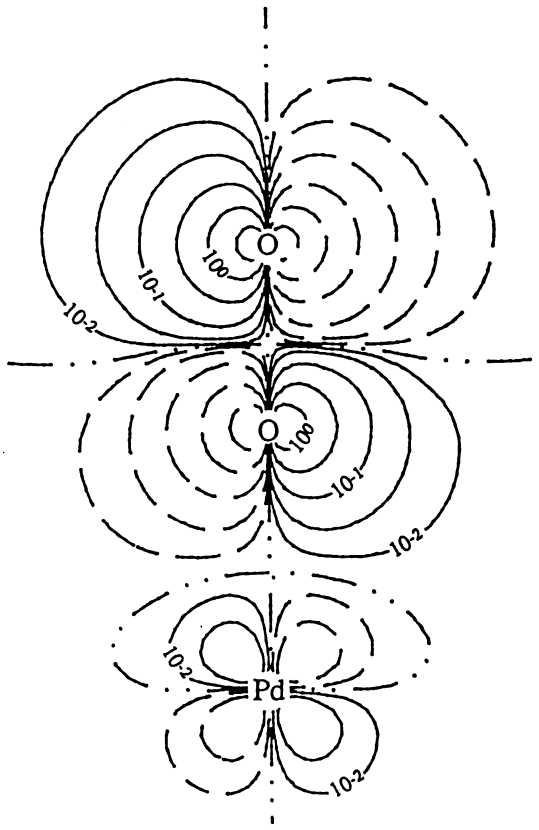

Fig. 10. Contour map of the frontier orbital of the PdO_2 adcluster with n=1.0. The Pd-O distance is 2.00 Å and the O-O distance is 1.40 Å. Solid and broken lines correspond to plus and minus signs in the MO and the double dotted line shows the node of the MO. The contours values are $10^{0.5}$, 10^{0}, $10^{-0.5}$, 10^{-1}, $10^{-1.5}$, and 10^{-2}.

In Table 2, we summarize the influence of the electrostatic term $E^{(1)}$ on the adsorption energy and the geometric and spectroscopic parameters of the PdO_2 system. The electrostatic interaction is important for stabilizing the adsorbed O_2 as mentioned before. On the other hand, the bond lengths and

force constants calculated with and without $E^{(1)}$ are very similar. This is because the image force is a long-range force which depends on 1/r, and the chemical bondings in O-O and Pd-O are mainly described by the short-range forces which depend exponentially like two-center overlap integrals. Thus, the electrostatic term $E^{(1)}$ is an important interaction, but influences to a less extent to the geometric and spectroscopic parameters of the adsorbed molecules. This is in fact our general experience; viz., the chemical difference is described by $E^{(0)}$ rather than $E^{(1)}$.

In the calculations above, we included the electrostatic effect $E^{(1)}$ after the SCF calculation. However, a better method is to include it in the SCF process. We examined the difference of these two procedures for this system and found that it was very small [6].

TABLE 2. The adsorption energy, geometry, and vibrational frequency calculated from the PdO_2 adcluster in the highest spin coupling model.

	Adsorption energy[a] (kcal/mol)	Bond length (Å)		Vibrational frequency (cm^{-1})	
		$R_{Pd\text{-}O}$	$R_{O\text{-}O}$	$\omega_{Pd\text{-}O}$[b]	$\omega_{O\text{-}O}$
$E^{(0)}$ alnoe	6.4	2.15	1.39	329	1229
$E^{(0)}+E^{(1)}$	21.9	2.15	1.40	338	1250
Experiment	7.5 ~12.3[c]		1.32±0.05[d]	485[e]	1035[f]

[a] Relative to the HF energy of Pd (^1S)+O_2 ($^3\Sigma_g^-$); -178.48500 hartree.
[b] O_2 is assumed to vibrate as a unit.
[c] Reference 43-46.
[d] For O_2 on a Pt(111) surface. Reference 41.
[e] For O_2 on a Pt(111) surface. Reference 40.
[f] Reference 42.

B. Paired-spin coupling

In the paired spin coupling model, the same amounts of α- and β-spin electrons occupy the frontier MO. In the linear Pd-O_2 system, the frontier MOs are mainly composed of the degenerate π* MOs of O_2. At the separated limit, the triplet state of O_2 has two α- (or β-spin) electrons, so that the adsorbed state is not continuously connected to the separated limit without introducing further assumptions. Note however that for adsorptions of closed-shell molecules, this model gives a continuous potential curve between the separated and adsorbed states.

Figure 11 is a display of the $E(n)$ curve, calculated as a function of n. The curves are lower convex in contrast to the upper ones of Figure 8. At n=0.25, the tangent of the curve for $R_{O\text{-}O}$=1.35 Å becomes equal to the chemical potential -μ of the solid palladium metal (5.12 ev) [39], and the adcluster is most stable there in the range of $\partial E/\partial n \leq -\mu$. Therefore, about 0.25 electrons flow into the adcluster from the bulk metal; the adcluster has a noninteger number of electrons. When the chemical

potential μ of the metal is regulated, the number of electrons *n* transferred into the adcluster is regulated. The effect of a promoter and an extended electric field may be represented in this way.

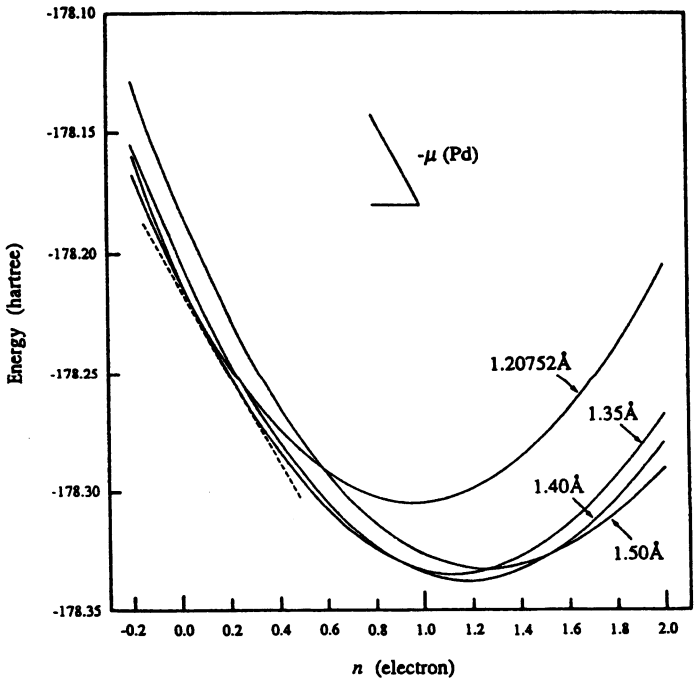

Fig. 11. *E(n)* curves of the Pd-O_a-O_b system in the paired spin coupling model for the O-O distances of 1.20752, 1.35, 1.40 and 1.50 Å and the Pd-O_a distance fixed at 2.00 Å.

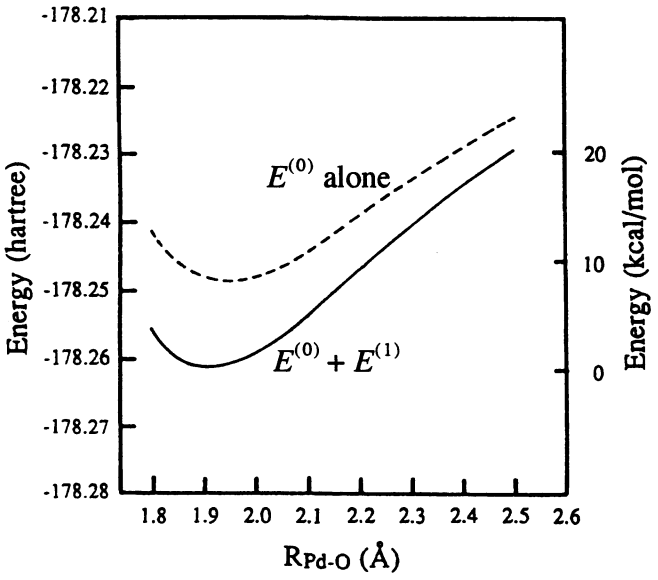

Fig. 12. Potential energy curves for Pd-O vibration calculated by the paired spin coupling model. The O-O length was fixed at 1.35 Å. Broken and solid lines were calculated, respectively, without and with the image force correction $E^{(1)}$.

The gross charge of Pd-O_a-O_b at n=0.25 is -0.35 (O_a), -0.20 (O_b), and +0.30 (Pd): The negative charge of O_a is larger than that of O_b and the Pd atom is positively charged. 0.30 electrons are supplied

by the adsorbed Pd and 0.25 electrons from the bulk metal. We think it natural that the Pd atom adsorbed by O_2 has positive charge, though this was not the case in the highest-spin coupling model.

Figure 12 shows the potential energy curve as a function of the Pd-O distance of the Pd-O_2 adcluster with fixed n of 0.25, though the number of electrons n should be optimized as the functions of these distances. Broken and solid lines are calculated respectively without and with the image force term $E^{(1)}$. The geometry and the vibrational frequency of the adsorbed system are calculated from these curves and shown in Table 3. The Pd-O and O-O lengths calculated by the paired-spin coupling model are a little shorter than those by the highest-spin coupling model, and the force constants are a little larger. A reasoning for these small differences is given in ref. 7.

TABLE 3. Geometry and vibrational frequency calculated from the PdO_2 adcluster in the paired spin coupling model.

	Bond length (Å)		Vibrational frequency (cm^{-1})	
	R_{Pd-O}	R_{O-O}	ω_{Pd-O}[a]	ω_{O-O}
$E^{(0)}$ alnoe	1.96	1.30	389	1259
$E^{(0)}+E^{(1)}$	1.93	1.31	399	1279
Experiment		1.32±0.05[b]	485[c]	1035[d]

[a] O_2 is assumed to vibrate as a unit.
[b] For O_2 on a Pt(111) surface. Reference 41.
[c] For O_2 on a Pt(111) surface. Reference 40.
[d] Reference 42.

5. Halogen Chemisorption on Alkali Metal Surfaces

This section is an exposition of an interesting application of the DAM and the SAC/SAC-CI method to the electron transfer processes between halogen molecule and alkali metal surfaces [26]. They are 'harpooning', surface chemiluminescence, and surface electron emission [53,54].

Figure 13 shows an illustration of the phenomena. When a halogen molecule approaches the surface to some distance, an electron jumps into the molecule: this large distance electron transfer is called 'harpooning'. When the halogen molecule receives an electron, it becomes an anion, is elongated, and attracted to the surface. When it collides with the surface, a photon and an electron are ejected out of the surface, namely, the surface chemiluminescence and electron emission occur. Up to three electrons are transferred from the surface to the molecule.

We studied these electron transfer processes by the *ab initio* method using the Hartree-Fock MO and SAC/SAC-CI methods. The basis set for Cl is ECP+ (3s3p)/[2s2p] [55]+ s,p functions with the exponent 0.049 [56]+ d-polarization function with ζ = 0.514 [57]. For K and Rb atoms, we used ECP+ (10s5p)/[3s3p] bases [58], and for Na (11s5p)/[4s1p]+ two p functions with the exponents 0.030 and 0.091 [57]. The alkali metal distance was fixed to that observed for the crystals (Na: 3.7083

Å, K: 4.6185 Å, Rb: 4.95 Å) [59] and the work functions are 2.75 eV for Na, 2.30 eV for K and 2.16 eV for Rb metal [60-62].

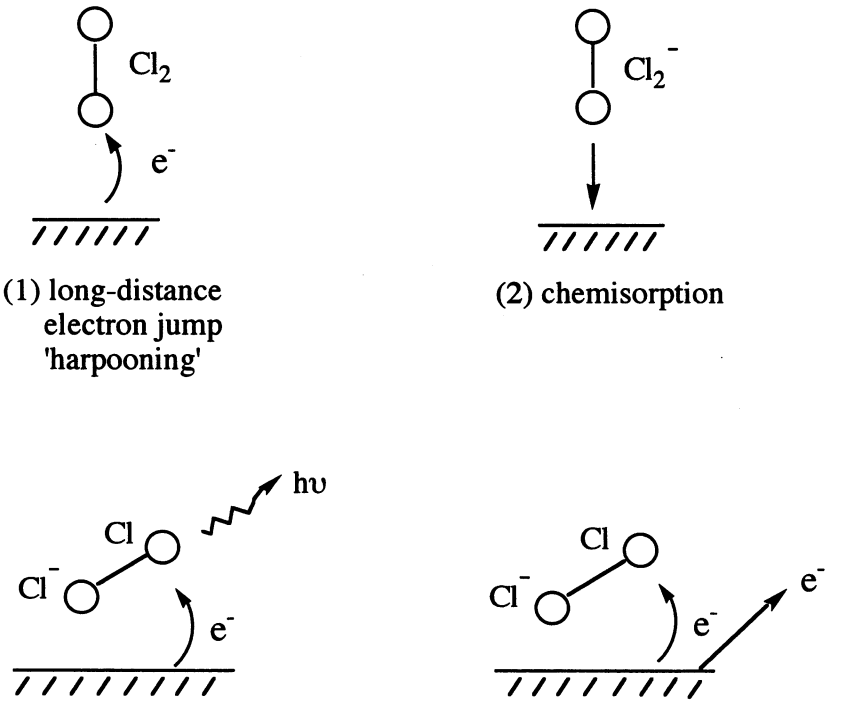

(1) long-distance electron jump 'harpooning'

(2) chemisorption

(3) surface chemiluminescence

(4) surface electron emission

Fig. 13. Electron transfer processes involved in the chemisorption of halogen molecule on alkali metal surfaces.

A. Harpooning

Harpooning is a long-distance jump of an electron from a metal surface to a molecule. It was explained as an electron tunneling from the alkali metal surface to the halogen molecule [53,54]. However, this process should be strongly vibronic, since the electron affinity of X_2^- is very much dependent on the X-X distance: a large electron affinity of X_2 is obtained only after an elongation of the distance. We show here the DAM picture of the harpooning, which is quite different from those given previously [53,54].

We assume that Cl_2 molecule approaches the surface in the end-on form, since the σ^* MO of Cl_2 is the electron-accepting orbital. We believe that the electron transfer occurs as a Frack-Condon process, as will be shown later, so that the Cl-Cl distance was fixed to 2.0025 Å, the calculated optimized distance: the experimental equilibrium distance is 1.987 Å [38]. We do not take into account the molecular vibrational effect. The alkali metal surface is represented by two metal atoms dipped onto the electron bath as illustrated in Figure 14. We consider here the sodium, potassium and rubidium surfaces.

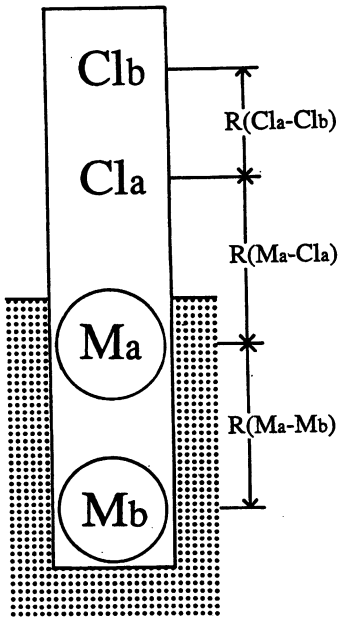

Fig. 14. Dipped adcluster model used for the study of " harpooning" .

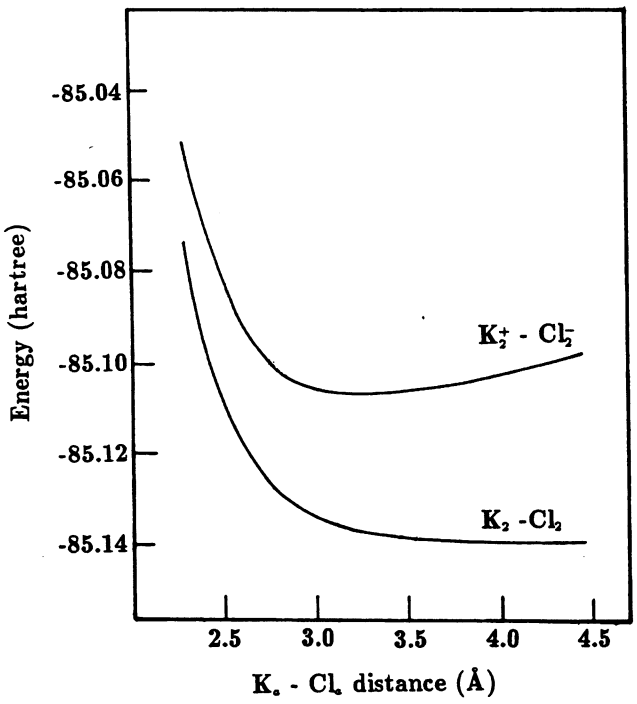

Fig. 15. Potential energy curve for the K_2-Cl_2 cluster model calculated by the SAC/SAC-CI method.

We first examine the cluster model, representing the potassium surface by only two potassium atoms, which is certainly a very crude model. Figure 15 shows the potential energy curves of the two lowest states calculated by the SAC/SAC-CI method. The lowest curve is for the interaction between the two neutral K_2 and Cl_2: it is repulsive throughout the interaction. The higher curve is attractive and represents the interaction between the electron transferred states, K_2^+ and Cl_2^-, but it is always less stable than the non-transferred neutral ground state. The reason is simple: this electron transfer is

realized by eliminating one electron from the bonding MO of K_2 and transferring it to the antibonding MO of Cl_2. Therefore, from this figure, we can not expect the occurrence of the harpooning. Maybe, the cluster size is too small and the vibrational effect of Cl_2 must be taken into account.

We next apply the DAM using the molecular orbital model explained in § 2B. The adcluster M_2 interacting with Cl_2, is dipped onto the electron bath of the alkali metal and the electron transfer is permitted. Figure 16 shows the *E(n)* curves calculated at different separations of Cl_2 from the surface. The curves were calculated using the paired spin coupling model and the highest spin coupling model, and the active orbital was chosen to be the σ^* MO of Cl_2.

In the paired spin coupling model, the energy of the system increases with increasing the number of electrons, *n*, transferred to Cl_2, so that the tangent of the *E(n)* curve can never become equal to $-\mu$. In the highest spin coupling model, on the other hand, the *E(n)* curve is an upper convex and its tangent can become larger (in absolute value) than $-\mu$ when the Cl_a-M_a distances is smaller than 6, 7, and 8 Å for M=Na, K, and Rb, respectively. Since the *E(n)* curves are upper convex, one electron (an integral number, one) is transferred from the surface to Cl_2, as explained in § 2A. This one electron transfer is just the harpooning of an electron from the surface to Cl_2, which is the DAM picture of the harpooning. We note that we could explain the harpooning as a Franck-Condon process without resorting to the vibronic coupling. We also used the picture of *tunneling* on the *E(n)* surface from *E(0)* to the point at which the derivative $\partial E/\partial n$ is equal to $-\mu$, since between these two points the derivative is always less than $-\mu$. However, this concept of *tunneling* is on the *n*-space and different from that on the *R*-space.

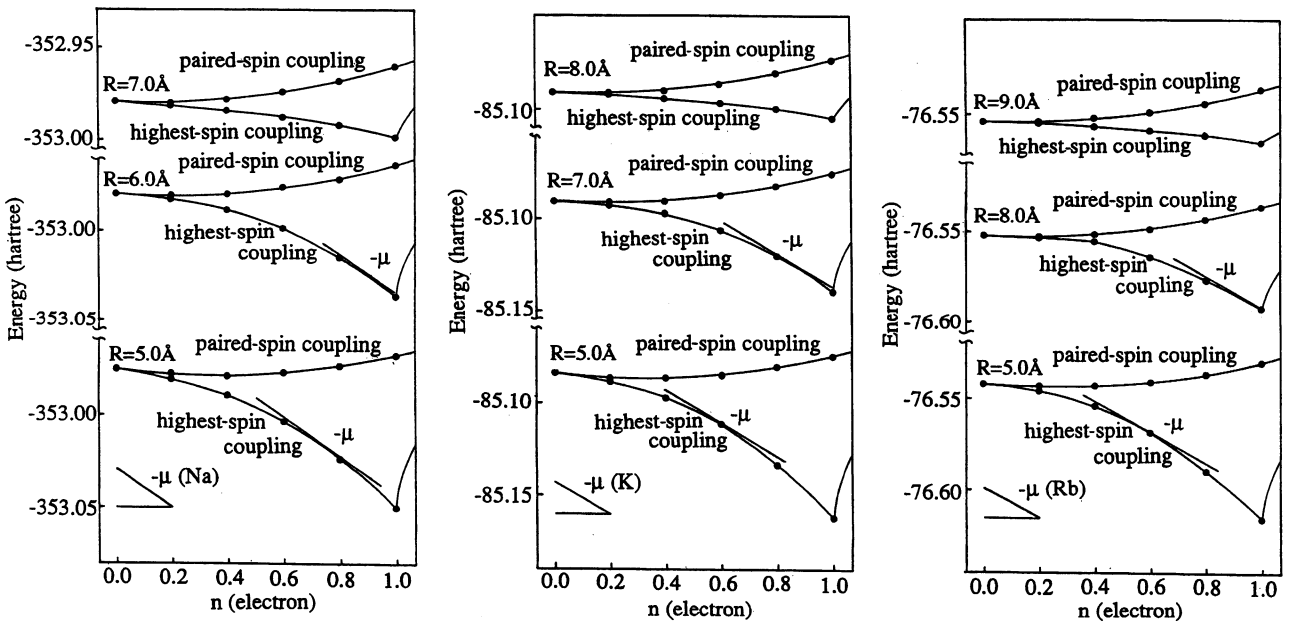

Fig. 16. E(n) curves calculated by the DAM for the Cl_2-M_2 adcluster at several different M_a-Cl_a distances: (a) M=Na, (b) M=K, (c) M=Rb.

Table 4 shows the gross charge of the adcluster at the Franck-Condon state just after the harpooning. It shows that the one electron transferred from the bulk metal to the adcluster is localized on Cl_2: the negative charges on M_2 are quite small. Further, M_a is positively charged even in this situation, in accordance with the picture of the image force. The outside chlorine atom Cl_b is a bit more negatively charged than the inside one Cl_a: the result which is different from other observations. However, when we optimize the Cl-Cl distance after the harpooning, Cl_a becomes more negative than Cl_b, as shown later.

TABLE 4. Gross charge of the adcluster at the Franck-Condon state just after the 'harpooning'

Metal M	M_a-Cl_a Distance (Å)	Gross charge					
		Cl_b	Cl_a	Cl_2	M_a	M_b	M_2
Na	6.0	-0.508	-0.476	-0.984	+0.164	-0.180	-0.016
K	7.0	-0.499	-0.490	-0.989	+0.073	-0.084	-0.011
Rb	8.0	-0.500	-0.493	-0.993	+0.064	-0.071	-0.007

In summary, the harpooning in the DAM picture is the Franck-Condon one-electron transfer process from the *bulk* alkali metal to Cl_2 in the *highest-spin coupling* mechanism. The harpooning distances calculated by the DAM are 6, 7, and 8 Å for Na, K, and Rb surfaces, respectively. These distances are shorter than those estimated by the conventional tunneling mechanism: for example, it is estimated to be 10 Å for the Na surface [53].

B. Chemisorption process of Cl_2^-

When the harpooning occurs, Cl_2 becomes Cl_2^-. Since one electron is accommodated in the σ^* MO, the Cl-Cl distance is elongated. Figure 17 shows the potential curve of the adcluster, K_2-Cl_2^- as a function of the Cl-Cl distance with the fixed K_a-Cl_a distance of 7.0 Å, the distance at which the harpooning begins to occur. It was calculated by the Hartree-Fock method. The harpooning occurs at the Cl-Cl distance of 2.0025 Å shown by an arrow, as a Franck-Condon process, and afterwards, the Cl-Cl distance is elongated to 2.64 Å with a large stabilization of about 48 kcal/mol. The binding energy of Cl_2^- is calculated to be only 7 kcal/mol on the surface, very weak in comparison with the experimental binding energy, 29 kcal/mol of a free Cl_2^- [38]. Since the energy gain by the elongation ~48 kcal/mol is much larger than the binding energy 7 kcal/mol, we predict that a neutral Cl atom would be ejected out from the surface after the harpooning.

We assume that this excess energy is dissipated somewhere, say, to the alkali metal surface and calculate the adiabatic potential curve of Cl_2^- on the surface. The potential curve shown in Figure 18

was calculated for the K_2-Cl_2^- adcluster as a function of the K_a-Cl_a distance: the Cl-Cl distance was optimized at each K_a-Cl_a distance. Starting from the K_a-Cl_a distance of about 7 Å, the harpooning distance, the potential curve was attractive, and the minimum was obtained at the K_a-Cl_a distance of 3 Å. The stabilization energy there was about 27 kcal/mol.

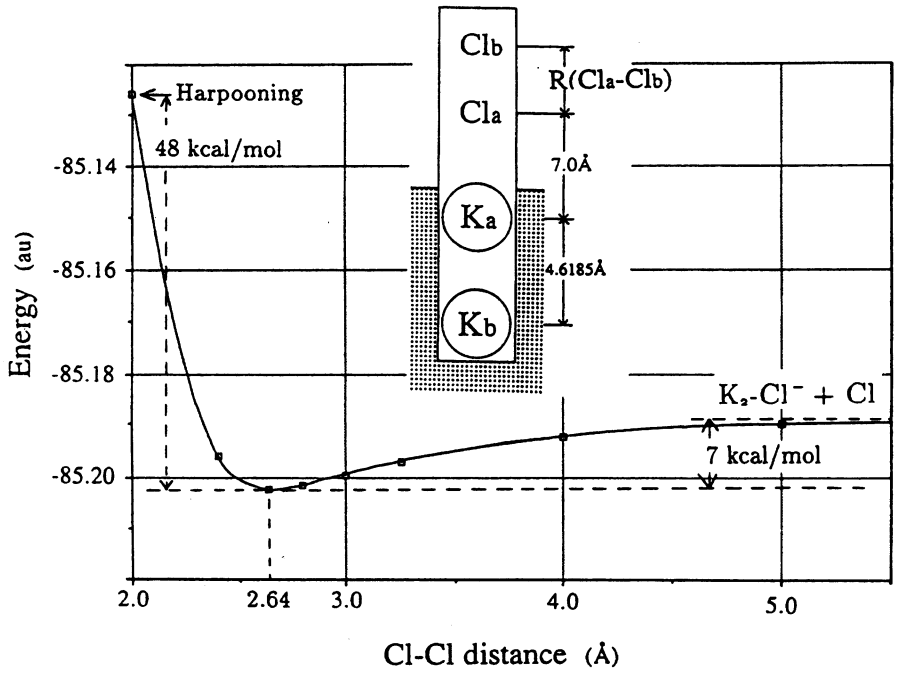

Fig. 17. Potential curve of the adcluster in the Hartree-Fock level as a function of the Cl-Cl distance just after the harpooning. The K_a-Cl_a distance was fixed at 7.0 Å.

TABLE 5. Stabilization energy of the K_2-Cl_2^- system after the harpooning and the optimized Cl-Cl distance and the gross charge

K_a-Cl_a distance (Å)	Optimized Cl-Cl distance(Å)	Stabilization Energy (kcal/mol)	Gross Charge			
			Cl_b	Cl_a	K_a	K_b
7.0	2.0025[a]	0.0	-0.499	-0.490	+0.073	-0.084
7.0	2.64	-48.07	-0.424	-0.578	+0.078	-0.077
6.0	2.65	-51.25	-0.378	-0.625	+0.097	-0.094
5.0	2.73	-54.29	-0.255	-0.749	+0.137	-0.133
4.0	2.78	-65.28	-0.158	-0.843	+0.204	-0.203
3.0	2.92	-75.07	-0.067	-0.875	+0.141	-0.199
2.5	2.94	-62.19	-0.076	-0.814	+0.032	-0.142
2.0	2.70	-41.70	-0.324	-0.515	-0.081	-0.080

[a] Franck-Condon state just after the harpooning.

Table 5 shows the more detailed information of the process. It shows the stabilization energy relative to the Franck-Condon state after the harpooning: the Cl-Cl distance was optimized at each K_a-

Cl_a distance. The gross charges of the adcluster are shown at each optimized geometry. We see that the stabilization energy at the potential minimum of Figure 18 is as large as 75 kcal/mol relative to the Franck-Condon state after the harpooning. This energy should be dissipated in the system. The charge polarization of Cl_2 is very large, and at the potential minimum, the Cl-Cl distance increases to about 2.9 Å and Cl_b is almost neutral (-0.067) though Cl_a is strongly negative (-0.875).

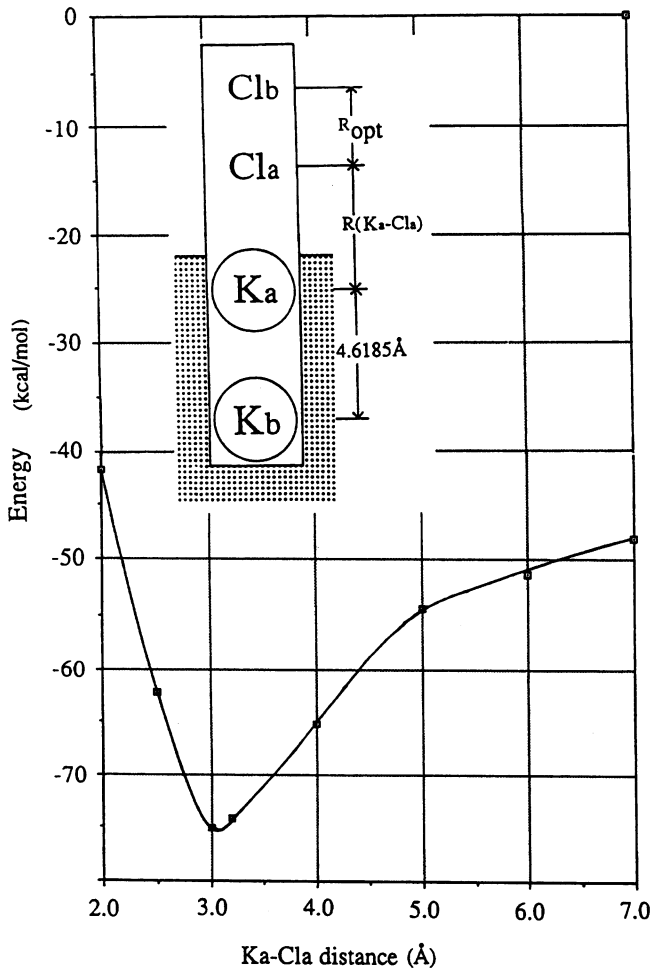

Fig. 18. Potential curve of the adcluster in the Hartree-Fock level as a function of the K_a-Cl_a distance. The Cl-Cl distance was optimized at each K_a-Cl_a distance. The energy is relative to the energy of the system just after the harpooning shown by the arrow in Fig. 17 (Cl-Cl distance is 2.0025 Å).

C. Surface chemiluminescence process

We expect from Figure 18 that Cl_2^- would collide strongly with the alkali metal surface, and then chemisorbed dissociatively. In this collisional process, two interesting electron transfer processes occur, which are surface chemiluminescence and electron emission. We study these electronic processes by the SAC/SAC-CI method.

Figure 19 shows the surface chemiluminescence spectrum observed by Anderson, et al. [63] for the chemisorption of Cl_2 on the potassium surface. The maximum intensity appears at about 440 nm and the spectrum is spread from 800 to 300 nm; the decay from the maximum at 440 nm to 300 nm is

very sharp. Can we explain these features of the chemiluminescence spectrum by the SAC/SAC-Cl method?

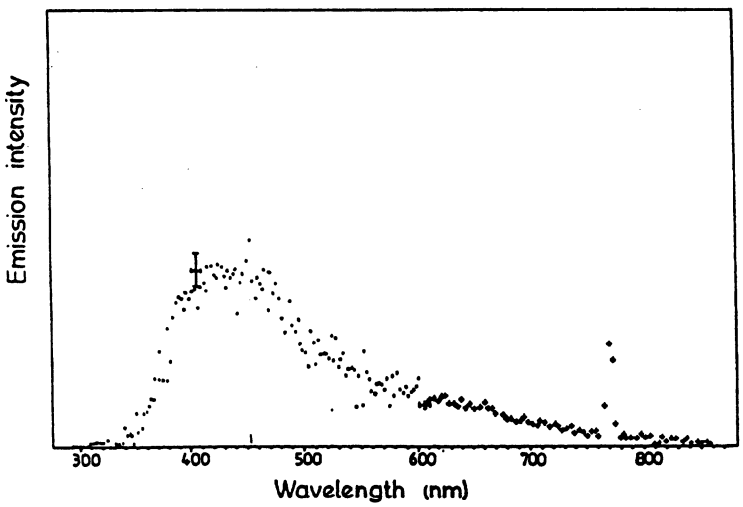

Fig. 19. Observed surface chemiluminescence spectrum for the Cl_2^- potassium surface system (cited from ref. 47).

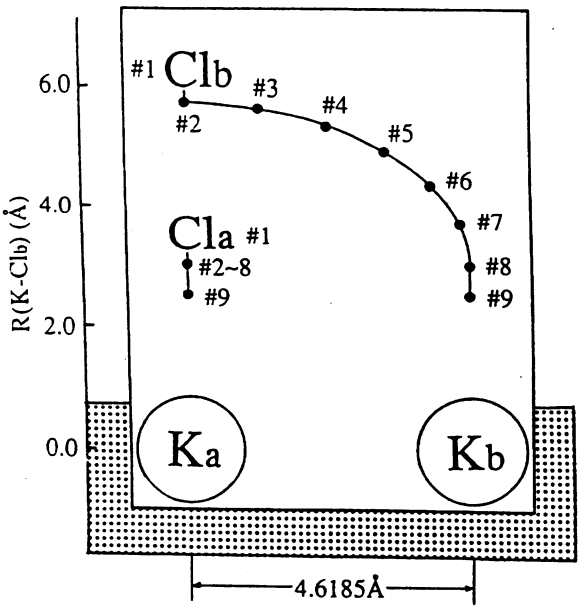

Fig. 20. Assumed reaction pathway for the surface chemiluminescence and surface electron emission processes.

Figure 20 shows the geometry of the model adcluster used in the study of the chemiluminescence and electron emission. The Cl_2 molecule would approach the surface in the end-on geometry, but after the collision the dissociative chemisorption would proceed to form two KCl molecules. The adcluster shown in Figure 20 gives a minimum possible model: the chemisorption reaction proceeds from the end-on position #1 to #2, where Cl_a is captured to K_a, and then Cl_b moves towards K_b successively through #3~#7 and captured by K_b at #8. The final state of the dissociative

TABLE 6. Energies of the K_2^+-Cl_2^{2-} and K_2-Cl_2^{2-} systems (au)

Structure	From K_2 K_2^+-Cl_2^{2-}	From bulk K_2-Cl_2^{2-}
#2	-85.26768	-85.20538
#4	-85.31470	-85.24579
#6	-85.36152	-85.28239
#8	-85.40445	-85.30826

TABLE 7. Gross charge for the initial and final states of chemiluminescence and electron emission

	Gross charge[a]			
	Cl_b	Cl_a	K_a	K_b
initial state				
#1	-0.361	-0.614	+0.039	-0.064
#2	-0.381	-0.614	+0.017	-0.022
#3	-0.358	-0.725	+0.110	-0.027
#4	-0.158	-0.778	-0.017	-0.047
#5	-0.081	-0.866	-0.029	-0.024
#6	-0.044	-0.893	-0.056	-0.007
#8	-0.428	-0.428	-0.072	-0.072
#9	-0.340	-0.340	-0.160	-0.160
final state of chemiluminescence				
#1	-0.893	-0.893	+0.687	+0.099
#2	-0.857	-0.883	+0.652	+0.088
#3	-0.855	-0.854	+0.585	+0.124
#4	-0.996	-0.947	+0.737	+0.206
#5	-0.993	-0.957	+0.682	+0.268
#6	-0.986	-0.965	+0.613	+0.338
#8	-0.979	-0.979	+0.479	+0.479
#9	-0.923	-0.923	+0.423	+0.423
final state of electron emission				
#2	-1.013	-0.928	+0.959	+0.812
#5	-0.949	-0.931	+0.937	+0.943
#6	-0.936	-0.947	+0.956	+0.927
#8	-0.975	-0.975	+0.975	+0.975
#9	-0.971	-0.971	+0.971	+0.971

[a] For the numbering of atoms, see Figure 20.

adsorption is represented by the geometry around #8, as will be shown below. The geometry #9 represents an inward vibrational position of the potassium chloride. The Cl_a-K_a distance is 3.25 Å for #1, 3.0 Å for #2~#8, and 2.5 Å for #9. The Cl_a-Cl_b distance at #1 and #2 is 2.73 Å.

The chemiluminescence would occur in the course of the chemisorption process shown in Figure 20. As shown in Figure 13(3), it is said that the chemiluminescence accompanies the second electron transfer from metal to halogen. An interesting question here raised is "from where the second electron originates?". Does it originate from the bulk metal or from the local K_2 site directly interacting with Cl_2? In order to investigate this problem, we calculated by the SAC/SAC-CI method the total energies of the adclusters with the formal charges of K_2^+-Cl_2^{2-} and K_2-Cl_2^{2-}, the former being the product of the electron transfer from the local K_2 site and the latter from the bulk metal. Table 6 shows the result. We see that the former is always more stable than the latter for the geometries #2~#8. This is probably due to the existence of the additional coulumbic attraction in the former. We therefore conclude that the second electron originates from the local K_2 site directly interacting with Cl_2^-. The chemiluminescence problem would be solved by calculating the potential curves of the two lower states of the adcluster K_2-Cl_2^- by the SAC/SAC-CI method.

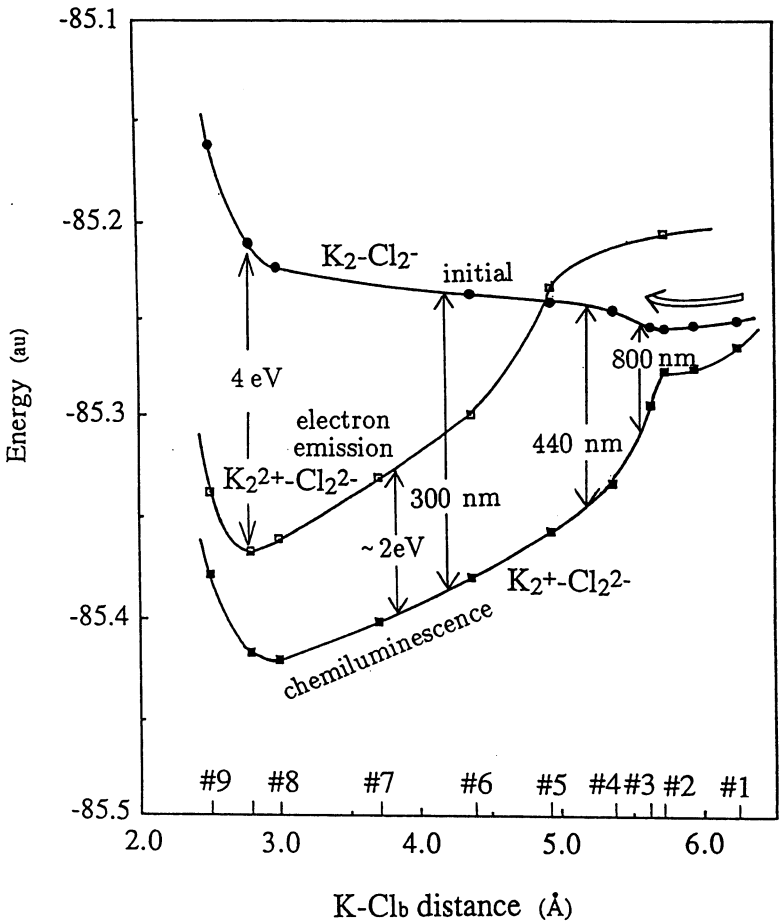

Fig. 21. Potential curves of the Cl_2^- potassium surface system for the surface chemiluminescence and electron emission processes calculated by the SAC/SAC-Cl method.

We show the potential curves calculated by the SAC/SAC-CI method in Figure 21. Table 7 shows the gross charge of the system. These results show the initial and final states of both chemiluminescence and electron emission. In Figure 21, the final state potential curves are distinguished by 'chemiluminescence' and 'electron emission'. The initial state is common to both processes. We discuss in this section only the chemiluminescence process.

The energy difference between the initial and final states of Figure 21 corresponds to the energy of the emitted chemiluminescence photon. Investigating the gross charge shown in Table 7, we see that the initial state is well represented by K_2-Cl_2^{2-} in all the geometries, Cl_a being more negative than Cl_b except for the geometries #8 and #9. The final state of the chemiluminescence is written, on the other hand, as K_2^+-Cl_2^{2-}. Therefore, as expected, this chemiluminescence corresponds to the charge-transfer transition: one electron is transferred from potassium to Cl_2.

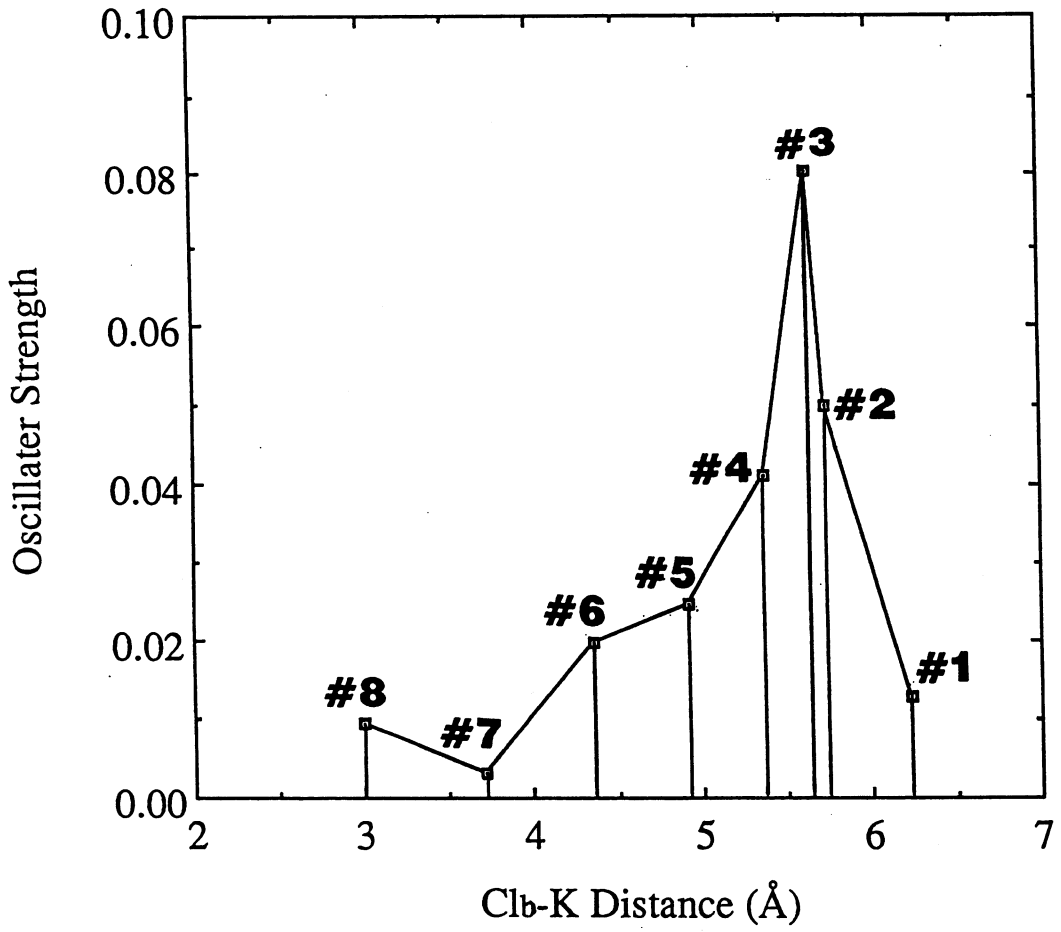

Fig. 22. Oscillator strength for the chemiluminescence along the reaction coordinate.

The dynamics of this system may roughly be described as follows. The system proceeds from the right to the left on the initial state curve and makes a transition to the chemiluminescence final state with emitting a photon. The energy of the emitted photon is given by the energy difference between the initial and final states plus some part of the kinetic energy of the accelerated Cl_2^- in the initial state. The

wave numbers shown in Figure 21 correspond to the former one. We show in Figure 22 the calculated oscillator strength for the chemiluminescence transition along the reaction coordinate. The experimentally observed surface chemiluminescence spectrum [63] shown in Figure 19 is well understood from the present theoretical results.

The experimental spectrum spread from 800 nm to about 300 nm with the peak maximum at about 400 nm. This peak position corresponds to about #4 geometry in Figure 21. The calculated intensity has a peak at #3 geometry but it is also large at #4 geometry. The intensity of the observed spectrum rapidly decreases from about 400 nm and becomes zero at about 300 nm. This rapid decrease is understood to be due to the transition to the electron emission channel: the crossing at about geometry #5 facilitates this transition. The calculated transition probability has a maximum at geometry #3, while the experimental peak occurs between the geometries #4 and #5. This shift is probably due to an addition of the kinetic energy of Cl_2^- to the energy of the emitted photon.

From the above analysis, we conclude that the chemiluminescence transition occurs in the median of the course of the dissociative adsorption, roughly at around #4 and #5 geometries. After passing #5, the transition to the electron emission channel increases rapidly.

D. Surface electron emission process

Surface electron emission process is also studied by the SAC/SAC-CI method. Theoretically, this process corresponds to the ionization process and can be dealt with by the SAC/SAC-CI method. We use the same model adcluster shown in Figure 20. Since the final state is neutral, it corresponds to two K^+-Cl^-. Namely, this is the two-electron process in which one electron is transferred from the surface to the halogen molecule anion X_2^-, and at the same time, another electron is emitted out of the surface as shown in Figure 13(4). We assume that these two electrons belong to the local K_2 site directly interacting with X_2^-, since they are so strongly correlated in this process. It is difficult to expect such a strong correlation if one or two of these electrons belong to the electron bath of the bulk metal.

The potential curve for the final state of the surface electron emission calculated by the SAC-CI method is given in Figure 21. The initial state is common to both chemiluminescence and electron emission processes. The electron emission process occurs after the chemiluminescence process, since the process proceeds from the right-hand side on the initial-state curve. The electron emission occurs in the geometries whose numberings are larger than #5, where the initial and final state curves of the electron emission cross each other. The excess (kinetic) energy of the emitted electron is given by the energy difference between the initial and final states plus some part of the kinetic energy in the initial state. The former is about 4 eV at the turning point of the initial state curve, namely at about #8~#9 geometries, where the equilibrium geometry of the final state also exist: i.e., two KCl. Therefore a large transition probability is expected at #8~#9 geometries from these features of the potential curves

of the initial and final states. A large transition probability is also expected at the crossing point at about #5 geometry and may be calculated by the Landau-Zener model.

Figure 23 shows the exoelectron energy distribution measured for Cl_2 on yttrium [64]. A similar spectrum was also measured for Cl_2 on Rb-dosed yttrium [64]. We see a maximum peak at about 4 eV in accordance with the above expectation.

The final state of the electron emission process is almost the two potassium chloride as described above. This is confirmed from the charge distribution shown in Table 7. For example, the charge distribution at #6 geometry is Cl_b(-0.936), Cl_a(-0.947), K_a(+0.956), and K_b(+0.927).

In Figure 21, the difference between the final-state potential curves of the electron emission and the chemiluminescence is about 2 eV at any geometry of the reaction pathway. This is because the difference corresponds to the work function of the potassium surface: the experimental value is 2.3 eV.

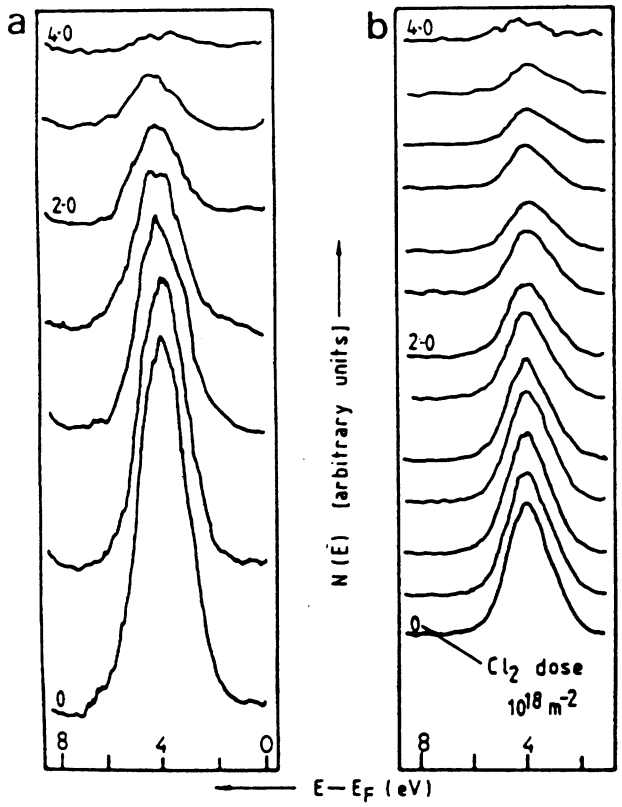

Fig. 23. Exoelectron energy distribution measured for (a) Cl_2 on yttrium and (b) Cl_2 on Rb-dosed yttrium (cited from ref. 64).

E. Brief summary

The electron transfer processes in the chemisorption of halogen molecules on alkali metal surfaces were studied and their natures were clarified as follows.

(1) The harpooning process was explained by the DAM as a Franck-Condon process. It is a one-electron transfer process from the bulk metal to Cl_2 through the highest-spin coupling mechanism. The harpooning distance for the Cl_2 molecule is calculated to be 6, 7, and 8 Å for sodium, potassium, and rubidium surfaces, respectively.

(2) Receiving one electron from the surface, Cl_2^- is elongated and stabilized. Since this stabilization energy is larger than the Cl-Cl binding energy, neutral Cl atom is expected to be emitted out of the surface after the harpooning.

(3) Both of the surface chemiluminescence and electron emission processes are well described by the SAC/SAC-CI method, since these processes involve the ground and excited states and the states having different numbers of electrons. The observed surface chemiluminescence spectrum and the excess-energy distribution spectrum of emitted electrons were well understood from the present results.

6. O_2 Anion Species in Gas Phase

O_2 molecules chemisorbed on metal surfaces show a lot of interesting chemistry. Before studying such chemistry in the next and subsequent sections, we show here the bondings and the potential curves of the dioxygen anion species O_2^- and O_2^{2-} in their isolated free states [65] for giving a comparative basis.

The Gaussian basis is the Huzinaga-Dunning (9s5p)/[4s2p] set [56] plus diffuse s, p functions (α=0.059) and polarization d functions (α=0.30). This basis set gives the electron affinity of oxygen atom as 0.97 eV, after electron correlation is included, in comparison with the experimental value of 1.31 eV.

TABLE 8. Bond length R_e, vibrational frequency ω_e, dissociation energy D_e, electron affinity EA, and gross charge of the O_2^- and O_2^{2-} molecules in a gas phase and of the superoxide O_2^- and peroxide O_2^{2-} species on a silver surface.

Species	Method	*Re* (Å)	ω_e (cm^{-1})	D_e (eV)	EA (eV)	Gross charge (per O_2)
O_2^-	SAC-CI	1.44	1010	4.00	-6.24	-1
	exptl.	1.35	1090	4.09		-1
O_2^{2-}	SAC	1.67	545	-2.94		-2
O_2^- on Ag surface	SAC-CI, DAM	1.47	974, 1055	(0.70)[a]		-0.54, -0.65
	exptl.		1053			
O_2^{2-} on Ag surface	SAC-CI, DAM	1.66	689			-1.4
	exptl.	1.47±0.05	628, ca. 697			

[a] Hump height.

We calculated the potential curves of O_2^- and O_2^{2-} by the SAC/SAC-CI method: O_2^{2-} was calculated by the SAC method, since it is a closed-shell molecule, and O_2^- was calculated by the SAC-CI method as a cation produced from O_2^{2-}. Figure 24 shows the potential curves and Table 8 gives a

summary of the spectroscopic constants. The superoxide O_2^- is a stable molecule with the dissociation energy of 4.00 eV (experimental value is 4.09 eV). The calculated equilibrium length and the vibrational frequency are 1.44 Å and 1010 cm^{-1} in reasonable agreement with the experimental values 1.35 Å and 1090 cm^{-1}. On the other hand, the peroxide O_2^{2-} is only a transient species though it has a minimum at $R_{O\text{-}O}$=1.67 Å with the hump height of 0.703 eV. The repulsive tail in the longer region is shown to be entirely due to the electrostatic repulsion between the negatively charged oxygen atoms [65].

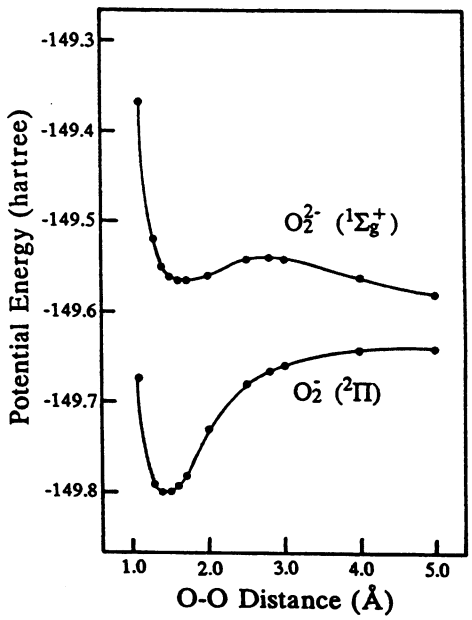

Fig. 24. Potential energy curves for the ground states of dioxygen anion species, O_2^- and O_2^{2-}, calculated by the SAC/SAC-Cl method [65].

7. Molecular and Dissociative Adsorption of O_2 on Silver Surface

Oxygen chemisorbed on a silver surface shows several important catalytic reactions. Partial oxidation of ethylene giving ethylene oxide and formaldehyde synthesis from methanol are particularly important reactions took place on a silver surface. Despite their usefulness in chemical industry , the nature of the active oxygen species and the detailed mechanisms of the reactions are not yet known. It is important to clarify the stabilities, reactivities, and other properties of the oxygen species adsorbed on a silver surface.

We studied the nature of the O_2 species adsorbed on a silver surface using the DAM [48-49]. Since O_2 molecule exists in some different electronic states on the surface, the SAC-CI method was useful since it describes several different electronic states in a good similar accuracy. Based on these studies, we have further studied the mechanism of the partial oxidation of ethylene on a silver surface [66,67], and the oxidation mechanism of propylene on a silver surface [68]. In this and succeeding sections, we give a review on these studies.

Experimentally, four different species are known for the adsorbed oxygens on a silver surface [69-82]: namely, physisorbed species (O_2) [69], molecularly adsorbed species, which are superoxide (O_2^-) [41,70,71] and peroxide (O_2^{2-}) [41,72-78], and dissociatively adsorbed species (O^- and/or O^{2-}) [41,74,79-81].

Some theoretical papers have been published on the oxygen chemisorption [47,51,83-89]. The GVB-CI study by Upton et al. [47] gave geometric and spectroscopic parameters of O_2 on an Ag(110) surface in good agreement with experimental data. However, the adsorption energy relative to the separated system were not reproduced: they were negative. Similarly negative adsorption energies have been obtained by the MP3 calculations [85] and by the GVB and correlation-consistent CI calculations [86,87]. All of these studies were based on the cluster model, so that the effect of the bulk metal was only insufficiently included in the calculations. Further, no ab initio studies have been able to describe dissociative adsorptions of O_2 on the Ag surface.

We think that the reason of the failure lies in the model adopted, that is, the cluster model. The effect of the electron transfer from the bulk metal to the adcluster and the electrostatic image force interaction between admolecule and surface are expected to be important for this system, but they are not well included in the cluster model. We therefore use here the DAM which include these effects as explained in the previous section.

We summarize the calculational method used. The Gaussian basis set for the silver atom was (3s3p4d)/[3s2p2d] and the Kr core was replaced by the relativistic effective core potential [90]. For oxygen, we used the (9s5p)/[4s2p] set of Huzinaga-Dunning [91] augmented with the diffuse anion s, p basis [40] of α=0.059 and the polarization d functions of α=0.30. The HF calculations were carried out with the use of the program GAMESS [92]. For the SAC/SAC-CI calculations, the active occupied orbitals for the Ag_2O_2 adcluster consists of the 4d, 5s and 5p orbitals of Ag and the 2p orbitals of O, and those for the Ag_4O_2 adcluster the 5s and 5p orbitals of Ag and the 2p orbitals of O. The program system SAC85 [37] was used for the SAC/SAC-CI calculations.

Before doing electron correlation calculations, we have applied to the Ag_2O_2 adcluster shown in the inset of Figure 25 the molecular orbital model of the dipped adcluster using the highest spin coupling model. The resultant *E(n)* curve is shown in Figure 25. The distance between the O-O axis and the Ag-Ag axis was fixed at 2 Å and the O-O distance was changed from 1.20 Å, which is an equilibrium length of O_2 [38], to 1.35 Å, which is an equilibrium length for O_2^- [38,93]. The curves were upper convex and the curvature was discontinuous at n=0.0 and n=1.0. At n=0.0, R_{OO}=1.20 Å was more stable, but at n=1.0, R_{OO} =1.35 was more stable. The tangent of the curves becomes equal to the experimental chemical potential -μ of the solid silver metal (4.52 eV) [94] at n=0.6-0.7. Therefore, as judged from the equilibrium condition of (2.2), one electron flows from the bulk metal into the adcluster after some barrier.

We assume that this one-electron flow is valid not only for this molecular orbital model, but also for the cases in which electron correlations are taken into account. We calculate hereafter the correlated

wave functions for this one-electron transferred adcluster using the SAC/SAC-CI method.

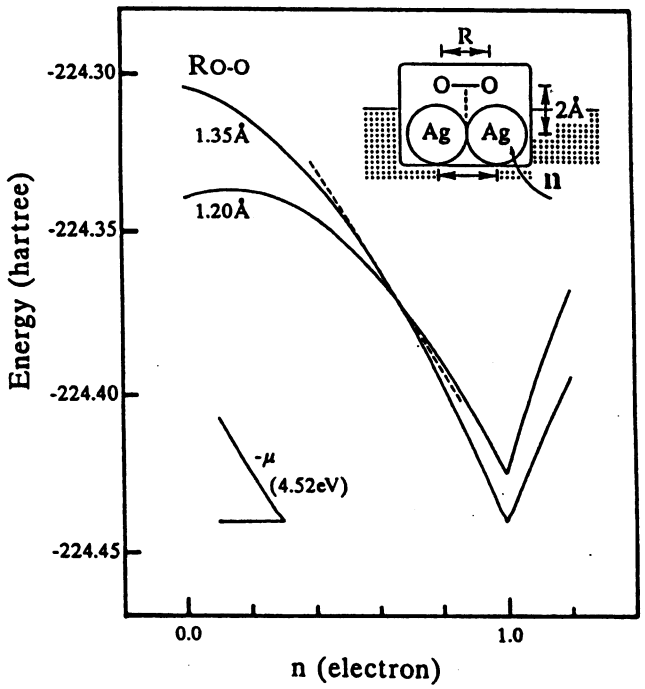

Fig. 25. *E(n)* curve for the Ag_2O_2 adcluster in the highest spin coupling model with the Ag_2-O_2 distance of 2.00 Å and the Ag-Ag distance of 2.8894 Å. The O-O distance was changed from 1.20 to 1.35 Å.

A. Approach of O_2 to silver surface

We first study the energetics for the approach of an O_2 molecule onto the Ag surface. The geometry of the reaction path is shown as an inset of Figure 26. The active site of the Ag surface was represented by Ag_2, and an O_2 molecule approaches the surface in a side-on bridge form keeping C_{2v} symmetry. The Ag-Ag distance was fixed at 2.8894 Å, which is an equilibrium distance in solid silver [59]. Figure 26 shows the potential energy curves of the Ag_2O_2 adcluster as a function of the Ag_2-O_2 distance. The curves were calculated for the O-O distance fixed at 1.35 Å, which is an equilibrium distance of an O_2 anion [38,93]. The asterisks show the energies for the optimized O-O distances.

We first examine the cluster model and the results are given in Figure 26 by the broken lines with n=0, which shows that the electron transfer from the bulk metal to the adcluster was not considered. However, we have included the image force correction even in this cluster model calculations. The $^3B_2$ (n=0) state is the ground state of the separated system, namely, the $^1\Sigma_g^+$ state of Ag_2 plus the $^3\Sigma_g^-$ state of O_2. The energy of the dissociation limit was estimated by optimizing the O-O distance at the Ag_2-O_2 distance of 5.0 Å, and is shown by the asterisk in Fig. 26. There, the optimized O-O length is 1.29 Å, in comparison with 1.27 Å, the optimized length for the free O_2 molecule (the experimental value is 1.207 Å [38]). The potential curve of the $^3B_2$ state rises monotonically as O_2 approaches Ag_2, showing that no chemisorption occurs along this state. The $^3A_2$ state is an electron

transferred state from Ag_2 to O_2, but no electron is supplied from the bulk metal (n=0). The image force term included works to stabilize the system. Though the system is stabilized as O_2 approaches the surface, the energy is always higher than the separated system. This state corresponds to the molecularly adsorbed species obtained by the conventional cluster model and the adsorption energy is negative as in the previous studies. The cluster model thus failed to describe the stabilization in the chemisorption process.

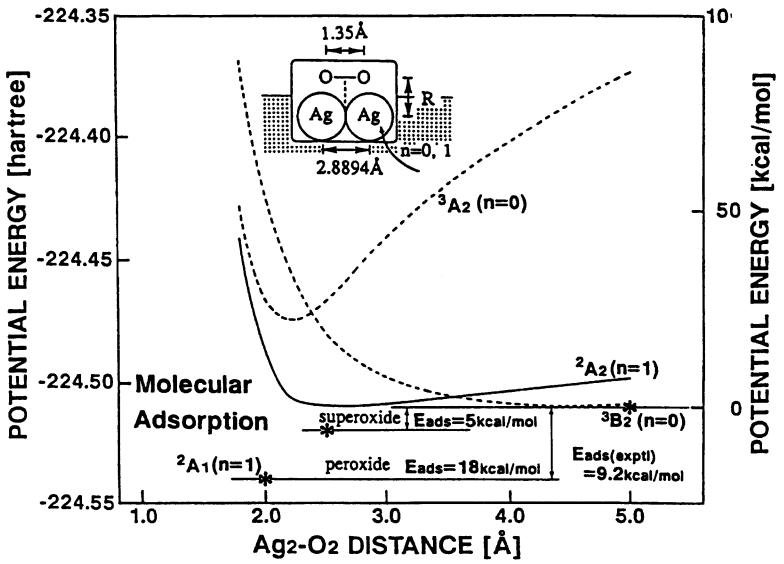

Fig. 26. Potential energy curves for the approach of O_2 onto Ag_2 in the Ag_2O_2 adcluster model. n denotes the number of electrons transferred from the bulk metal to the adcluster.

On the other hand, when we use the DAM and admit one-electron transfer from the bulk metal to the adcluster, namely n=1, the potential of the $^2A_2$ state becomes attractive and a minimum was found at $R(Ag_2\text{-}O_2)$=2.6 Å. When the O-O distance was further optimized at this minimum, we got R(O-O)=1.5 Å and the system was stabilized up to the asterisk shown in Figure 26. This $^2A_2$ state corresponds to the superoxide species, O_2^-. There is another state, $^2A_1$, which also results from one-electron transfer from the bulk metal to the adcluster. This $^2A_1$ state corresponds to the peroxide species, O_2^{2-}, and has a potential minimum at $R(Ag_2\text{-}O_2)$=2.0 Å and R(O-O)=1.66 Å. The corresponding energy was shown by the asterisk in Figure 26. The calculated adsorption energies of the superoxide and peroxide species were 5.5 and 17.8 kcal/mol, respectively, in comparison with the experimental molecular adsorption energy of 9.2 kcal/mol on Ag(111) and 9.3 kcal/mol on Ag(110) [80,112].

This was the first successes of obtaining the positive adsorption energy for the O_2 chemisorption on a silver surface [48,49]. The main reason of the failure of the cluster model was that it did not include the effect of the electron transfer from the bulk metal. In the cluster model, all the electrons transferred to O_2 must be supplied from Ag_2 destabilizing the Ag_2 cluster, but in the DAM some of the electrons are supplied from the bulk metal. We thus conclude that the electron transfer from the bulk metal to the adcluster is essential for the occurrence of chemisorption of O_2 on an Ag surface. This is

why even a so small adcluster, Ag_2O_2 could describe successfully the O_2 chemisorption on a Ag surface. Further, we have also confirmed that the stabilization of the charged O_2 admolecule by the electrostatic image force of the Ag metal is also important.

B. Vibrational potential of O_2 on silver surface

We next examine whether the DAM describes well the properties of the O_2 species chemisorbed on the Ag surface .We show in Figure 27 the potential curves of the O_2 species for the elongation of the O-O distance on the Ag_2 site keeping the C_{2v} symmetry. These potential curves were calculated using the DAM with the Ag_2O_2 adcluster and n=1. The distance between the Ag_2 and O_2 axes were kept at 2.0 Å. As before, the $^2A_2$ and $^2B_1$ states correspond to the superoxide species and the $^2A_1$ state to the peroxide species.

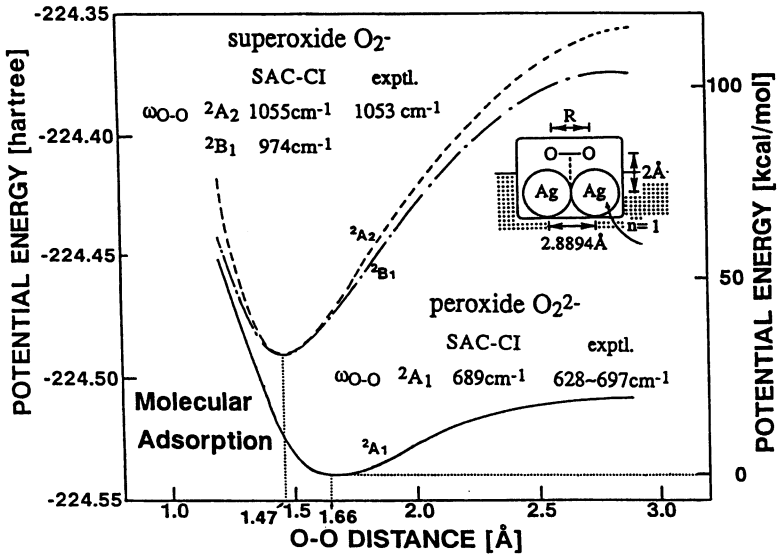

Fig. 27. Potential energy curves for the O-O elongation of the Ag_2O_2 adcluster.

We summarize in Table 9 the adsorption energy, geometry, vibrational frequency, and gross charge calculated for these three oxygen species on the silver surface. The O-O bond length of the superoxide was calculated at 1.47 Å and that of the peroxide at 1.66 Å. In contrast, the experimental value for peroxide is 1.47 Å [41], and the value calculated by Upton et al. [47] is 1.55 Å. The O-O vibrational frequency of the superoxide was calculated at 1055 ($^2A_2$) and 974 cm^{-1} ($^2B_1$) in comparison with the experimental value of 1053 cm^{-1} [72,73]. For the peroxide species, the theoretical value is 689 cm^{-1} in comparison with the experimental values of 628 to 697 cm^{-1} [72-76]. The agreement is excellent showing that the present model describes well the molecular adsorption state of O_2 on a silver surface. The gross charge of the oxygen of the superoxide is -0.27 ($^2A_2$) or -0.33 ($^2B_1$), and so O_2^- is actually $O_2^{(0.5\text{-}0.6)-}$. In peroxide, the gross charge on oxygen is about -0.7, and so O_2^{2-} is actually $O_2^{1.4-}$. Backx et al. estimated the charge of -1.7 from the consideration of the vibrational frequency as a

function of the number of electrons in the π^* antibonding orbitals [75,76]. The calculated distance of O_2 from the surface is 2.6 Å for superoxide and 2.0 Å for peroxide, shorter for peroxide reflecting its larger adsorption energy.

TABLE 9. Adsorption energy, vibrational frequency, and gross charge of the molecular adsorption species of O_2 on a silver surface calculated from the Ag_2O_2 adcluster.

Species	State	Adsorption energy (kcal/mol)	Bond length (Å)		O-O vibrational frequency (cm^{-1})	Gross charge (per O_2)
			$R(Ag_2-O_2)$	R(O-O)		
Superoxide	$^2A_2$	5.5	2.6	1.47	1055	-0.54
	$^2B_1$	···	···	1.47	974	-0.65
	Exptl.	9.2-9.3[a]	···	···	1053[b]	···
Peroxide	$^2A_1$	17.8	2.0	1.66	689	-12.4
	Exptl.	9.2-9.3[a]	···	1.47±0.05[c]	628-697[d]	···

[a] Reference 80. [b] Reference 72,73. [c] Reference 41,77. [d] Reference 72-76.

C. Dissociative adsorption of O_2 on silver surface

It is expected that the dissociative adsorption is led from the peroxide species ($^2A_1$), because the curves of the superoxide species ($^2A_2$, $^2B_1$) in Figure 27 rise more rapidly than that of the peroxide as the O-O distance is elongated. However, the potential curve of the peroxide rises monotonically up to R(O-O)=2.8894 Å, which is twice as large as the O-O distance of the free O_2 molecule. For realizing the stabilization of the dissociative state, two oxygen atoms must be separated further on the surface. We, therefore, need a larger Ag surface so that we next consider the dissociation of O_2 on the linear Ag_4 cluster.

We carried out the DAM calculations using the Ag_4O_2 adcluster with n=1. The geometry of the adcluster is shown in the inset of Figure 28. The O-O distance was elongated from 1.20 Å to 8.6682 Å keeping C_{2v} symmetry and the Ag_4-O_2 distance was kept to 2.0 Å. Different from the calculations for the Ag_2O_2 adcluster given above, the SAC/SAC-CI calculations for the Ag_4O_2 adcluster were done keeping the 4d orbitals of silver to be frozen. Figure 28 shows the potential energy curves of the ground and excited states of the Ag_4O_2 adcluster with n=1 for the elongation of the O-O distance and Table 10 is a summary of the calculated properties of the dissociative adsorption state. Here, we got the potential minima of not only the molecular adsorption states ($^2A_1$, $^2A_2$, and $^2B_1$), but also the dissociative adsorption state ($^2A_1$) at R(O-O)=7.0 Å. When we further optimized the Ag_4-O_2 distance at R(O-O)=5.7788 and 7.0 Å, it became shorter to 1.60 and 1.90 Å, respectively, and the corresponding energies are shown by the asterisks in Figure 28. The system is most stable at R(O-O)=5.7788 Å and $R(Ag_4-O_2)$=1.60 Å. The dissociated oxygens are adsorbed at the twofold bridge site of the Ag surface, as illustrated in the *rhs* inset of Figure 28, and the Ag-O bond length was calculated to be 2.16 Å,

which agrees with the observed distance of 2.06-2.17 Å [81]. The gross charge of oxygen at the optimized geometry is -0.98 and so the dissociated oxygen in essentially O^-.

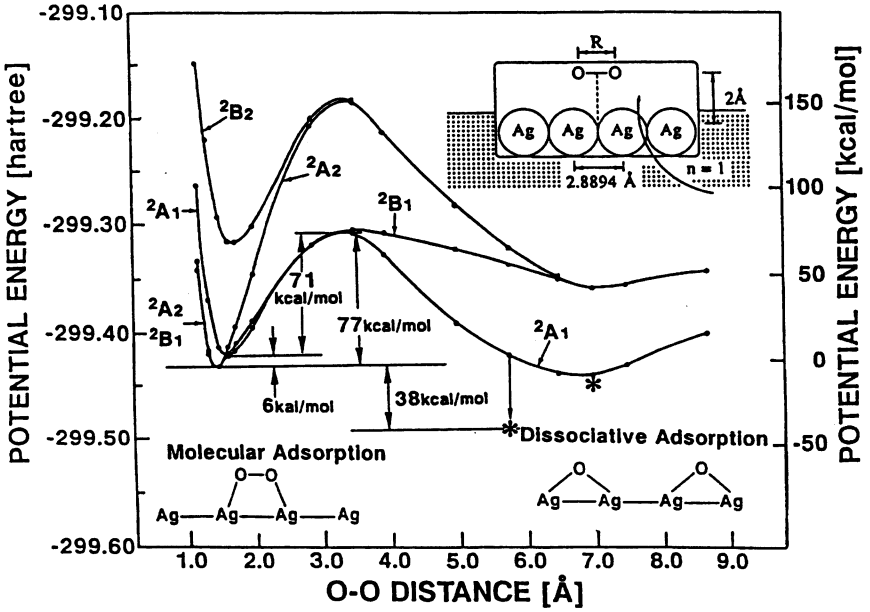

Fig. 28. Potential energy curves for the O-O elongation process in the Ag_4O_2 adcluster.

TABLE 10. Adsorption energy, geometry, and gross charge of the dissociative adsorption species of O_2 on a Ag surface calculated from the Ag_4O_2 adcluster.

Method	State	Adsorption energy (kcal/mol)	Bond length (Å) R(Ag-O)	Bond length (Å) R(O-O)	Gross charge (per O)
Theoretical	$^2A_1$	44.0, 61.4	2.16	5.78	-0.98
Experimental		40.8-44.0[a]	2.06-2.17[b]		

[a] Reference 80. [b] Reference 81.

The dissociative adsorption state is lower by 38.5 and 43.6 kcal/mol than the molecular superoxide and peroxide, respectively. The former value is an average of the values, 37.6 and 39.4 for the superoxide species, $^2A_2$ and $^2B_1$, respectively. By the thermal desorption spectra of O_2 adsorbed on Ag(111) and Ag(110) [80], the dissociative adsorption state was observed to be lower by 31.6 and 34.7 kcal/mol, respectively, than the molecular adsorption state. Using the adsorption energy for molecular species, the adsorption energy for the dissociated oxygen was calculated as 44.0 or 61.4 kcal/mol, in comparison with the experimental values 40.8-44.0 kcal/mol. The energy barrier between the molecular and dissociative adsorptions lies at R(O-O)=3.5 Å with a height of 77.2 kcal/mol from the superoxide species and 71.2 kcal/mol from the peroxide species. This barrier may be too large, in comparison with that in Figure 27, and this may be attributed to the neglect of the correlations of the d electrons for the Ag_4O_2 adcluster. Further, it was shown that the Ag(111) surface does not give the

dissociative adsorption, while the Ag(110) surface readily give the dissociative adsorption [80,112]. The structure of the present Ag_4 adcluster is close to the Ag(111) surface.

Thus, using the DAM, we were able to describe the dissociative adsorption of O_2 on a silver surface. This was the first such result and the reason was again the importance of the electron transfer from the silver bulk metal to the adcluster. Since the gross charge on the oxygen is large in this process, the electrostatic image force correction was also important [49].

D. End-on superoxide on silver surface

We have separately studied the end-on superoxide species adsorbed on a silver surface using the AgO_2 adcluster [50]. We have shown that even a single Ag atom can give positive adsorption energy if we use the DAM. We had the potential curves essentially similar to those shown in Figure 26. The ground state of the end-on O_2 adsorption on silver was shown to be the superoxide and the Ag-O-O angle being bent at about 110 degree. This result is similar to that of Broomfield et al. [51]. The bent geometry is about 10 kcal/mol more stable than the linear one. The O-O bond of the superoxide is moderately relaxed since the π^* MOs are formally occupied by three electrons.

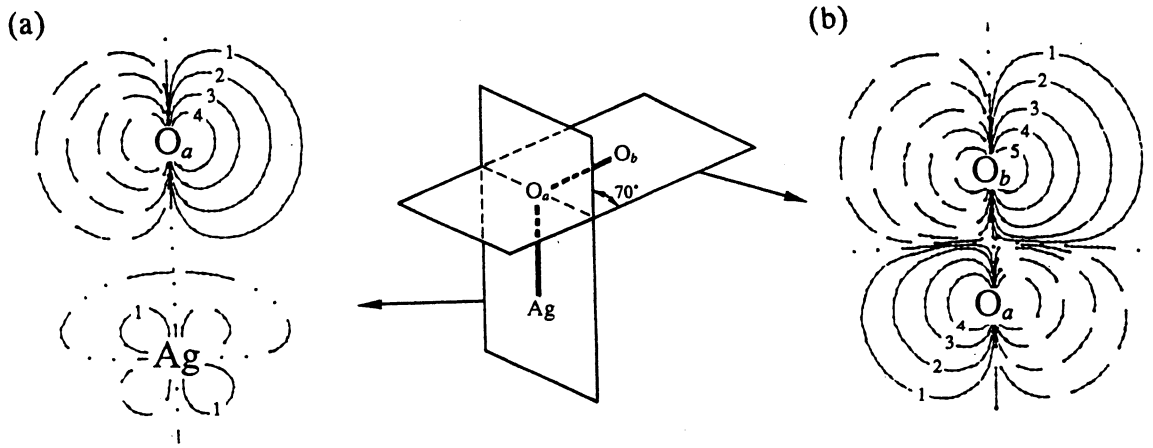

Fig. 29. Contour maps of the frontier orbital of the superoxide on silver calculated for the $Ag\text{-}O_a\text{-}O_b$ with the declining angle θ of 70°; (a) and (b) are the maps on the planes including the $Ag\text{-}O_a$ and $O_a\text{-}O_b$ bonds, respectively. Solid and broken lines correspond to plus and minus signs in the orbital. Double dotted line shows the node of the MO. The numbers 1-5 on the contours correspond to the values 0.01, 0.03, 0.10, 0.30, 1.00, respectively.

We designate this system as $Ag\text{-}O_a\text{-}O_b$. It was found that O_a is more negative than O_b: their net charges were -0.50 and -0.32, respectively. This charge distribution agrees with the stabilization due to the image force. Further, a more important result was the reactivity difference between these two oxygen atoms. Figure 29 shows the counter map of the frontier orbital of the superoxide on a silver surface. It is the out-of-plane π^* MO which is singly occupied. The in-plane π^* MO is doubly occupied. In Figure 29 we see that this frontier MO is localized on the superoxide (the contours near the Ag atom are small), and between O_a and O_b, the frontier orbital density is much higher on O_b. Namely, the outside oxygen O_b is more reactive than the inside oxygen. Furthermore, since the frontier

orbital, which is SOMO, is mainly composed of the π^* MO of O_2, one-electron flow into this orbital causes a breaking of the O-O bond. We will see later that this reactivity difference between O_a and O_b is very important in studying the mechanism of the reactions involving the superoxide species.

The charge distribution of the end-on superoxide is favorable for the approach of electron-rich molecules: by the frontier orbital control, the electron-rich molecule would attack the outside oxygen of the end-on superoxide. The electrostatic repulsion in this attacking process is reduced, since the negative charge on the outside oxygen atom is smaller than that on the inside one. On the other hand, in the side-on form there is no charge polarization between the two oxygen atoms.

8. Partial Oxidation of Ethylene on Silver Surface

The heterogeneous selective oxidation of olefins to epoxides on sliver

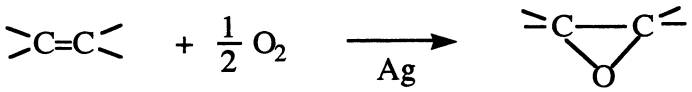

olefin epoxide (8.1)

is an exceedingly important industrial catalytic reaction, and as such has received long and extensive study [95-101]. During the past 20 years, many studies [102-120] have been devoted to getting a better understanding of the reaction mechanism of the epoxidation, with the ultimate goal to be able to increase the selectivity for epoxide formation. Most of them were carried out for ethylene epoxidation and actually, silver catalysts are used in industry to produce several million tons of ethylene oxide yearly [95-98]. One of the main questions about the mechanism of ethylene oxidation is the roles of the adsorbed molecular and atomic oxygen. The mechanistic details of the epoxidation and that of the competing combustion to carbon dioxygen and water are far from understood, and also, the nature of the active oxygen species on the catalyst surface for either of these reactions has not been conclusively demonstrated.

One particularly interesting aspect of the epoxidation reaction is its uniqueness: not only is silver a uniquely effective catalyst for heterogeneous epoxidation, but also ethylene is the only hydrocarbon which may be epoxidized with high selectivity [95-101]. A selectivity as high as 85-87% has been reported experimentally by promoted supported silver catalyst [99-104]. Recent experimental studies show that, except for ethylene, only a few olefins such as styrene [121,122], 3,3-dimethylbutene [123], norbornene [124], and butadiene are epoxidized over silver with high selectivity. In contrast, other olefins such as propylene, butenes and pentenes are epoxidized over silver but with extremely low selectivity [114-120]. The selectivity reported for propylene was only 2 to 4% [114-117]. Due to the unfavorable selectivity of this reaction, it is of limited utility for the commercial production of propylene oxide, and considerably less attention has been devoted to the oxidation of propylene on silver than to that of ethylene.

In this section we give an account of our research on the mechanism of the partial oxidation of ethylene on a silver surface [66,67] and in the next section we want to clarify the reason why complete oxidation dominates for propylene on the same silver catalyst [68].

We already know the existence of at least four adsorbed species [72-75]: physisorbed species (O_2), molecularly adsorbed species, superoxide (O_2^-) and peroxide (O_2^{2-}), and atomically adsorbed species (O^- and/or O^{2-}). Since ethylene is not adsorbed on a clean silver surface [99-101,105,106], it was thought that ethylene in a gas phase reacts with the adsorbed oxygen on a silver surface [125].

Among the various adsorbed oxygen species, the active species for the partial oxidation of ethylene has not yet been identified. Many studies support the notion that molecularly adsorbed oxygen is the active species for partial oxidation, while total oxidation involves atomically adsorbed oxygen [126,127]. Herzog showed that atomically adsorbed oxygen produced from N_2O gave only CO_2 and H_2O at low temperature, at which surface migration can not occur [126,128]. Campbell compared the reactivity of Ag(111) with Ag(110) and showed that the Ag(110) surface can dissociate O_2 more easily than the Ag(111) surface, but the selectivity for the formation of ethylene oxide is higher on Ag(111) [12].

If the molecularly adsorbed oxygen is the active species of the partial oxidation and the atomically adsorbed species gives CO_2 and H_2O by complete oxidation, the overall reaction on the silver surface is written as

$$O_2(g) \rightarrow O_2(a), \tag{8.2}$$

$$C_2H_4(g) + O_2(a) \rightarrow C_2H_4O(g) + O(a), \tag{8.3}$$

$$C_2H_4(g) + 6O(a) \rightarrow 2CO_2(g) + 2H_2O(g). \tag{8.4}$$

where we assumed that the atomic oxygen is supplied on by (8.3). Then, the overall reaction is written as

$$7\ C_2H_4\ (g) + 6O_2(g) \rightarrow 6\ C_2H_4O(g) + 2CO_2(g) + 2H_2O(g). \tag{8.5}$$

If this mechanism is correct, the maximum conversion of ethylene into ethylene oxide would be 6/7 (85.7%) [129]. However, some recent experiments have exceeded this limit, and have achieved the selectivity of 85-87% by adding NaCl to the catalyst [130,131]. Deng et al. studied the promoting effects of Re and Cs and concluded that Re and Cs could enhance the selectivity reaching over 85.7% [102-104]. Based on these results, it has been suggested that the reaction may proceed by the mechanism that differs from the above one. Van Santen and de Groot [132] studied the reactivity of atomically adsorbed oxygen and showed that both ethylene oxide and carbon dioxide were obtained in the absence of molecularly adsorbed oxygen.

Some theoretical studies have been reported for this reaction mechanism. Carter and Goddard studied this reaction in detail using the *ab initio* generalized valence bond correlation consistent configuration interaction (GVB-CCCI) method [86,87]. They concluded that the surface atomic oxyradical anion (SAO) is the selective species for the formation of ethylene oxide and proposed that

the key to high epoxidation yields is to keep the oxygen coverage above θ=0.5 to ensure a large concentration of SAO. Van den Hoek et al. investigated the role of subsurface oxygen [88]. They showed that ethylene reacts with adsorbed atomic oxygen to form epoxide, and that subsurface oxygen enhances the epoxide formation by chemisorbed oxygen. Jørgensen and Hoffmann [133] studied this reaction using the extended Hückel method and concluded that atomically adsorbed oxygen is active for partial oxidation.

Here we show our recent theoretical study on the mechanism of partial oxidation of ethylene on a Ag surface [66,67]. We calculated the energy diagrams of the reactions of ethylene with both molecularly adsorbed and atomically adsorbed oxygens on a Ag surface. We assumed the Eley-Rideal mode, namely the reaction between the adsorbed oxygen species and a gaseous ethylene. The DAM was used to include the effects of the bulk metal such as the electron transfer between adcluster and surface and the image force. Geometry optimizations for calculating the reaction path were performed using the *ab initio* unrestricted Hartree-Fock (UHF) method and the energies at the optimized geometries were calculated by the second-order Møller-Plesset (MP2) methods including the image force correction. The Gaussian basis set used is of double-zeta accuracy and some additional functions were added for improvement. They are shown to reproduce well the known geometries and the energetics of the reactions.

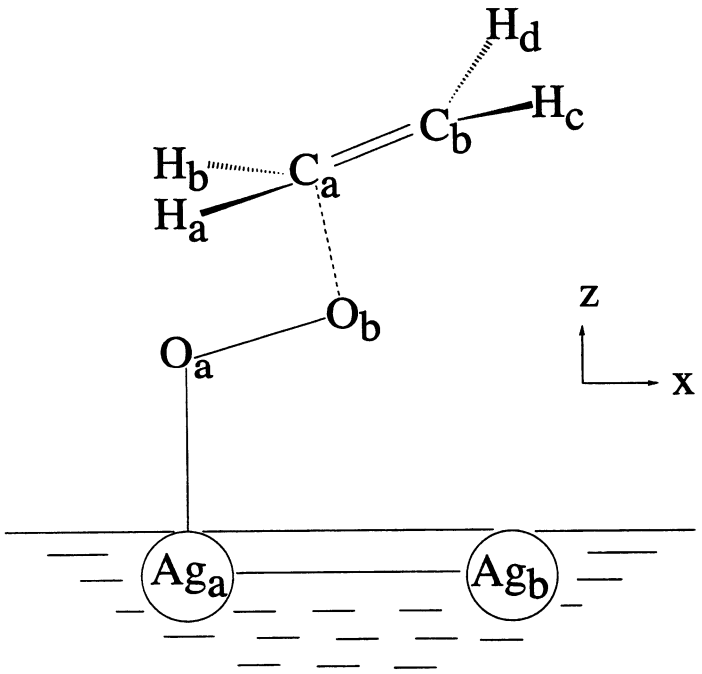

Fig. 30. Model adcluster used. Geometries were optimized in the Cs symmetry except for the Ag-Ag distance and the O_a-Ag-Ag angle fixed at 2.8894 Å and and 90.0°, respectively.

A. Reactions with molecularly adsorbed oxygen

(i) Epoxide formation We first study the epoxidation reaction of ethylene with the molecularly adsorbed superoxide on a silver surface. Figure 30 shows the favorable initial attack of ethylene to

superoxide. Starting from this geometry, we optimized the geometries of the intermediates and the transition states (TSs) along the reaction pathway. The Ag-Ag distance and the Ag_b-Ag_a-O_a angle were fixed at 2.8894 Å and 90.0°, respectively, but all the other geometrical parameters were fully optimized. The results are shown in Figure 31. The reaction proceeds from the left to the right, and the energy is in kcal/mol relative to the free system, i.e., $Ag_2 + O_2 + C_2H_4$.

The energy diagram given in Figure 31 shows that the reaction leading to ethylene oxide proceeds very smoothly: the reaction is exothermic, there are no very high barriers, and there are no too stable intermediates. We therefore conclude that the epoxide formation reaction from the superoxide species on a silver surface proceeds very smoothly. We note that the exothermicity of the overall reaction is partially due to the formation of the atomically adsorbed oxygen on the silver surface.

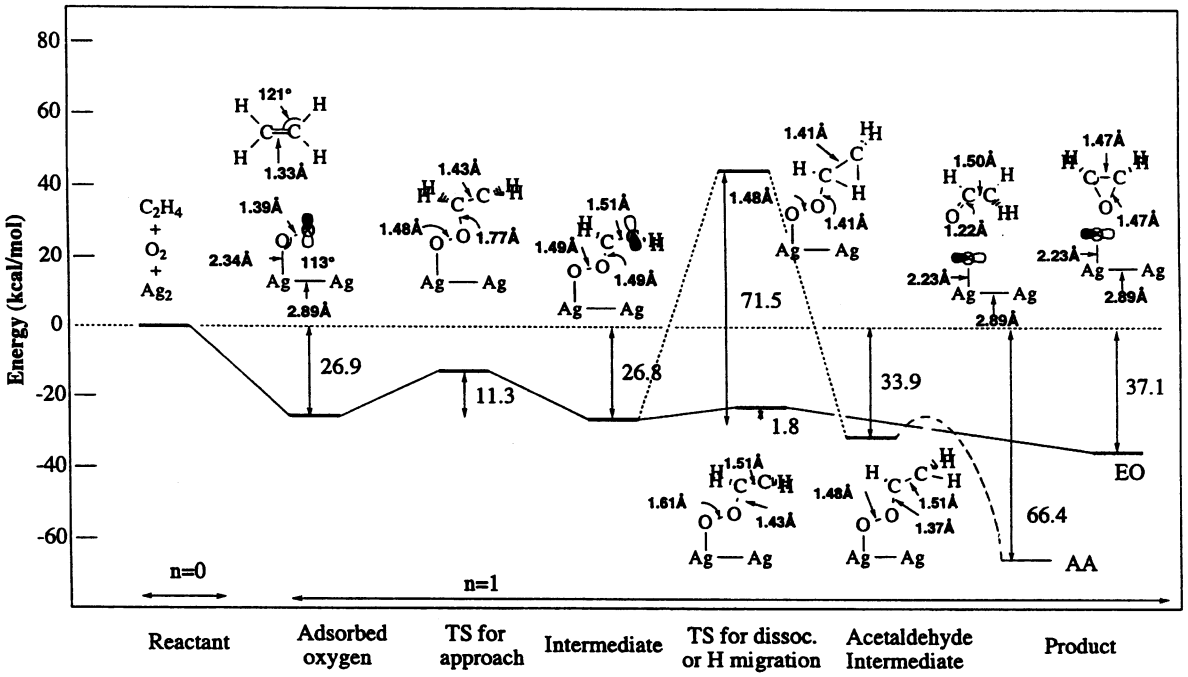

Fig. 31. Energy diagram for the reaction between ethylene and molecularly adsorbed superoxide on Ag surface. The routes leading to ethylene oxide (EO) and acetaldehyde (AA) are shown by the solid and broken lines, respectively.

We examine each reaction step in more detail. The first step of this reaction is the adsorption of molecular O_2 on the Ag surface, in which one electron is transferred from the bulk metal to the adcluster, i.e., n=1. The transferred electron mainly occupies the out-of-plane π^* orbital of O_2, and the in-plane π * MO of O_2 remains singly occupied. The optimized geometry is bent end-on as explained in § 7D. The ground state for the end-on adsorption of O_2 is the superoxide. The adsorption energy of superoxide is calculated to be 7.4 kcal/mol at the UHF level and 26.9 kcal/mol at the MP2 level. The experimental molecular adsorption energies are 9.2, 9.3, and 24.1 kcal/mol for the Ag(111) [80], Ag(110) [80], and electrolytic Ag [134] surfaces, respectively. The next step is the attack of ethylene onto the terminal oxygen atom O_b which is more reactive than the inside one O_a, leading to the TS and the intermediate with the energy barrier of 11.3 kcal/mol. The energy level of the intermediate is

similar to that of initial step. In the TS the σ bond between O_b and C_a is formed and the in-plane π bond of O_2 and the π bond of C_2 are broken. The O_a-O_b distances of the adsorbed oxygen state, the TS, and the intermediate are 1.39, 1.48, and 1.49 Å, respectively, and the C_a-C_b distance increases from 1.33 to 1.43, and then to 1.51Å, respectively. Note that the O-O distances of the free O_2^- and peroxide are 1.35 Å, and 1.47 Å, respectively [41,77]. The O_b-C_a distances of the latter two are 1.77 and 1.49Å, respectively.

Since the C-C π bond is broken in the intemediate, the calculated energy barrier for the rotation around the C_a- C_b axis is small: calculated to be 2.3 kcal/mol. This result agrees with the experimental fact that both cis- and trans-$C_2H_2D_2O$ molecules are produced from the cis- $C_2H_2D_2$ in this catalytic reaction [114].

When this intermediate is produced, the formation of ethylene oxide is an easy path as shown by the real line, leaving an atomic oxygen on the Ag surface: the energy barrier of this process is only 1.8 kcal/mol. In this process, the O_a-O_b distance increases from 1.49Å to 1.61Å, and then to infinity, and the O_b-C_b distance decreases from 2.44Å to 2.37Å and further to 1.47Å. The mode of the negative force constant certainly corresponds to this change of the geometry, i.e., O_a-O_b stretching and O_b-C_a-C_b bending.

The reaction shown in Figure 31 proceeds with n=1, i.e., with an excess electron supplied from the bulk metal, except for the free state. The heat of reaction is 37.1 kcal/mol.

(ii) Acetaldehyde formation. We next study the formation process of acetaldehyde from ethylene and molecularly adsorbed superoxide on the Ag surface. In Figure 31, the path is given by the broken line. When acetaldehyde is produced, it is further oxidized to CO_2 and H_2O by combustion in the presence of adsorbed oxygen and therefore it is an intermediate in the complete oxidation process [135].

The formation of acetaldehyde starts from the intemediate shown in the center of Figure 31: up to it the reaction path is common to the epoxidation reaction. H_a bound to C_a in the intermediate migrates to C_b, giving a stable conformation denoted as acetaldehyde intermediate in Figure 31. However, the energy barrier for this H_a migration is as high as 71.5 kcal/mol. This step is therefore energetically forbidden. This is a reason of the high selectivity of the epoxide formation process starting from the superoxide species summarized in the preceding section.

(iii) Effect of silver surface. The effect of the silver surface may be twofold: one is to provide a reactive species adsorbed on the surface and the other to provide electrons to the reaction site as considered in the DAM. Figure 32 shows the energy diagram for the reaction between ethylene and gaseous oxygen without the silver surface. Two energy diagrams correspond to the calculations with n=1 and n=0. The former involves an excess electron but the latter is neutral. For n=1, we used the optimized geometries shown in Figure 31, and, for n=0, we performed the geometry optimization for

the present purpose. The geometries illustrated in the upper and lower sides correspond to those for n=0 and n=1, respectively. For n=0, the O-O distance is calculated to be 1.37 Å for the intermediate, which is smaller than the corresponding value 1.49 Å for n=1. The same is true for all the intermediates and TSs.

Comparing Fig. 32 with Fig. 31, we clearly see the catalytic activity of the silver surface for the epoxidation reaction. Without the surface, the reaction is endothermic and the pathway has a large barrier. Electron transfer (n=1) certainly reduces the barrier, but the direct interaction with the actual silver atoms on the surface is quite important. Clearly, the exothermicity of the reaction shown in Fig. 31 is due to the formation of the atomically adsorbed oxygen on the surface. Thus, both of the two effects summarized at the beginning of this subsection are important for the catalytic activity of the silver surface.

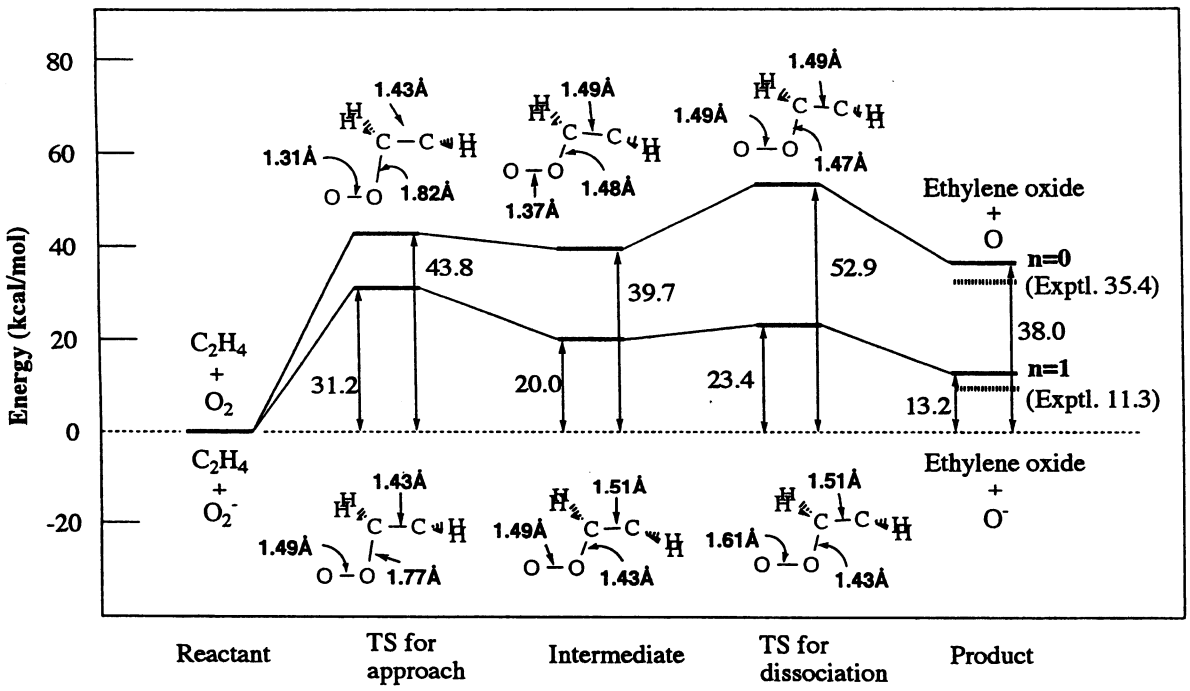

Fig. 32. Energy diagram for the reactions between ethylene and gaseous oxygens (neutral O_2 (n=0) and O_2 anion (n=1)). The upper geometries are for n=0, and the lower geometries for n=1.

B. Reactions with atomically adsorbed oxygen

When ethylene oxide is ejected out of the Ag surface, the atomically adsorbed oxygen O^- is left on the surface. It is also produced by the dissociative adsorption of O_2 on the surface, and the dissociative state is more stable than the molecular adsorption state. In our calculation, the dissociated oxygen has its singly occupied orbital in the 2p orbital parallel to the surface.

Figure 33 shows the energy diagram for the reaction of ethylene with the atomically adsorbed oxygen on the Ag surface. When ethylene attacks atomic oxygen on the surface, the most favorable approach is to form the C_a-O_a bond as illustrated in Figure 33. It is similar to the approach of ethylene to the superoxide species shown in Figure 31. The calculated energy barrier from the adsorbed oxygen to the intermediate is however, as small as 1.5 kcal/mol, reflecting the reactivity of the atomic oxygen.

In the TS and the intermediate, the C_a-O_a distance was calculated to be 1.80 and 1.43 Å, respectively. The C-C bond changes from 1.33 Å in ethylene to 1.43 Å in the TS and then to 1.51 Å in the intermediate: it changes from the double bond to the single bond. In the intermediate, the reactive site is the p orbital on the C_b atom shown in the figure. Up to this intermediate, the reaction proceeds quite smoothly.

The next step from this intermediate is very important, since it determines the selectivity of the atomically adsorbed oxygen. If C_b attacks the oxygen to form the C_b-O_a bond, ethylene oxide is formed. If C_b attacks another C-H bond, causing the hydrogen migration, acetaldehyde is a product, which is an intermediate for the complete oxidization product.

For the hydrogen migration reaction, the barrier was calculated to be 39.1 kcal/mol, which is high but lower than the barrier, 71.5 kcal/mol, of the reaction in which the superoxide species was involved (see Figure 31). This process were calculated using the adcluster with n=1.

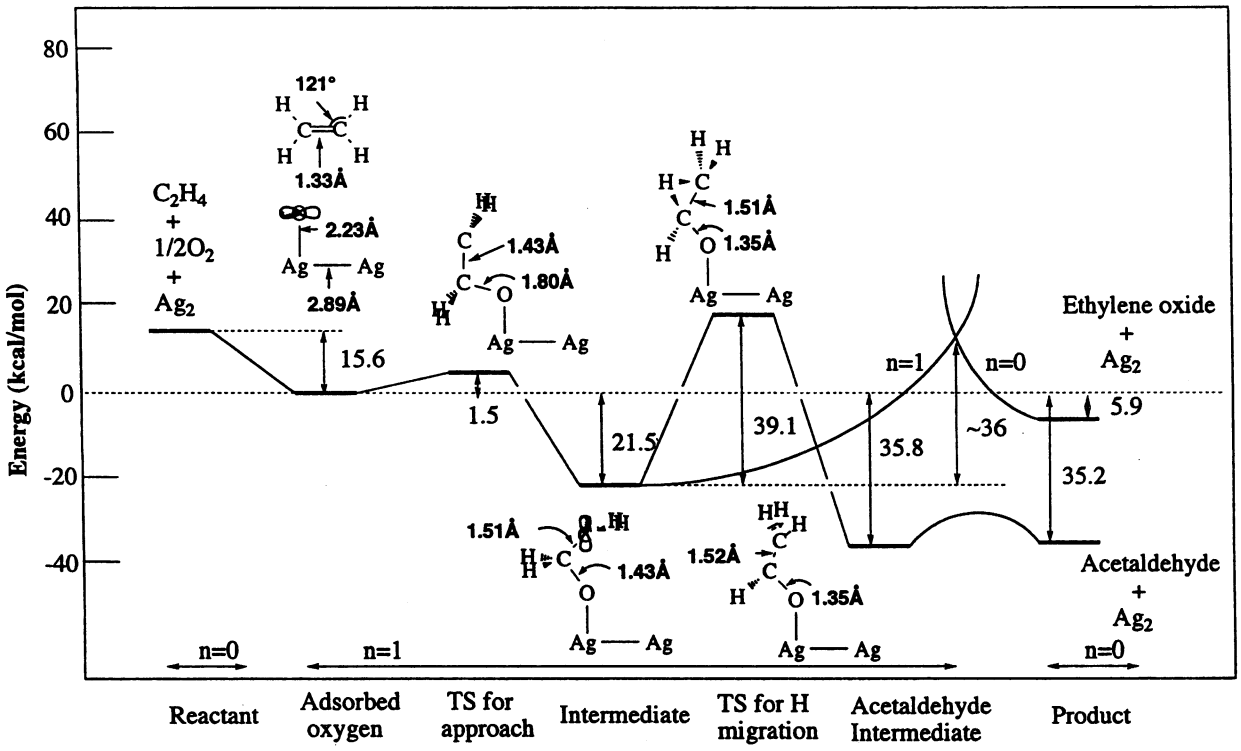

Fig. 33. Energy diagram for the reaction between ethylene and atomically adsorbed oxygen on Ag surface.

Unfortunately, the structure of the TS to form the C_b-O_a bond could not be determined by the geometry optimization procedure using both of the n=1 and n=0 adclusters. If the pathway from the intermediate to ethylene oxide is one step, it is a quite interesting step since it involves both geometrical changes and *one electron back-transfer* from the admolecule to the bulk metal. In the DAM picture, the intermediate in Figure 33 is naturally described with n=1, i.e., with one additional electron supplied from the bulk metal to the adcluster, but the product, ethylene oxide plus Ag_2 should be neutral, i.e., n=0. Therefore, we calculated two potential curves, one starting from the intermediate

and the other from ethylene oxide plus Ag_2 using n=1 and n=0, respectively. All the geometrical parameters were assumed to change linearly, except for the Ag-O distance which was fixed to 2.180Å.

The potential curve for n=1 increases monotonically from the intermediate to the product, while the curve for n=0 also increases monotonically from ethylene oxide and Ag_2 to the intermediate, and the two energy curves crosses. The energy difference between the crossing point and the intermediate is about 36 kcal/mol, which may be considered as the energy barrier of this process. Namely at this 'TS', one electron is transferred back to the metal.

The selectivity giving either ethylene oxide or acetaldehyde would be dependent on the heights of the barriers of the two processes and on the stabilities of the two products. The calculated energy barriers for the two processes are similar, 39.1 and about 36 kcal/mol, respectively. On the other hand, the energy difference between the two products and the intermediate are +15.6 and -13.7 kcal/mol, respectively, which means endothermicity and exothermicity from the intermediate, respectively. From the above data alone, it is difficult to decide which is a preferential process, though the acetaldehyde formation may be favorable for the exothermicity. However, it may safely be said that both ethylene oxide and acetaldehyde are formed from ethylene and atomically adsorbed oxygen on the Ag surface. This is in agreement with the observation by Van Santen and de Groot [132] that from atomically adsorbed oxygen both ethylene oxide and CO_2 were obtained. Furthermore, this fact is very important since it would be a reason for the experimental maximum selectivity more than 6/7 [99-101].

Based on the above analysis, we further note that both electron acceptor and donor may work to reduce the barrier of the electron transfer step: they work to stabilize the n=1 and n=0 curves, respectively. The effects of Ce and halogen as promoters of catalyst are well known experimentally [99-101]. We speculate that these promoters act in this electron transfer step. Design of the promoter or co-catalyst which is effective to this electron-transfer step is of crucial importance, since it would be a key for raising up the selectivity over 6/7.

C. Overall mechanism of epoxidation of ethylene

We summarize here our results on the mechanism of the partial oxidation of ethylene on a silver surface. The present theoretical results partially support the experimental findings summarized by Ayame [99-101].

The calculated energy barriers and the heats of the reactions are summarized in Table 11. The primarily important species for the epoxidation of ethylene on a silver surface is the superoxide O_2^- which is molecularly adsorbed on the surface in the bent end-on geometry. Ethylene attacks the terminal oxygen atom of the superoxide, as shown in Figure 30, with the barrier of about 11 kcal/mol, and then the reaction proceeds quite smoothly leading to ethylene oxide as shown in Figure 31. The overall reaction is exothermic by 37 kcal/mol from $C_2H_4 + O_2 +$ Ag surface or by 10 kcal/mol from C_2H_4 + superoxide on Ag surface. The second exothermicity is due to the larger adsorption energy of the atomic oxygen than that of the superoxide.

On the contrary, the complete oxidation of ethylene from the superoxide species is forbidden due to the existence of the large barrier (72 kcal/mol) in the hydrogen migration step, though this reaction

is largely exothermic by 66 kcal/mol from the initial compounds or by 40 kcal/mol from the superoxide on Ag and C_2H_4. When silver surface does not exist, the epoxidation reaction is a very unfavorable reaction having high energy barrier and endothermicity. Thus, the partial oxidation of ethylene by the superoxide on the Ag surface is highly efficient and selective.

TABLE 11. Comparison of the energy barrier and the heat of reaction for the epoxidation and acetaldehyde formation by the molecularly and atomicaaly adsorbed oxygens (kcal/mol).

Reaction	Energy barrier	Heat of reaction[a)]
Molecularly adsorbed oxygen		
$O_2(a)/Ag + C_2H_4 \rightarrow C_2H_4O + O(a)/Ag$	11.3	10.2
$O_2(a)/Ag + C_2H_4 \rightarrow CH_3CHO + O(a)/Ag$	71.5	39.5
Atomically adsorbed oxygen		
$O(a)/Ag + C_2H_4 \rightarrow C_2H_4O + Ag$	~36	21.5 (24.7)
$O(a)/Ag + C_2H_4 \rightarrow CH_3CHO + Ag$	39.1	50.8 (52.3)
Without Ag surface		
$O_2^- + C_2H_4 \rightarrow O^- + C_2H_4O$	31.2	-13.2 (-11.3)
$O_2 + C_2H_4 \rightarrow O + C_2H_4O$	52.9	-38.0 (-35.4)

a) Values in parantheses show the experimental values.

The atomically adsorbed oxygen, which is left on the surface after completion of the epoxidation reaction by the superoxide or which may exist by the dissociative adsorption of O_2 on the surface, has two reaction channels leading to ethylene oxide and to complete oxidation. The selectivity here seems to be small and both products would be obtained. This would be the reason why some experiments reach the selectivity larger than 6/7. In the process leading to ethylene oxide, the electron back-transfer from the reaction adsorbate complex to the metal surface should be important and related to the barrier. Both electron donor and acceptor would be effective for reducing the barrier of this process.

D. Comparison with previous experimental and theoretical studies

Many experimental and theoretical studies have been performed for the reaction mechanism of the silver-catalyzed epoxidation of ethylene. However, a mechanism totally consistent with all the observations seems not to has been presented. In this section, we try to explain many experimental results in view of the present theoretical results.

The Eley-Rideal (ER) mechanism in which gas-phase ethylene reacts with the adsorbed oxygen has widely been accepted, because ethylene is not adsorbed on a clean silver surface [99-101,105,106]. High temperature, used in the experimental condition, also supports the ER mechanism. However, a

Langmuir-Hinshelwood (LH) mechanism was not ruled out since ethylene adsorbs on an Ag^+ site induced by oxygen adsorption [105,106]. Therefore, we have checked the possibility of the reaction between the adsorbed oxygen and the adsorbed ethylene using the Ag_2-O_2-C_2H_4 adcluster with n=0 and 1, but no stable geometries and species were found: the present calculation supports the ER mechanism.

There remained a controversy regarding the active oxygen species. Early studies concluded that the catalytic activity unique to silver is originated by the existence of the molecularly adsorbed oxygen, which was not detected or rare on other metal surfaces. More direct evidence for molecular oxygen as the active species has been obtained by several studies: e. g., only complete oxidation occurs when N_2O pulse giving atomically adsorbed oxygen is used, but the epoxidation reaction occurs when O_2 pulse giving molecularly adsorbed oxygen, at least initially, is used [128]. The assumption that molecular and atomic oxygens cause the partial and total oxidation reactions, respectively, gives an upper limit for the selectivity of 6/7. Recent experiments giving higher selectivity than 6/7 may conflict with this assumption.

On the other hand, a mechanism assuming atomic oxygen as an active species was suggested from the experimental data that only atomically adsorbed oxygen exist at high temperature in an industrial condition, since molecular oxygen desorbs or dissociates. A theoretical study by Carter and Goddard supports this mechanism [86,87]. The electronic structure of the active atomic species is oxyradical anion and a spin transfer from the oxyradical anion to ethylene, giving Ag-O-CH_2-CH_2· intermediate, is important in both of the Carter and Goddard and our studies. Kilty et al. assigned their IR peaks to the Ag-O-CH2-CH2· intermediate [136,137]. This observation means that this intermediate has a life time long enough to be observed, which is in accordance with our results shown in Fig. 33: the barrier starting from this intermediate to acetaldehyde and to ethylene oxide are both rather high, 39 and 36 kcal/mol, respectively. Furthermore, the mechanism assuming only atomic oxygen to be an active species may conflict with the surface dependence of the selectivity; the selectivity of partial oxidation is lower on Ag(110) than on Ag(111), although oxygen dissociation is preferred on Ag(110) [80]. Furthermore, a copper surface which leads to the dissociative adsorption of O_2 more easily than silver does not catalyze the epoxidation of ethylene, while formaldehyde formation from methanol in which atomic oxygen is assumed to be an active species [138] is catalyzed not only by silver but also by copper.

Our theoretical study implies that the selectivity of the molecularly adsorbed oxygen is high and that of the atomically adsorbed oxygen is low. When O_2 molecule in a gas phase reacts with the Ag surface, the first product is molecularly adsorbed superoxide species, which is highly reactive with ethylene to give ethylene oxide. This reactivity of the molecularly adsorbed oxygen explains the high selectivity of the silver catalyst. The result that the atomically adsorbed oxygen can also give ethylene oxide, though in low selectivity, explains the experimental selectivity exceeding 6/7. Thus, the mechanism presented here can unambiguously explain the high selectivity of silver catalyst. For increasing the selectivity, the catalyst and/or promoter design for the reaction involving atomic oxygen is important, without affecting the high selectivity of the molecularly adsorbed superoxide.

9. Oxidation Mechanism of Propylene on Silver Surface

Though silver is an effective catalyst for the epoxidation of ethylene (85-87% conversion) [99-104], it is a very poor catalyst for the epoxidation of propylene (2-5% conversion) [114-117]. A relatively small substitution of hydrogen with methyl group,

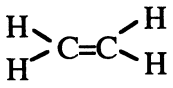

ethylene

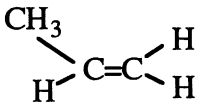

propylene

causes such a drastic change of the reaction. It is interesting to understand why. Further, in chemical industry, propylene oxide is an important material, so that to know why silver is so poor for the conversion of propylene to propylene oxide is a starting point for a design of a new effective catalyst. This section is a summary of our recent study on the oxidation mechanism of propylene [68].

It is known experimentally that silver is an effective catalyst of epoxidation only for few olefins such as ethylene [95-101], butadiene, styrene [121,122], 3,3-dimethylbutene [123], and norbornene [124], but in contrast, other olefins such as propylene, butene, and pentene are led to complete oxidation [114-120]. To clarify the reason of this kind of selectivity is a purpose of this section.

Two possible reasons may be considered for the difference in the reaction of ethylene and propylene on a silver surface. One possibility is that the reaction routes are the same but the methyl substituent causes a large change in the barrier height and/or in the stability of the intermediates in the course of the reaction. Another possibility is that an entirely different reaction route comes out for the existence of the methyl group. We have investigated these two possibilities. As in the case of ethylene, we study the reactions of the two active oxygen species on a silver surface : the molecularly adsorbed superoxide species and the dissociatively adsorbed atomic oxygen species.

The calculational methods are the same as those in the preceding section. The DAM [6-7] was used to include the effect of the bulk metal such as the electron transfer and the image force. The basis sets are the same as before and the geometries of the reactants, intermediates, transition states, and the products were optimized by the Hartree-Fock method and the energies were calculated by the MP2 method in order to include the effects of electron correlations.

A. Attack on olefinic carbon

We first study the reaction route which is essentially the same as that of ethylene [66]: the reaction starts from the interaction between the adsorbed oxygen and the doubly bonded carbon atom of propylene. Figure 34 is an illustration of the adcluster for the initial interaction of propylene with the superoxide species. Since two carbons in propylene are different, two different attacks were considered. The interaction with atomic oxygen was similarly considered.

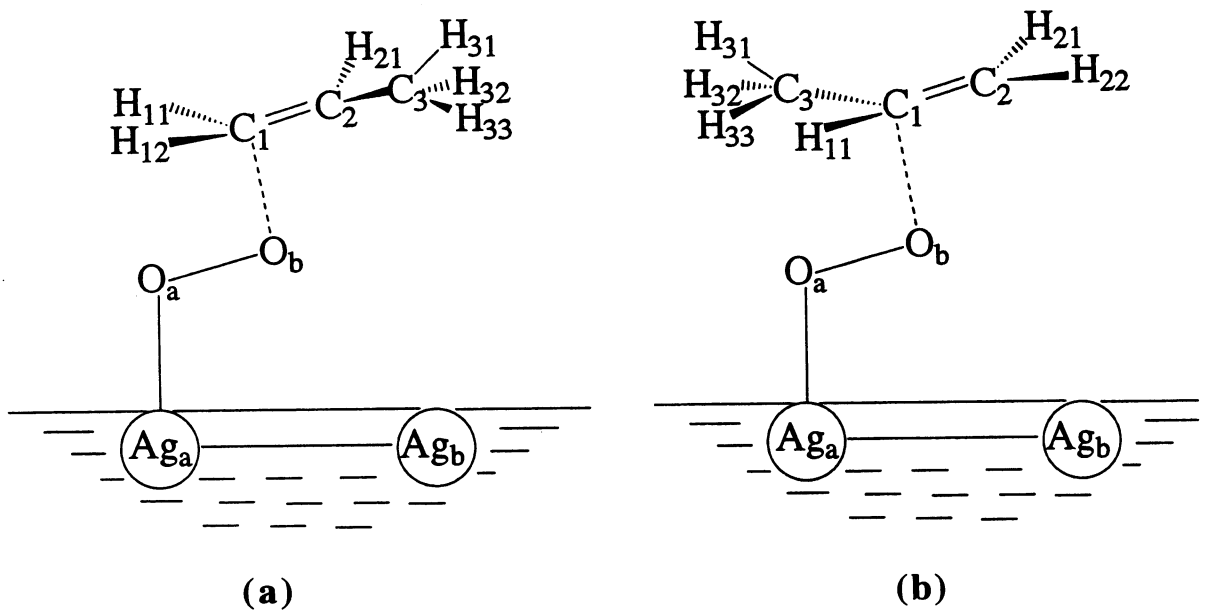

Fig. 34. Model adclusters for the olefinic carbon attack mechanism:
(a) on the terminal olefinic carbon, (b) on the central olefinic carbon.

Figure 35 shows the corresponding reaction route and the energy diagram for the reactions involving molecular superoxide species. It is for the attack on the terminal carbon atom. The reaction may be written as

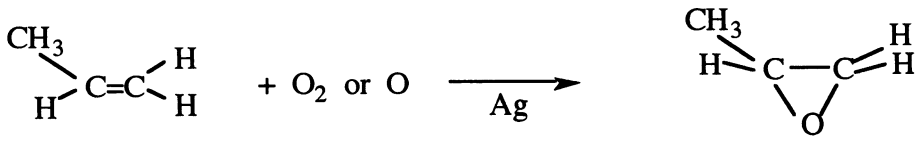

propylene oxide (9.1)

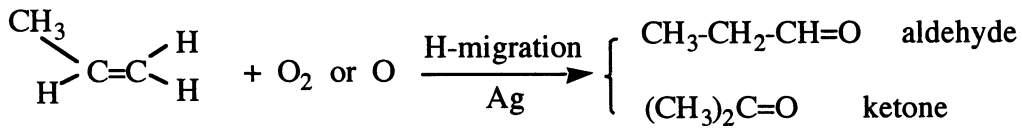

(9.2)

In (9.2), aldehyde is a product of the terminal C attack and ketone is a product of the central C attack (Figure 34), and they are further oxidized to CO_2 and H_2O.

Looking at Figure 35, we were surprised by its close similarity with Figure 31 for ethylene : the substitution of one hydrogen with methyl group does not cause a large change for the reaction route and the energetics. In this reaction mechanism, the route going to propylene oxide should be quite smooth without any high barrier and without any too stable intermediate, while the route leading to the aldehyde should be essentially blocked up by the existence of a high energy barrier in the hydrogen migration step. The diagram for the reaction of the superoxide with the central carbon atom of propylene (Figure 34b) was similar to Figure 35 [68]. Thus, if the reaction proceeds along this reaction route, propylene oxide should be produced in high selectivity due to the catalytic activity of the superoxide species adsorbed on silver.

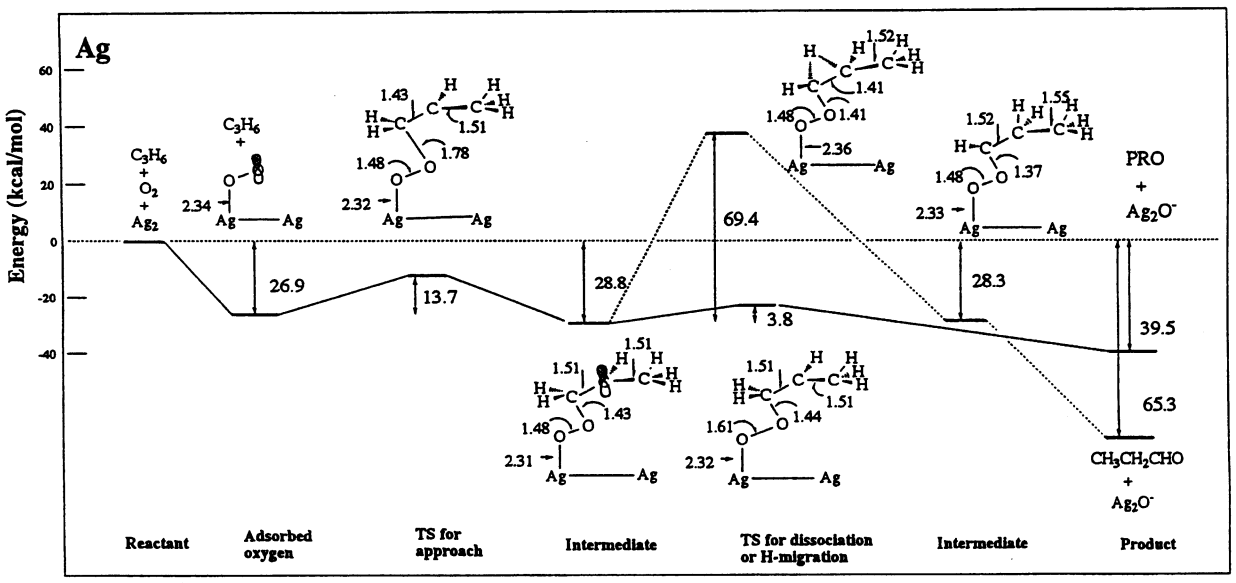

Fig. 35. Energy diagram for the reaction between the terminal carbon atom of propylene and the molecularly adsorbed superoxide on a Ag surface. The routes leading to propylene oxide and aldehyde are shown by the solid and broken lines, respectively.

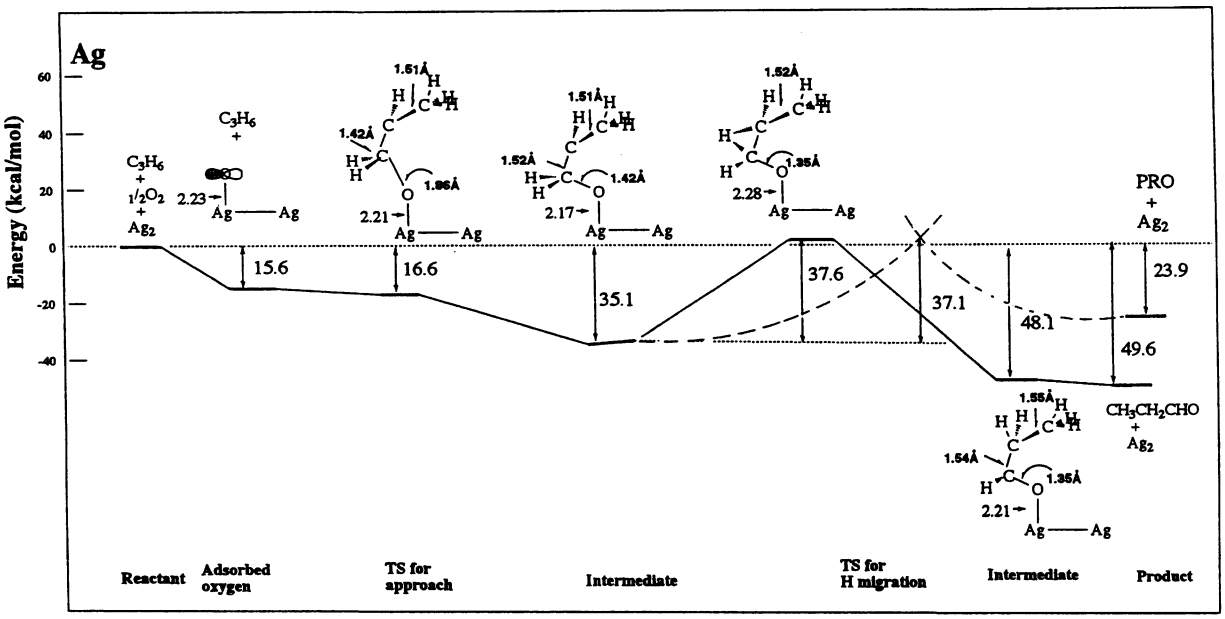

Fig. 36. Energy diagram for the reaction between terminal carbon atom of propylene and the atomically adsorbed oxygen on a Ag silver.

Figure 36 shows the reaction route and its energy diagram for the reaction of the dissociatively adsorbed atomic oxygen on silver with propylene. This figure corresponds to the attack on the terminal carbon, but the one for the attack on the central carbon was similar. We again notice a close similarity of Figure 36 to Figure 33 for ethylene: the heights of the barriers leading to propylene oxide and aldehyde are similar and the aldehyde product is more thermally stable than propylene oxide. (Note that the barrier for the olefinic C-attack was calculated to be -1.0 kcal/mol, a negative value which might be thought to be strange but possible because the energy was calculated by the MP2 method at the

geometry of the transition state optimized by the HF method.) Therefore, if the reaction proceeds along the route, propylene oxide should be produced though the selectivity of the atomic oxygen species must be low.

The results obtained from Figures 35 and 36 mean that if the reaction proceeds through the oxygen attack on the olefinic carbon of propylene, silver should be as good catalyst as for ethylene for the epoxidation. However, this result contradicts with the experimental observation that the conversion of propylene into propylene oxide is only 2-5% on the silver catalyst [114-120]. We therefore have to examine another possibility that a reaction route entirely different from those of ethylene may exist. Since propylene has a methyl group, but ethylene does not, we next examine the reaction route involving the reaction of this methyl group with the reactive oxygen on a silver surface.

B. Attack on allylic hydrogen

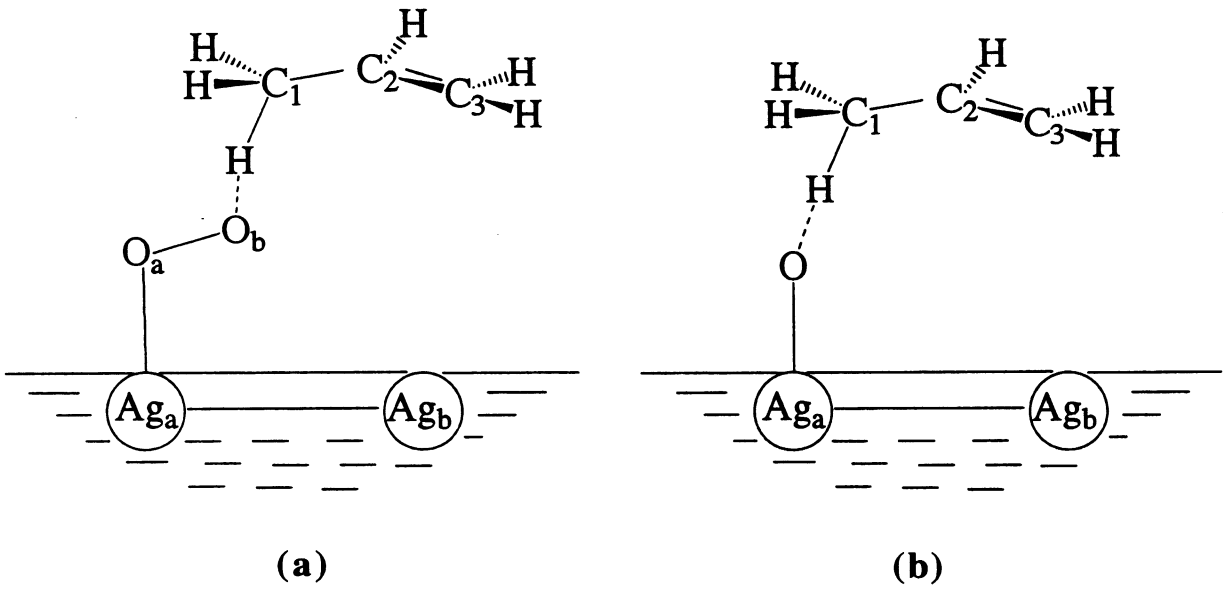

Fig. 37. Model adcluster for the allylic H attack mechanism. (a) Reaction with molecularly adsorbed superoxide species. (b) Reaction with atomically adsorbed oxygen.

Propylene is different from ethylene by an existence of a methyl group. We examine here the reaction route involving the reaction of this methyl group with the superoxide and the atomic oxygen on a silver surface. Figure 37 shows the initial attack of the superoxide (Figure 37a) and atomic oxygen (Figure 37b) on the methyl hydrogen, and the reaction proceeds as follows.

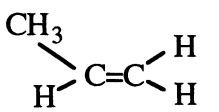

$$+ O_2/Ag \longrightarrow CH_2\text{-}CH\text{-}CH_2/Ag + H\text{-}O\text{-}O/Ag \qquad (9.3)$$

$$\longrightarrow CH_2\text{-}CH\text{-}CH_2/Ag + O/Ag + HO/Ag \qquad (9.4)$$

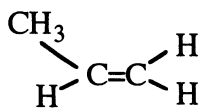

$$+ O/Ag \longrightarrow CH_2\text{-}CH\text{-}CH_2/Ag + HO/Ag \qquad (9.5)$$

These reactions produce the allyl intermediate adsorbed on the silver surface which is oxidized further to CO_2 and H_2O. Since allyl radical or anion is a rather stable intermediate, this reaction route is feasible.

Figure 38 shows the optimized reaction route for the attack of superoxide on the methyl hydrogen of propylene as given by (9.3) and (9.4). The present result was added to the previous one for the carbon attack given in Figure 35. The optimized geometries of the intermediates and the transition states for the present H-attack are given in the lower side, while those for the previous C-attack are given on the upper side. The energy levels of the intermediates and the transition states for the present reaction route are lower than those of the previous one. The barrier for the attack on the methyl hydrogen was calculated to be 10.8 kcal/mol, which is lower than the barrier for the carbon attack, 13.7 kcal/mol, and then the system becomes allyl intermediate and the hydroperoxy group adsorbed on silver ((9.3)). This intermediate is also more stable than the previous one, but the hydroperoxy group is unstable and further converted into OH and O as given by Eq. (9.4) : the barrier in this step is only 2.8 kcal/mol and the stabilization energy is as large as 42.6 kcal/mol. When two site interaction between allyl and silver surface is further allowed, the system is further stabilized by 18.1 kcal/mol. Thus, the reaction route starting from the allylic H attack is always lower than that starting from the olefinic C attack, so that the reactions represented by (9.3) and (9.4) should proceed more easily than the reactions given by (9.1) and (9.2).

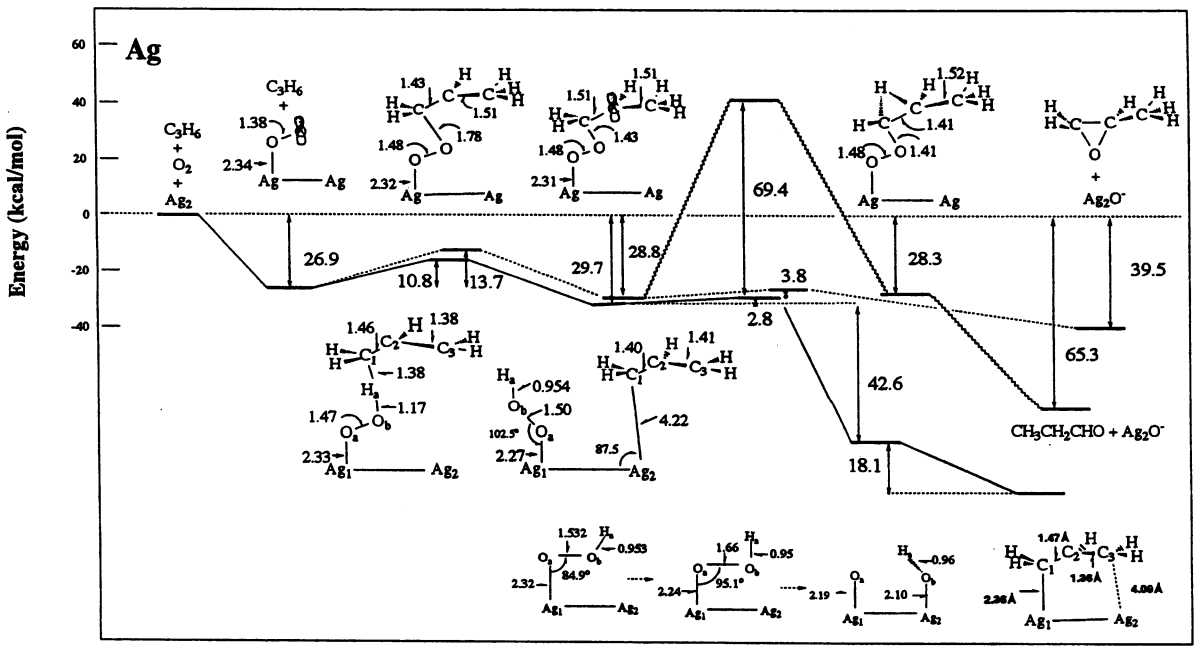

Fig.38. Comparison of the energy diagrams for the reactions between propylene and molecularly adsorbed oxygen. The route for the allylic H attack is shown by the solid line, and those for the carbon attack are shown by the broken and waved lines.

We next examine the similar reaction given by (9.5) involving the atomic oxygen adsorbed on silver. Figure 39 shows the optimized reaction route and its energetics. The lower figures give the

optimized geometries for the allylic H-attack and the upper ones for the olefinic C-attack. The barrier for the allylic H-attack is essentially zero: only 0.1 kcal/mol. The allyl intermediate is more stable than the intermediate of the previous C-attack: when two site interaction between allyl and silver surface is allowed, it is further stabilized by 18.1 kcal/mol. Thus, again, for the atomic oxygen on the silver surface, the allylic H-attack is an easier reaction than the olefinic C-attack. The allyl intermediate thus produced is stable on the silver surface so that it will be further attacked by the oxygen species on the surface and would finally be converted into CO_2 and H_2O.

Thus, for both superoxide and atomic oxygen on a silver surface, the reaction starting from the allylic H-attack proceeds more easily than the one starting from the olefinic C-attack. Therefore, the conversion to propylene oxide does not effectively occur on a silver surface.

However, the present study clearly shows that the route leading to propylene oxide also exists on a silver surface. Since propylene oxide is an important material in chemical industry, it is interesting whether we can block up the route leading to the allylic intermediate.

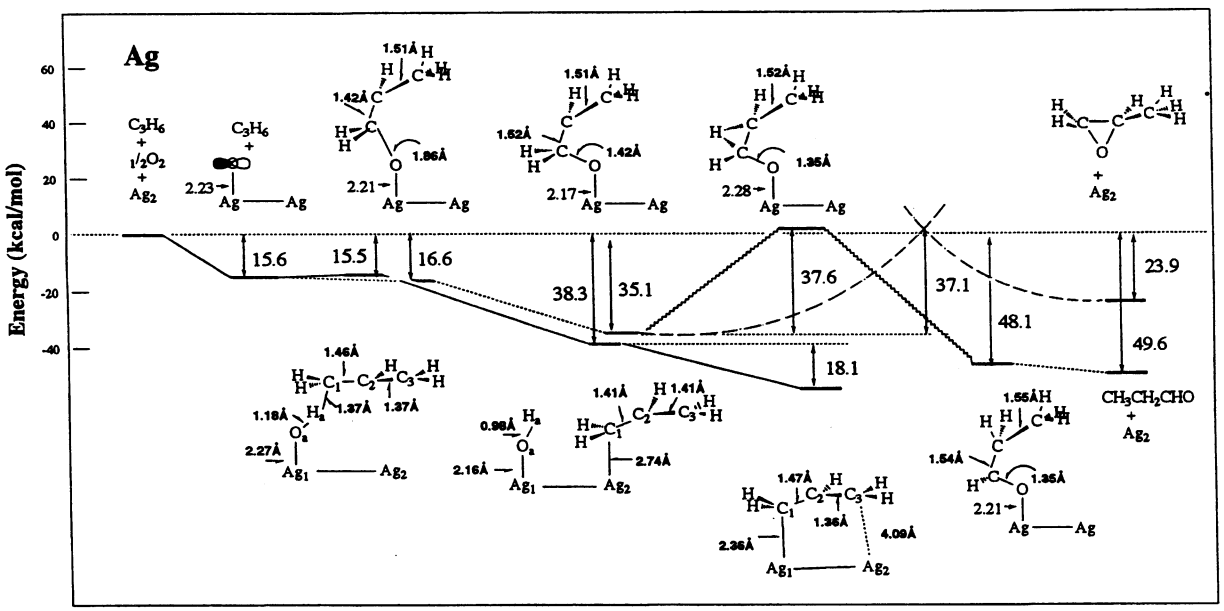

Fig. 39. Comparison of the energy diagrams for the two reactions between propylene and atomically adsorbed oxygen on a Ag surfaces.

Finally, we have investigated the nature of the allyl intermediate adsorbed on a silver surface. Figure 40 shows the optimized geometry of the allyl intermediate on Ag_2 calculated with n=0 and n=1. We see that the adsorption energy is larger with n=1 than with n=0, indicating that the allyl species on silver is actually an allyl anion species. Actually, the charge on the allyl group was -0.52 for n=1, while it was -0.27 in the case of n=0.

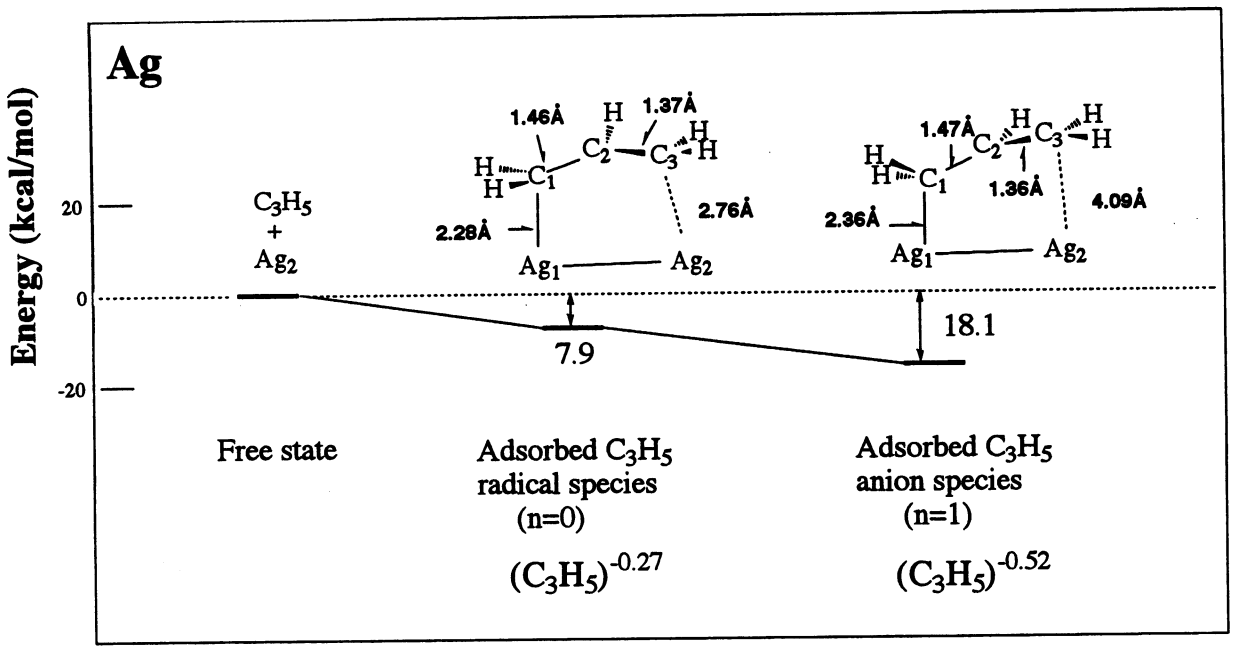

Fig. 40. Stability of the allyl species adsorbed on the Ag_2 cluster in the neutral (n=0) and anion (n=1) states.

C. Brief summary

Figure 41 is a summary of the reaction of propylene on a silver surface. The allylic hydrogen is more reactive than the olefinic carbon, due to the stability of the allyl anion species on the silver surface, so that propylene is converted to allyl intermediate and further converted to CO_2 and H_2O. If an olefin does not have an allylic hydrogen, like ethylene, styrene, etc., it is converted to epoxide in high selectivity. Even if it has an allylic hydrogen but the allyl intermediate is not stable like in norbornene, the route leading to epoxide is more preferable. This explains the selectivity of the silver surface for the epoxidation reactions of olefins.

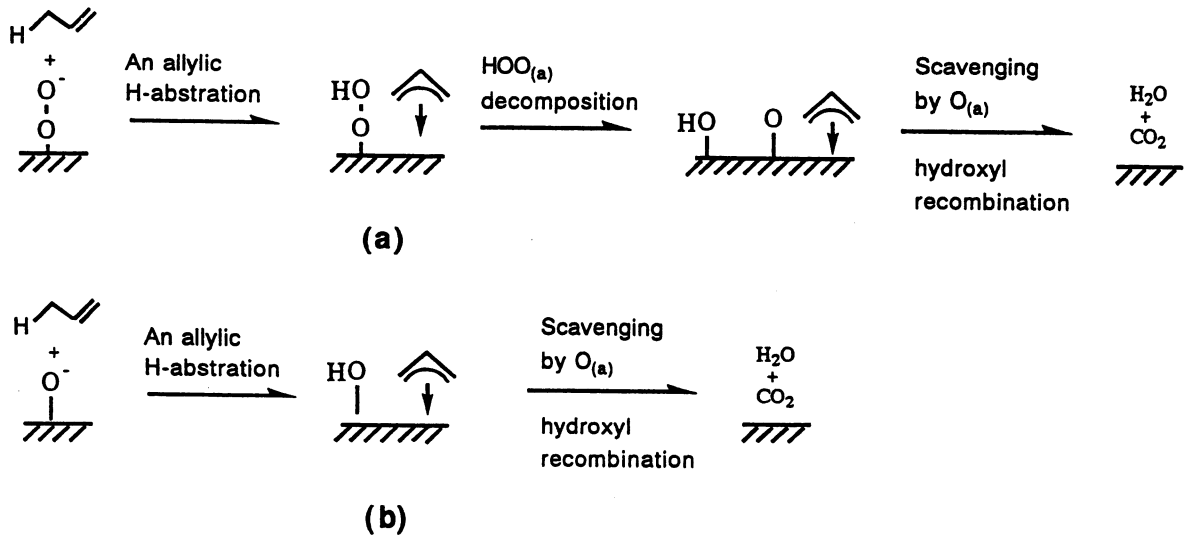

Fig. 41. Mechanism of the complete oxidation of propylene over a silver surface: (a) with molecularly adsorbed oxygen, (b) with atomically adsorbed oxygen.

10. Concluding Remarks

Dipped adcluster model (DAM) is a model for describing chemisorptions and catalytic reactions on a metal surface. It is useful especially when electron transfer between surface and adsorbates is important. This review has given an overview of the studies on the surface chemistry using the DAM performed in my laboratory. The DAM has raised interesting and important questions about the quantum chemistry of a partial system involving non-integer number of electrons. The molecular orbital model summarized here seems to work well, but we have to develop electron correlation theory of such system. The existence or the non-existence of the surface magnetism is closely related with the integral or non-integral nature of electron transfer, respectively, between the adcluster and the surface. For the palladium-O_2 system, we showed a numerical example that the highest spin coupling leads to one-electron transfer, but the paired spin coupling gives the transfer of electrons in a non-integral number. In the halogen chemisorption on alkali-metal surfaces, the long-range electron transfer, called harpooning, is understood as a one-electron transfer process in the DAM. It is a tunneling of an electron in the electron-number space, not in a coordinate space. The SAC/SAC-CI method is shown to be excellent in describing the surface chemiluminescence and surface electron emission of this system.

We have studied the chemisorptions and the reactions of O_2 adsorbed on a silver surface. O_2 is a triplet molecule in its ground state and therefore a bit special, different from most other closed-shell molecules. The highest-spin coupling is appropriate for the chemisorptions of this molecule and leads to a one-electron transfer from the bulk metal to the admolecule. We have demonstrated that the DAM combined with the SAC/SAC-CI method can describe well the different oxygen species adsorbed on a silver surface. This was the first successful result firstly obtained by using the DAM. Kosloff and his coworkers [139] studied the dissociation dynamics of O_2 on silver surfaces using the potential calculated by the DAM.

We have shown that the active species for the epoxidation of ethylene is the molecularly adsorbed superoxide, and the atomically adsorbed oxygen is less selective. For getting a better selectivity, the point of the catalysis design is to improve the selectivity of atomic oxygen by say adding some promoters. The step the promoter is effective is the electron back-transfer process giving ethylene oxide, so that both electron donating and accepting promoters should be effective. For the epoxidation of propylene, silver ia a very poor catalyst. We have clarified the reason. The active oxygen species are the same as in ethylene, but there are two oxidation paths : one leading to propylene oxide and the other leading to allyl anion species on a silver surface. The path leading to the allyl anion species was shown to be more favorable than the one leading to propylene oxide. This is a reason of a very low selectivity of the silver catalyst. The essence of an effective catalyst design is therefore to find a way of blocking up the route leading to the allyl anion species.

From the examples of the applications of the DAM, the usefulness of the DAM may become clear. Without the DAM, such studies must have been totally impossible. There are still many surface phenomena for which the DAM is appropriate. Indeed, Fan et al. clarified the oxidation mechanism of methanol [140] and Hyodo et al. studied the O_2 and NO adsorbed on a palladium surface [141], both

using the DAM. It is indeed our pleasure if this model serves to understand and clarify the mechanisms of such surface phenomena.

Acknowledgements

The author would like to deeply thank Dr. Zhen-Ming Hu for his very kind help in preparing this manuscript. Part of the calculations were performed using the computers at the Institute for Molecular Science. The studies summarized here were partially supported by the Grants-in-Aid for Scientific Research from the Ministry of Education, Science, and Culture and partially by the New Energy and Industrial Technology Development Organization (NEDO).

References

1. T.B. Grimley and C. Pisani, J. Phys. Chem. **7**, 2831 (1974).
2. C. Pisani, Phys. Rev. B **17**, 3143 (1978).
3. W. Ravenek and F.M.M. Geurts, J. Chem. Phys. **84**, 1613 (1986).
4. Y. Fukunishi and H. Nakatsuji, J. Chem. Phys. **97**, 6535 (1992).
5. J.L. Whitten and H. Yang, Surf. Sci. Rept. **24**, 56 (1996).
6. H. Nakatsuji, J. Chem. Phys., **87**, 4995 (1987).
7. H. Nakatsuji, H. Nakai, and Y. Fukunishi, J. Chem. Phys. **95**, 640 (1991).
8. H. Nakatsuji, H. Morita, H. Nakai, Y. Murata and K. Fukutani, J. Chem. Phys. **104**, 714 (1996).
9. H. Nakatsuji, T. Hayakawa and T. Yonezawa, J. Am. Chem. Soc. **103**, 7426 (1982); see also, H. Nakatsuji, J. Am. Chem. Soc. **96**, 24 (1974).
10. T. Fujita, H. Nakai and H. Nakatsuji, J. Chem. Phys. **104**, 2410 (1996).
11. M. Hidaka, T. Fujita, H. Nakai and H. Nakatsuji, Chem. Phys. Lett. in press.
12. C.T. Campbell, Surf. Sci. **157**, 43 (1985); J. Catal. **94**, 436 (1985).
13. H. Nakatsuji and M. Hada, J. Am. Chem. Soc. **107**, 8264 (1985); H. Nakatsuji, M. Hada and T. Yonezawa, J. Am. Chem. Soc. **109**, 1902 (1987).
14. H. Nakatsuji, Y. Matsuzaki and T. Yonezawa, J. Chem. Phys. **88**, 5759 (1988).
15. H. Nakatsuji, M. Hada and T. Yonezawa, Surf. Sci. **185**, 319 (1987).
16. H. Nakatsuji and Y. Fukunishi, Intern. J. Quantum Chem. **42**, 1101 (1992).
17. H. Nakatsuji, M. Yoshimoto, Y. Umemura, S. Takagi and M. Hada, J. Phys. Chem. **100**, 294 (1996); M. Yoshimoto, S. Takagi, Y. Umemura and H. Nakatsuji, J. Catal. submitted.
18. H. Nakatsuji, M. Hada, H. Ogawa, K. Nagata and K. Domen, J. Phys. Chem. **98**, 11840 (1994).
19. H. Nakatsuji, M. Yoshimoto, M. Hada, K. Domen and C. Hirose, Surf. Sci. **336**, 232 (1995).
20. Y. Fukunishi and H. Nakatsuji, Surf. Sci. **291**, 271, 281 (1993); **316**, 168 (1993).

21. H. Nakatsuji, Mathematical Science (Suuri Kagaku), **304**, 46 (1988). (in Japanese).
22. Y. Fukunishi, M. Hada and H. Nakatsuji, Catalysis, **33**, 270 (1991). (in Japanese).
23. H. Nakatsuji, H. Nakai and M. Hada, in *Metal-Ligand Interactions: From Atoms, to Cluster, to Surface*, D.R. Salahub and N. Russo (Eds.), NATO ASI Series, C378, Reidel, Dordrecht (1992), p251.
24. H. Nakatsuji, in *New Functionality Materials, Vol. C. Synthetic Process and Control of Functionality Materials*, T. Tsuruta, M. Doyama and M. Seno (Eds.), (1993), p15.
25. H. Nakatsuji, M. Hada, H. Nakai and Y. Fukunishi, Catalysis, **36**, 33 (1994). (in Japanese).
26. H. Nakatsuji, R. Kuwano, H. Morita and H. Nakai, J. Mol. Catal. **82**, 211 (1993).
27. For example, see, F.W. Bobrowicz and W.A. Goddard, in *Modern Theoretical Chemistry,* H.F. SchaeferⅢ(Eds.), Plenum, New York (1977), p.79.
28. J.H. Jeans, *The Methematical Theory of Electricity and Magnetism*, Cambridge University, New York (1966), Chap. VIII.
29. H. Nakatsuji and K. Hirao, J. Chem. Phys. **68**, 2053 (1978).
30. H. Nakatsuji, Chem. Phys. Lett. **59**, 362 (1978).
31. H. Nakatsuji, Chem. Phys. Lett. **67**, 329 (1979).
32. H. Nakatsuji, Chem. Phys. Lett. **67**, 334 (1979).
33. See for example, H. Nakatsuji and M. Ehara, J. Chem. Phys. **102**, 6822 (1995); H. Nakatsuji, J. Hasegawa, and M. Hada, J. Chem. Phys. **104**, 2321 (1996).
34. M. Hada, Y. Imai, M. Hidaka and H. Nakatsuji, J. Chem. Phys., **103**, 6993 (1995).
35. H. Nakatsuji, Acta Chim. Hungarica, **129**, 719 (1992).
36. H. Nakatsuji, in *Computational Chemistry - Reviews of Current Trends,* J. Leszczynski (Eds.), World Scientific (1997).
37. H. Nakatsuji, *Program System for SAC and SAC-CI Calculations,* Program Library No. 146 (Y4/SAC), Data Processing Center of Kyoto University, 1985; H. Nakatsuji, *Program Library SAC85(No. 1396),* Computer Center of the Institute for Molecular Science, Okazaki, 1986.
38. K.P. Huber and G. Herzberg, *Molecular Spectra and Molecular Structure, Ⅳ. Constants of Diatomic Molecules*, Van Nostrand Reinhold, New York (1979).
39. H.B. Michaelson, J. Appl. Phys. **48**, 4729 (1977).
40. J.L. Gland, B.A. Sexton and G.B. Fisher, Surf. Sci. **95**, 587 (1980).
41. D.A. Outka, J.Stohr, W. Jark, P. Stevens, J. Salomons and R.J. Madix, Phys. Rev. B **35**, 4119 (1987).
42. R. Imbihl and E. Demuth, Surf. Sci. **173**, 395 (1986).
43. X.Guo, L. Hanley and J.T. Yates, Jr., J. Chem. Phys. **90**, 5200 (1989).
44. X.Guo, A. Hoffman and J.T. Yates, Jr., ibid. **90**, 5787 (1989).
45. A. Hoffman, X. Guo, J.T. Yates, Jr., J.W. Gadzuk and C. W. Clark, ibid. **90**, 5793 (1989).

47. T.H. Upton, P. Stevens and R.J. Madix, J. Chem. Phys. **88**, 3988 (1988).
48. H. Nakatsuji and H. Nakai, Chem. Phys. Lett. **174**, 283 (1990).
49. H. Nakatsuji and H. Nakai, J. Chem. Phys. **98**, 2423 (1993).
50. H. Nakatsuji and H. Nakai, Can. J. Chem. **70**, 404 (1992).
51. K. Broomfield and R.M. Lambert, Mol.Phys. **66**, 421 (1989).
52. H. Metiu and P. Dax, Annu. Rev. Phys. Chem. **35**, 507 (1984).
53. J.K. Norskov, D.M. Newns and B.I. Lundqvist, Surf. Sci. **80**, 179 (1979).
54. P.A. Dowben, CRC Crit. Rev. Solid State Mat. Sci. **13**, 191 (1987).
55. W.R. Wadt and P.J. Hay, J. Chem. Phys. **82**, 284 (1985).
56. T.H. Dunning, Jr. and P.J. Hay, in *Modern Theoretical Chemistry,* H. F. Schaefer (Eds.), Plenum, New York (1977), p. 1.
57. S. Huzinaga (Eds.), *Gaussian Basis Sets for Molecular Calculations*, Elsevier, Amsterdam (1984).
58. P.J. Hay and W.R. Wadt, J. Chem. Phys. **82**, 299 (1985).
59. L. E. Sutton et. al., *Tables of Interatomic Distances and Configuration in Molecules and Ions,* The Chemical Society, London (1965).
60. R.J. Whitefield and J.J. Brady, Phys. Rev. Lett. **26**, 380 (1971).
61. Th.G J. van Orischot, M. van den Brink and W.H.M. Sachtler, Surf. Sci. **29**, 189 (1972).
62. V.B. Lazarev and Y.I. Malov, Fiz. Met. Metalloved **24**, 565 (1967).
63. D. Anderson, B. Kasemo, and L. Wallden, Surf. Sci. **152/153**, 576 (1985).
64. M.P. Cox, J.S. Foord, R.M. Lambert, and R.H. Prince, Surf. Sci. **129**, 399 (1983).
65. H. Nakatsuji and H. Nakai, Chem. Phys. Lett. **197**, 339 (1992).
66. H. Nakatsuji, H. Nakai, K. Ikeda and Y. Yamamoto, Surf. Sci. Submitted.
67. H. Nakatsuji, Z.M. Hu, H. Nakai and K. Ikeda, Surf. Sci. submitted.
68. Z. M. Hu, H. Nakai and H. Nakatsuji, to be submitted.
69. D. Schmeisser, J.E. Demuth and P.H. Avouris, Phys. Rev. B **26**, 4857 (1982).
70. P.B. Clarkson and A.C. Cirillo Jr., J. Catal. **33**, 392 (1974).
71. K.C. Price and A.M. Bradshow, Surf. Sci. **126**, 49 (1983).
72. C. Pettenkofer, I. Pockrand and A. Otto, Surf. Sci. **135**, 52 (1983).
73. C. Pettenkofer, J. Eickmans, U. Erturk and A.Otto, Surf. Sci. **151**, 9 (1985).
74. A. Sexton and R.J. Madix, Chem. Phys. Lett. **76**, 294 (1980).
75. C. Backx, C.P.M. de Groot and P. Biloen, Surf. Sci. **104**, 300(1981).
76. C. Backx, C.P.M. de Groot and P. Biloen, Appl. Surf. Sci. **6**, 256 (1980).
77. J. Stohr and D.A. Outka, Phys. Rev. B **36**, 7891 (1987).
78. M.A. Bartreau and J. Madix, Chem. Phys. Lett. **97**, 85 (1983).
79. H.A. Engelhardt, A.M. Bradshow and D. Menzel, Surf. Sci. **40**, 410 (1973).
80. C.T. Campbell, Surf. Sci. **157**, 43 (1985).
81. A. Pushmann and J. Haase, Surf. Sci. **144**, 559 (1984).

82. K. Bange, T.E. Madey and J.K. Sass, Chem. Phys. Lett. **113**, 56 (1985).
83. J.H. Lin and B.J. Garrison, J. Chem. Phys. **80**, 2904 (1984).
84. A. Selmani, J. Andzelm and D.R. Salahub, Intern. J.Quantum Chem. **29**, 829 (1986).
85. M.L. McKee, J. Chem. Phys. **87**, 3143 (1987).
86. E.A. Carter and W.A. Goddard , J. Catal. **112**, 80 (1988).
87. E.A. Carter and W.A. Goddard , Surf. Sci. **209**, 243 (1989).
88. P.J. van den Hoek, E.J. Baerends and R.A. van Santen, J. Phys. Chem. **93**, 6469 (1989).
89. I. Panas, P. Siegbahn and U. Wahlgren, J. Chem. Phys. **90**, 6791 (1989).
90. P.J. Hay and W.R. Wadt, J. Chem. Phys. **82**, 270 (1985).
91. T.H. Dunning Jr., J. Chem. Phys. **53**, 2823 (1970).
92. B.R.Brooks, P. Saxe, W.D. Laidig and M. Dupuis, Program System *GAMESS*, Program Library No. 481, Computer Center of the Institute for Molecular Science (1981).
93. P.H. Krupenie, J. Phys. Chem. Ref. Data **1**, 423 (1972).
94. A.W. Dweydari and C.H.B. Mee, Phys. Status Solidi. A **27**, 223 (1975).
95. R.A. van Santen and H.P.C.E. Kuipers, Adv. Catal. **35**, 265 (1987).
96. W.M.H. Sachtler, C. Backx and R.A. van Santen, Cat. Rev. Sci. Eng. **23**, 127 (1981).
97. X.E. Verykios, F.P. Stein and R.W. Coughlin, Cat. Rev. Sci. Eng. **22**, 197 (1980).
98. K.A. Jørgensen, Chem. Rev. **89**, 431 (1989).
99. A. Ayame, *Series of Lectures on Catalysis VII, Fundamental Industrial Catalytic Reactions,* Catalytic Society of Japan, Murakami Y (Ed.), Tokyo (1985), pp.170-185, in Japanese.
100. A. Ayame and H. Kanoh, Shokubai **20**, 381(1978), in Japanese.
101. H. Miura, A. Ayame, H. Kanoh, K. Miyahara and I. Toyoshima, Shinku **25**, 302 (1982).
102. J. Yang, J. Deng, X.Yuan and S. Zhang, Applied Catalysis A, General **92**, 73 (1992).
103. J. Deng, J. Yang, S. Zhang and X.Yuan, J. Catal. **138**, 395 (1992).
104. Y. Peng, S. Zhang, L. Tang and J. Deng, Catalysis Lett. **12**, 307 (1992).
105. E.L. Force and A.T. Bell, J. Catal. **38**, 440 (1975).
106. E.L. Force and A.T. Bell, J. Catal. **40**, 356 (1975).
107. R.B. Grant and R.M. Lambert, J. Catal. **92**, 364 (1985).
108. J.T. Gleaves, A.G. Sault, R.J. Madix and J.R. Ebner, J. Catal. **121**, 202 (1990).
109. M.A. Barteau, R.J. Madix, J. Am. Chem. Soc. **105**, 344 (1983).
110. J.T. Roberts, R.J. Madix and W.W. Crew, J. Catal. **141**, 300 (1993).
111. C.T. Campbell, J. Catal. **99**, 28 (1986).
112. C.T. Campbell and M.T. Paffett, Surf. Sci. **143**, 517 (1984).
113. C.T. Campbell and M.T. Paffett, Surf. Sci. **177**, 417 (1986).
114. N.W. Cant and W.K.J. Hall, J. Catal. **52**, 81(1978).
115. M. Imachi, M. Egashira, R.L. Kuczkowski and N.W. Cant, J. Catal. **70**, 177 (1981).
116. C. Henriques, M.F. Portela, C. Mazzocchia and E. Guglielminotti, *New Frontiers in Catalysis,*

Guczi, L. et al. (Eds.), (1993) pp.1995-1998.
117. M.F. Portela, C. Henriques, M.J. Pires, L. Ferreira and M. Baerna, Catal. Today, **1**, 101 (1987).
118. P.V. Geenen, H.J. Boss and G.T. Pott, J. Catal. **77**, 499 (1982).
119. I. L. C. Freriks, R. Bouwman and P.V. Geenen, J. Catal. **65**, 311 (1980).
120. M. Akimoto, K. Ichikawa and E. Echigoya, J. Catal. **76**, 333 (1982).
121. Y. Murakomo and K. Tanaka, Nippon Kagaku Kaishi **11**, 1603 (1977).
122. S. Hawker, C. Mukoid, J.P.S. Badyal and R.M. Lambert, Surf. Sci. **219**, L615 (1989).
123. C. Mukoid, S. Hawker, J.P.S. Badyal and R.M. Lambert, Catal. Lett. **4**, 57 (1990).
124. J.T. Roberts and R.J. Madix, J. Am. Chem. Soc. **110**, 8540 (1988).
125. G.H. Twigg, Proc. R. Soc.(London) A **188**, 92 (1946).
126. W. Herzog, Ber. Bunsenges. Phys. Chem. **74**, 216 (1970).
127. S. Tanaka and T. Yamashita, J. Catal. **33**, 392 (1974).
128. M. Kobayashi, M. Yamamoto and H. Kobayashi, *Proc. 6th. Intern. Congr. Catal.* A24, 1976.; M. Kobayashi, *Catalysis Under Transient Conditions,* A.T. Bell and L.L. Hegedus (Eds.), ACS (1982), p. 209.
129. M.A. Barteau and R.J. Madix, *The Chemical Physics of Solid Surfaces and Heterogeneous Catalysis*, D. A. King and D. P. Woodruff (Eds.), Elsevier, Amsterdam (1982), Vol. 4.
130. A. Ayame, N. Takeno and H. Kanoh, J. Chem. Soc. Chem. Commun. 617 (1982).
131. A. Ayame, T. Kimura, M. Yamaguchi, H. Miura, N. Takeno, H. Kanoh and I. Toyoshima, J. Catal. **79**, 233 (1983).
132. R.A. van Santen and C.P.M. de Groot, J. Catal. **98**, 530 (1986).
133. K.A. Jørgenson and R. Hoffmann, J. Phys. Chem. **94**, 3046 (1990).
134. X. Bao, J. Deng and S. Dong, Surf. Sci. **163**, 444 (1985).
135. L. Ya. Margolis, Adv. Catal. **14**, 429 (1963).
136. P. A. Kilty and W.M.H. Sachtler, *Catalysis Reviews*, Marcel Dekker, Inc., New York (1970), Vol. 10, p. 1.
137. P.A. Kilty, N.C. Rol and W.M.H. Sachtler, *Proc. 5th Int. Condr. Catal.,* Palm Beach (1972), No. 64.
138. H. Nakai, S. Kaimori, A. Matsubara and H. Nakatsuji, to be submitted.
139. O. Citri, R. Baaer and R. Kosloff, Surf. Sci. **351**, 24 (1996).
140. K. Fan, W. Wang and J. Deng, Bull. Chem. Soc. Jpn. **68**, 3035 (1995).
141. S. Hyodo and S. Noda, preprint.